NO-emission prediction in a Diesel Engine

Using a two zone in-cylinder simulation model

Y. Linden

P&E report number 2826

NO-emission prediction in a Diesel Engine

Using a two zone in-cylinder simulation model

by

Y. Linden

to obtain the degree of Master of Science
at the Delft University of Technology,
to be defended publicly on Tuesday July 4, 2017 at 13:00 AM.

Student number:	1279033	
Project duration:	december, 2015 – december, 2016	
Thesis committee:	Prof. Dr. D. J. E. M. Roekaerts,	TU Delft, chairman
	Ir. K. Visser,	TU Delft, supervisor
	Dr. Ir. R. Pecnik	TU Delft

TU Delft

Preface

The Royal Netherlands Navy, my employer for over fifteen years, gave me the opportunity to pursue a masters degree in engineering. The opportunity is one I greatly appreciate and also one I greatly enjoyed the past two years. After finishing the Naval College about ten years ago, I did not foresee returning to the school benches would be so interesting and pleasurable.

This thesis finalizes the last part of my two years education. The co-operation between Delft University of Technology and the Royal Netherlands Naval College, gave me the opportunity to profit from the equipment and knowledge of both. In Den Helder I was quickly welcomed and the support from the staff of the naval college, made my work possible. Ir. Henk Knol helped me with my thermodynamic 'struggles' and could more than once provide fresh insights and approaches to my challenges. The conversations where enjoyable and the help is greatly appreciated.
The friendly atmosphere in the Mechanical Laboratory (gebouw Medemblik) made it a nice workplace. A balance between engineering and the more regular coffee break topics provided an interesting and fun environment. My experiments would not be possible without the help and support of Ing. Chris Dijkstra, SGTTDE Marcel Roberscheuten and SGTTDW Arie van Oord. Your help is truly appreciated.

My renewed interest in Diesel Engines was mainly fostered by Ir. Rinze Geertsma. The discussions which led to my final topic of research and the help with the most difficult part of research - writing - is much appreciated. And, of course, all of this would not be possible without the guidance and support of my supervising professor. I am still impressed by the speed and accuracy with which he could pin-point weaknesses in my arguments, but also with the same speed and accuracy could put me back on track. Professor Ir. Klaas Visser thank you for your time, your knowledge and the motivational words which kept me on track the last months.

Finally, all would not be possible without the support of my friends and family. Writing a thesis can be time consuming at some points. Thank you for your understanding when study had the overhand on personal appointments and supporting me in times my results did not meet my expectations. When younger, living at my parents, I always did my homework at the kitchen table. Now, almost two decades later, this is still the place I go back to when struggling to tackle a problem. Mom, Dad, thank you.

Y. Linden
Delft, December 2016

Abstract

The diesel engine plays a dominant role in the field of (maritime) transportation and is expected to do so in the coming years. Depletion of fossil fuels and environmental impact are relevant concerns, widely acknowledged by the international community. NO_x contributes to acid deposition and eutrophication. Regulations on NO_x emissions become more stringent, such as the North Sea becoming a NECA area in 2021. In diesel engine emissions NO_x mainly consists of NO.

Given the relevance of NO-emissions a prediction tool is useful. Hohlbaum has suggested a 2-zone in-cylinder model approach to predict NO-emissions. The cylinder volume is divided in two zones, one containing fresh air, the other hosting secondary combustion. In the flame front, which separates both zones, primary combustion takes place at an air excess ratio smaller than unity. Air also passes the flame front, effecting the composition in secondary combustion zone, where NO-formation is calculated using the extended Zel'dovich formulation.
The inclusion of gas properties by means of an equations of state is investigated as an opportunity to reduce the uncertainty in the assumptions in the original model formulation. Measurements on a 4 cylinder MAN engine are used to evaluate simulation results.

Matching the simulated cylinder volume to the actual cylinder volume using the fuel flow, requires an additional tuning parameter - the partition of the cylinder volume in two zones at start of combustion - since the original assumption no longer holds.
The original tuning parameter - the air excess ratio in the flame front - in combination with the newly introduced tuning parameter proved insufficient to match the simulated to the measured fuel flow. Therefore, the constant air flow passing the flame front is adjusted. Changing the flow profile made it possible to match the simulated to the measured fuel consumption. The simulated NO emission where 2.7 times higher than the measured values in the operating point investigated.
A more complete analysis of flow profiles at different operating points is still required.

Contents

List of Figures

List of Tables

Nomenclature

Acronyms

ACT	Apparent combustion time
ADCF	Air defense and command frigate
AFR	Air fuel ratio
BDC	Bottom dead centre
CA	Crank angle
CFD	Computational fluid dynamics
DE	Diesel engine
EC	Exhaust valve closes
EO	Exhaust valve opens
EOC	End of combustion
FBN	Fuel bound Nitrogen
FFT	Fast fourier transformation
HRR	Heat release rate
HT	High temperature
IC	Inlet valve closes
IGM	Ideal gas mixture
IO	Inlet valve opens
IR	Inlet receiver
GAHRR	Gross apparent heat release rate
LHV	Lower heating value
LPF	Low pass filter
LT	Low temperature
MCR	Maximum continous rating
MVFP	Mean value first principle
NAHRR	Net apparent heat release rate
NLDA	Netherlands Defense Academy
OPV	Ocean-going patrol vessel
RHS	Right hand side
SFC	Specific fuel consumption
SOC	Start of combustion
SOI	Start of injection
TDC	Top dead centre
TU Delft	Delft University of technology

Symbols

Roman symbols

A	m^2	Area
C		Constant
D	m	Diameter
$\mathscr{F}$	[-]	Number of flows into and out of the system
H	J	Enthalpy
K_a		Equilibrium constant
L	m	Length
M	$kg\,mol^{-1}$	Molar mass
$\mathscr{M}$	[-]	Number of independent chemical reactions in the system

N_{eng}	RPM	Engine speed
N_i	mol	Amount of the i-th specie
$\mathcal{N}$	[-]	Number of species in the system
$\dot{Q}$	W	Heat flow
R	$\mathrm{J\,kg^{-1}\,K^{-1}}$	Gas constant
R	m	Radius
RH	[%]	Relative humidity
T	K	Temperature
U	J	Internal energy
U	$\mathrm{W\,m^{-2}\,K^{-1}}$	Overall heat transfer coefficient
V	$\mathrm{m^3}$	Volume
$\dot{W}_s$	W	Shaft work
X	[-]	Non-dimensional reaction coordinate
X_J	mol	Molar extend of the j-th reaction
Z	[-]	Non-dimensional rate of reaction
a	[-]	Activity coefficient
a	[-]	Vibe parameter linked to combustion efficiency
b_k	[-]	Weight factors in the multiple-Vibe model (k = 1, 2, 3,...)
c_p	$\mathrm{J\,kg^{-1}\,K^{-1}}$	Specific heat at constant pressure
c_m	$\mathrm{m\,s^{-1}}$	Mean piston speed
c_R	$\mathrm{mol\,m^{-3}}$	Concentration of rate controlling specie
c_v	$\mathrm{J\,kg^{-1}\,K^{-1}}$	Specific heat at constant volume
f	$\mathrm{kg\,s^{-1}}$	Mass flow
h	$\mathrm{J\,kg^{-1}}$	Specific enthalpy
h_k		Parameter polygon hyperbole heat release rate (k = [1,2,3])
k	$\mathrm{m^2\,s^{-2}}$	Turbulent kinetic energy
$k_{N,1f}$	[-]	Forward reaction coefficient of reaction N1
k_{FC}		Gain to control the fuel flow to zone II
m	kg	Mass
m_k	[-]	Form factors in the multiple-Vibe model
p	Pa	Pressure
r	$\mathrm{mol\,m^{-3}\,s^{-1}}$	Reaction rate
s	[-]	Slip factor
t	s	Time
u	$\mathrm{J\,kg^{-1}}$	Specific internal energy
v	$\mathrm{m^3\,kg^{-1}}$	Specific volume
y_2^*		Parameter polygon hyperbole heat release rate
y_4		Parameter polygon hyperbole heat release rate
y_6		Parameter polygon hyperbole heat release rate
y_i	[-]	Mole fraction of i-th component

Greek symbols

α	rad	Crank angle
α_{HT}	$\mathrm{W\,m^{-2}\,K^{-1}}$	Heat transfer coefficient
ϵ	[-]	error
ϵ_{HE}	[-]	Heat exchanger effectiveness
η	[-]	Efficiency
λ	[-]	Air excess ratio
λ_{CR}	[-]	Ratio between crank and connecting rod
ξ	$\mathrm{kg^2\,m^{-3}\,J^{-1}}$	Partial derivative of density to specific enthalpy at constant pressure and composition

ρ	$kg\,m^{-3}$	Density
Σ	mol	Final total number of mole
τ	[-]	Non-dimensional time
ϕ	m	nozzle diameter
φ	°	Crank angle
χ	$kg\,m^{-3}\,mol^{-1}$	Partial derivative of density to pressure at constant enthalpy and composition
ψ	$kg\,m^{-3}\,Pa^{-1}$	Partial derivative of density to composition at constant pressure and enthalpy

Subscripts

A	Air passing the flame front
a	Activation
Arr	Arrhenius
B	Bore
CD	Combustion duration
$comb$	Combustion
CR	Connecting rod
$CxHy$	Fuel composition
cyl	Cylinder
$diff$	Diffusion phase of combustion
E	Entering
eng	Engine
f	Fuel
FF	Flame front
HT	Heat transfer
i	i-th specie
in	Inflow
k	k-th flow
L	Leaving
$loss$	Loss from the control volume
m	Mechanical
Mag	Magnussen
mix	Mixing
out	Outflow
pre	Pre-mixed combustion
ref	Reference point
S	Stroke
sat	Saturation
sc	Scavenging
SV	Single volume
$total$	Total available
TR	Trapped
0	Total available fuel in the Vibe heat release model No fuel or motored condition in the Woshni heat loss model
I	Zone I
II	Zone II

1 Introduction

1.1. Background and relevance

The internal combustion engine concept developed by Rudolph Diesel in the late 19th century, quickly found application in many areas in the beginning of the next century. In present-day transportation the diesel engine (DE) plays a dominant role, both in number and in power generated. Seaborne shipments account for four fifth of total world merchandise trade by volume according to UNCTAD [32]. Fuels delivered to international maritime transport are almost only diesel or fuel oil and over 90 % for domestic maritime transportation are [11].
Mainly due to depletion of fossil fuels and environmental impact, various alternatives are sought for the diesel engine. However, current technologies do not render the diesel engine obsolete. Future technologies might include alternative, environmental friendlier, fuels for the diesel engine, perpetuating its role as reliable source of energy. For the coming years/decades, the diesel engine will be a dominant player in many fields, especially in transportation.

Depletion of fossil fuels and environmental impact are relevant concerns, widely acknowledged by the international community. Improvement in terms of (fuel) efficiency and emissions of the diesel engine and the use of diesel engines within operation concepts, is still a relevant area of research.
NO_x contributes to acid deposition and eutrophication. Acid deposition has an adverse effect on aquatic ecosystems and causes damage to vegetation, such as forests and crops. Eutrophication leads to severe reduction in water quality, impacts include decreased bio-diversity and toxicity effects EEA [12].
Emissions of nitrogen oxides from international transport are projected to increase. Regulations on NO_x emissions have become more stringent in the past decades and are expected to do so even more in the future. Ships built after 2011 have a maximum NO_x emission between 7.7 and 14.4 g/kWh (Tier II). The limit in NO_x emission control areas (NECA) lies between 2.0 and 3.4 g/kWh (Tier III) [11]. An increasing amount of areas is designated as NECA, such as for instance the North sea starting January 1st 2021, influencing north European shipping significantly.
Until now, regulations are only applied to static engine operating points and some engines are optimized for those specific operation conditions. Driven by developments in the automotive industrie, future regulations might also include transient restrictions on emissions. More importantly, efforts should be focussed on actually reducing emissions under real operating conditions, rather than meeting regulations.

Exploration and development of new concepts and control strategies can be done using models. Many types of models have been developed over the years and (with increasing computational power at lower cost) trends are emerging: simulations become more detailed and capture more complex phenomena (e.g. computational fluid dynamics - CFD); system boundaries widen, also capturing interaction between various components (e.g. the total ship model[24]) and while exploring a design, more options can be calculated.
Modeling is crucial in reducing emissions. The in-cylinder process of a diesel engine is complex. Not all occurring phenomena can be measured or even observed. Simulations increase understanding of the in-cylinder process and can predict values of variables which can not be measured directly, but influence emission formation significantly.

This thesis aims to predict NO-emissions based on a first principle model. While most emission-models consider the closed part of the diesel cycle, the proposed 2-zone model formulation allows for filling and emptying of the cylinder to be included in the simulation. Therefore, simulation of the complete diesel cycle is possible - simplifying integration in a complete diesel engine model. Conservation equations and the equation of state (EoS) are separated, so different EoS can be applied.

1.2. Research question

The proposed thesis investigates the possibility to include emission prediction capability in a mean value first principle (MVFP) DE-model based on (manufacturers) engine data and measured performance data. The choice of a MVFP DE-model for emission prediction is not the most obvious for emission prediction, as will be explained in the next sections. However, it would allow for emission prediction in existing DE-models used for system simulation. The aim is to avoid the necessity of specialized (expensive) measurement equipment and rely solely/mainly on build in sensors and widely available maintenance equipment (such as pV-measurement). Validation is seen as a built-in part of model development and necessity to asses the accuracy of the proposed model. The diesel engine located at the research facility of the Netherlands Defense Academy (NLDA) will be used for validation.

Given the relevance of NO-emissions, a good prediction tool would be useful. Hohlbaum has suggested a model approach to predict NO emissions and claimed pretty good agreement between simulated and measured results [18]. The inclusion of gas properties by means of an equation of state can be an opportunity to reduce the uncertainty with respect to the air flow passing the flame front in the original model.
Where Hohlbaum looks at mass and enthalpy, the proposed model will include pressure, volume and gas properties in order to gain more information.

The research question is: *Can NO emissions be accurately predicted using a first principle two-zone simulation model, manufacturers engine data and (easily available) engine performance measurements?*

The following sub-questions are identified:

- Can all parameters in a two-zone first principle simulation model be uniquely determined using manufacturers data and performance measurements?
- Is a model formulation possible, which uses state parameters which are commonly used in models of other diesel engine components to allow implementation of the in-cylinder model with other diesel engine models?
- Can the conservation equations and the equation of state be separated in the model formulation? This allows to choose the most suitable gas property database based on simulation requirements.
- Is it possible to accurately predict NO emissions based on the relative simple assumptions in a two zone model formulation?

2 Literature

2.1. Introduction

This section will give an overview of the literature relevant for the proposed thesis work. A division of topics is based on the identified subtasks. Many of the subtasks relate to the processes occurring in the cylinder and are (closely) related. A subdivision based on the type of model would also be possible. Two types of approaches are most common: a division of the cylinder volume in zones or packages models.
The division of the cylinder in different zones in simplest form is a zero-dimensional model, in which only one zone (the cylinder volume) is considered. The state in the cylinder is represented by (spacial) averaged variables. Limited data on the distribution of state variables in the volume is available. On the other end of the spectrum are CFD models, which use a fine grid to calculate state variables in each point. The complex phenomena (turbulent flow and combustion) occurring in the cylinder and the need to solve (full) Navier-Stokes equations, result in relative long calculation times. In between these two extremes, different approaches are possible, mostly compromising in capturing relevant phenomena at sufficient accuracy and computational time.
Package models follow the injected fuel. The flow of fuel is divided in multiple packages (hence the name). Each package is followed from injection to complete combustion, while covering all relevant intermediate events, such as droplet breakup, evaporation and ignition.

The process in a diesel engine is intermittent. Air can flow into the cylinder from the moment the inlet valves open (IO) until the inlet valves close (IC). From the moment all valves are closed the cylinder content (fresh air and some residual gas) are compressed. Around the point where the piston reaches top dead center (TDC) fuel is injected (SOI - start of injection). After an ignition delay combustion starts (SOC - start of combustion). Just before the piston reaches bottom dead center (BDC) the exhaust valve opens (EO). In modern day (charged) engines a positive pressure ratio exists over the cylinder (pressure in the inlet receiver is higher than the pressure in the exhaust receiver). The positive pressure ratio over the cylinder allows the inlet valve to open before the exhaust valve closes (EC). This valve overlap creates a scavenge air flow through the cylinder. The two main advantages of scavenge air are the removal of most/more residual gas and cooling of the cylinder (especially the exhaust valves).
Rather than simulating the complete cycle (one complete revolution for a 2-stroke engine or two complete revolutions for a 4-stroke engine), combustion models often consider only the closed part of the cycle (from IC to EO). This reduces model complexity since the gas exchange is not included. Of course information regarding the state of the gas in the cylinder at IC is required as an input for the calculations/simulations (and still needs to be determined). A different take is not to calculate at crank-angle level, but represent the in-cylinder process by a theoretical process description. For a diesel engine the theoretical process is covered by the Seiliger process. This approach reduces calculation time about a factor 400 Schulten [24] and is more suitable when using a DE-model in a larger system model.

The intermittent nature of the process influences the elegance of some formulations. Where open systems are best described by an enthalpy formulation (state variables: enthalpy h and pressure p), closed systems are best described by a formulation based on internal energy (state variables: internal energy u and specific vol-

ume v). By considering the cylinder content as a mixture of ideal gasses, which is common practice, complexity reduces. The state variables (temperature T and pressure p) are related by the ideal gas law ($pV = mRT$), and enthalpy and internal energy are only temperature dependent (related by c_p and c_v, respectively).

Independent of the formulation, three conservation laws are valid: conservation of mass, conservation of energy and conservation of momentum. The conservation laws form the basis of any model, often supplemented with consecutive equations. Conservation of mass states that no mass is lost or created:

$$\frac{dm}{dt} = \sum_i \dot{m}_{in,i} - \sum_j \dot{m}_{out,j} \tag{2.1}$$

where m is the mass in the volume considered, and the $\dot{m}_{in}$ and $\dot{m}_{out}$ the flows into and out of the considered volume, respectively. So, the accumulated mass is the difference between in- and outflow. During combustion many reactions occur. The amount of different species can increase or decrease, but total mass remains conserved.
Conservation of energy states [20]:

$$\frac{d\overline{u}}{dt} = \frac{1}{\overline{\rho}V}\left(\sum_i (\dot{m}h)_{in} - \sum_j (\dot{m}h)_{out} + \dot{Q} - \dot{W}_s - p\frac{dV}{dt} - \overline{u\rho}\frac{dV}{dt} + \overline{u}V\frac{d\overline{\rho}}{dt}\right) \tag{2.2}$$

in which u is the internal energy, h the enthalpy, ρ the density, V the volume, $\dot{W}_s$ the shaft work (not present in a DE cylinder) and $\dot{Q}$ the heat flow to or from the volume (either gained from combustion or exchanged with the cylinder wall/head). The formulation stems from a lumped parameter model and uses average values, which are indicated by an over-line.
Looking at the individual terms on RHS, one notices: total energy of incoming and leaving flows is the product of mass flow and enthalpy. Adapting an ideal gas approach makes this only temperature dependent ($dh = c_p dT$). Addressing shaft work and heat flow later, three terms remain. Two partial derivatives to the volume, which is known based on geometry and rotational speed and one partial derivative to the average density. Next to the already defined state variable temperature T, a second state variable is required to uniquely define the systems state (thus far nothing is said regarding what is in the cylinder; in a system containing k components, $k-1$ relations for the composition are required). For an open system pressure p would be a suitable choice; for a closed system specific volume v is often adapted (a nice bonus is the simple relationship with density). Using an equation of state, all properties can be calculated based on the two state variables.
Two elements of equation 2 are not yet addressed. First, shaft work is not present in a cylinder. The work performed by the volume on its surroundings is captured in the pdV term. Secondly, the heat flow is more complex. In a DE heat is added through the combustion of fuel. The total heat added can be calculated using the lower heating value (LHV) of the fuel. In practice combustion will not be perfect, however combustion efficiency η_{comb} will be high($> 99\%$). Far more difficult to calculate or measure is the time dependent heat flow from combustion (heat flow as function of crank-angle). The combination of flow (injection and turbulent mixing) and reaction kinetics will largely determine this time dependent heat release. The next subsection will address this subject in more depth.

Also captured in the heat flux $\dot{Q}$ is the loss to the surroundings. In case of a DE the surroundings are the cylinder liner/wall, the piston crown and the cylinder head with valves and injectors. Generally, a combination of cooling water and oil provides cooling to the engine (air cooling is mainly seen in small petrol engines). Applying a simple/common heat transfer relationship $\dot{Q} = UA\Delta T$, immediately shows several difficulties. The overall heat transfer coefficient U comprises of convective and radiant heat transfer and conduction through the material. The first two are not easily determined and many theories exist (see section 2.4.5). The area A available for heat exchange is fluctuating, but can be calculated based on geometry and rotational speed (Stapersma also presents an average area that can be used Stapersma [28]). The temperature difference ΔT between the gasses and the walls shows spatial and temporal gradients. Gas temperatures are highly non-uniform, the cylinder liner is warmer in the top than in the bottom due to the time exposed to the hot gasses, and cylinder head and valves are for instance influenced by the gas flows (large difference between hot exhaust gasses and scavenge air (Stapersma [28])).

To conclude a rather long introduction, the process in a DE cylinder is covered by basic conservation laws,

but the complex phenomena inside the cylinder make calculations/simulations difficult and an astute set of assumptions/hypothesis is required.

2.2. Heat release rate

Where possible, nomenclature in this text is in line with the work of Stapersma. Two definitions are adapted from Stapersma [27]. The net apparent heat release rate (NAHRR) is the net heat as observed from the temperature and volume evolution:

$$\text{NAHRR} = \dot{Q}_{comb} - \dot{Q}_{loss} \overset{\text{ideal gas}}{=} mc_v \frac{dT}{dt} + p\frac{dV}{dt} \tag{2.3}$$

The NAHRR is easy to measure, but covers not all heat produced. The NAHRR is the combination or balance of heat produced and heat lost. No assumptions are made regarding the loss. The gross apparent heat release rate (GAHRR) takes this into account:

$$\text{GAHRR} = \dot{Q}_{comb} \overset{\text{ideal gas}}{=} mc_v \frac{dT}{dt} + p\frac{dV}{dt} + \dot{Q}_{loss} \tag{2.4}$$

The GAHRR is a combination of "measurable" quantities supplemented with a "model" for the losses and sensitive to an accurate estimate of the heat loss.

Two mathematical formulations of the heat release rate are presented in this section, the Vibe function and the polygon-hyperbola substitute heat release. Both are clearly described by Merker et al. [19] and a short description of that formulation is presented here. Based on reaction kinetics Vibe (1970) provided the relation for the heat release:

$$\frac{Q_f(\varphi)}{Q_{f,total}} = 1 - e^{-a\left(\frac{\varphi-\varphi_{SOC}}{\Delta\varphi_{CD}}\right)^{m+1}} \tag{2.5}$$

The total heat release is the product of fuel mass and lower heating value $Q_{f,total} = m_f LHV$, φ_{SOC} is the crank-angle at which combustion starts and $\Delta\varphi_{CD}$ the combustion duration (expressed in crank-angle). At the end of combustion (EOC) a certain amount of energy is released (or fuel burned). Therefore, the parameter a is set by the combustion efficiency η_{comb}:

$$\frac{Q_f(\varphi)}{Q_{f,total}}|_{\varphi=\varphi_{EOC}} \equiv \eta_{comb} = 1 - e^{a} \tag{2.6}$$

The heat release rate from the degree of crank-angle is:

$$\frac{dQ_f}{d\varphi} = Q_{f,total}\, a(m+1)\left(\frac{\varphi-\varphi_{SOC}}{\Delta\varphi_{CD}}\right)^{m} e^{-a\left(\frac{\varphi-\varphi_{SOC}}{\Delta\varphi_{CD}}\right)^{m+1}} \tag{2.7}$$

In general this non-linear single-Vibe model offers too little freedom in shaping the heat release; only the duration can be varied Stapersma [27]. The distinct shape of premixed combustion can certainly not be captured with a single/linear Vibe function. By superimposing two Vibe functions more freedom in created to shape the heat release rate. The parameter a is the same for both functions, representing the end of combustion. The sum of both functions is the total heat released. Introducing the normalized quantities defined by Stapersma [27]:

$$X \overset{\text{def}}{=} \frac{\text{nr of fuel molecules broken up}}{\text{initial nr of molecules}} = \frac{n_f^{comb}(t)}{n_{f,0}} = \frac{m_f^{comb}(t)}{m_{f,0}^{comb}} \tag{2.8}$$

where the index 0 denotes the total mass of fuel available for combustion. The non-dimensional time τ is introduced:

$$\tau \overset{\text{def}}{=} \frac{\text{time since begin of combustion}}{\text{total combustion time}} = \frac{t - t_{SOC}}{\Delta t_{comb}} = \frac{\varphi - \varphi_{SOC}}{\Delta\varphi_{CD}} \tag{2.9}$$

where the subscript *SOC* is used to indicate the start of combustion (in contrast to Stapersma, who uses the subscript 0 to denote the start time). The non-dimensional rate of combustion can now be defined as:

$$Z \overset{\text{def}}{=} \frac{dX}{d\tau} \tag{2.10}$$

With the non-dimensional quantities defined, the double Vibe can mathematical be expressed as:

$$X = b_1 X_1 + b_2 X_2 \tag{2.11}$$

where the sum of the weighting factors must be one ($b_1 + b_2 = 1$). Now both Vibe functions are modeled with their own shape parameter m_i, but with a shared combustion duration parameter a.

$$X = b_1 \left(1 - e^{-a\tau^{m_1+1}}\right) + b_2 \left(1 - e^{-a\tau^{m_2+1}}\right) \tag{2.12}$$

and

$$Z = b_1 a(m_1+1)\tau^{m_1} e^{-a\tau^{m_1+1}} + b_2 a(m_1+1)\tau^{m_2} e^{-a\tau^{m_2+1}} \tag{2.13}$$

The degree of combustion is again equal to $X_{end} = 1 - e^{-a} = \eta_{comb}$.

The double Vibe-function can be easily associated with the peaky premix combustion followed by diffusive combustion, as can be seen in Figure 2.1 (The figure is only illustrative; and not meant to give a quantitative comparison between Vibe- and polygon-hyperbola heat release functions). Using the same superposition principle, more Vibe-functions can be used for a better representation of the heat release. Mathematically formulated by Ding Yu as Ding [10]:

$$X = \sum_{k=1}^{n} b_k X_k = \sum_{k=1}^{n} b_k \left(1 - e^{-a\tau^{m_k+1}}\right) \tag{2.14}$$

An anti-causual model is developed by Ding [10], which allows to reconstruct the heat release from measured pV-data. Next to that the work presents an effective method to smoothen a measured pressure signal by using a multiple Vibe-function.

Another mathematical description of the heat release rate is the polygon-hyperbola substitute heat release.

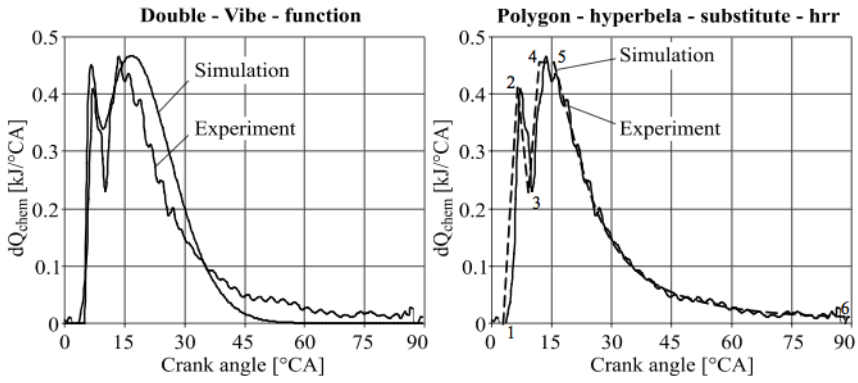

Figure 2.1: The double- Vibe function and polygon-hyperbola heat release rate (taken from Merker et al. [19])

Following the description given by Merker et al. [19], which describes the idea suggested by Schreiner (1993). A triangle, that serves in the description of premixed combustion, is superimposed on a polygonal port. The right part of Figure 2.1 shows an example and the definition of the different angles.

For the pre-mixed phase:

$$\frac{dQ_{f,pre}}{d\varphi} = y_2^* \frac{(\varphi - \varphi_1)}{(\varphi_2 - \varphi_1)} \qquad \text{with} \qquad \varphi_1 \le \varphi \le \varphi_2 \tag{2.15}$$

$$\frac{dQ_{f,pre}}{d\varphi} = y_2^* \frac{(\varphi_3 - \varphi)}{(\varphi_3 - \varphi_2)} \qquad \text{with} \qquad \varphi_2 \le \varphi \le \varphi_3 \tag{2.16}$$

For the diffusion phase:

$$\frac{dQ_{f,diff}}{d\varphi} = y_4 \frac{(\varphi-\varphi_1)}{(\varphi_4-\varphi_1)} \qquad \text{with} \qquad \varphi_1 \le \varphi \le \varphi_4 \tag{2.17}$$

$$\frac{dQ_{f,diff}}{d\varphi} = y_4 \qquad \text{with} \qquad \varphi_4 \le \varphi \le \varphi_5 \tag{2.18}$$

$$\begin{aligned}\frac{dQ_{f,diff}}{d\varphi} &= h_3 + h_1(\varphi-\varphi_1)^{h_2} \\ &= y_4 - \frac{y_4-y_6}{1-\left[\frac{\varphi_6-\varphi_1}{\varphi_5-\varphi_1}\right]^{h_2}} + \\ &+ \frac{y_4-y_6}{(\varphi_5-\varphi_6)^{h_2}-(\varphi_6-\varphi_1)^{h_2}}(\varphi-\varphi_1)^{h_2} \qquad \text{with} \qquad \varphi_5 \le \varphi \le \varphi_6\end{aligned} \tag{2.19}$$

For entire combustion:

$$\frac{dQ_{f,total}}{d\varphi} = \frac{dQ_{f,pre}}{d\varphi} + \frac{dQ_{f,diff}}{d\varphi} \tag{2.20}$$

The peak in the premix combustion is set by the parameter y_2^*. The parameters h_1, h_2 and h_3 define the parabola. The maximum height of the substitute heat release rate in the diffusion phase y_4 results from the condition that the center of the substitute heat release matches measurements. The quantity y_6 describes the conversion at the end of combustion.

So far, two mathematical descriptions for the heat release rate are presented. The models are purely em-

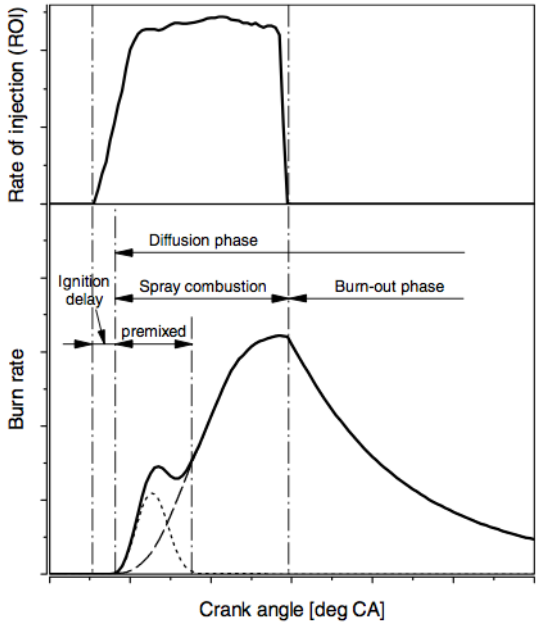

Figure 2.2: Sequence of combustion phases in a diesel engine (taken from Chmela et al. [8])

pirical and have no/little predictive capability. The multiple Vibe-method is preferred for this thesis, since the approach suggested by Ding [10] allows for smoothing a measured pressure signal and converting a measured pV-signal to the heat release rate. A drawback of this method can be inaccuracy in determining the location of TDC, which introduces uncertainty in the heat release rate.

A physics based model for ignition delay and premixed combustion, combined with diffusive combustion is developed by Chmela et al. [8]. The basis of this formulation are the rate equations formulated by Arrhe-

nius and Magnussen. The turbulence controlled rate equation by Magnussen is:

$$r_{Mag} = C_{Mag} c_R \frac{\sqrt{k}}{\sqrt[3]{V_{cyl}}} \tag{2.21}$$

where c_R is the concentration of the rate controlling species (fuel or air - depending on the AFR), k the turbulent kinetic energy and C_{Mag} a constant. The temperature controlled equation by Arrhenius is given by:

$$r_{Arr} = C_{Arr} c_F c_O e^{\frac{-k_2 T_a}{T}} \tag{2.22}$$

where c_F and c_O are the concentration of fuel and oxygen, T_a the activation energy and C_{Arr} and k_2 are constants. Ignition delay, pre-mixed combustion and diffusion combustion are modeled. Two stages are identified: the burning spray and the burn-out phase (injection stopped, but still fuel available for combustion). An overview of the combustion phases is presented in Figure 2.2. Radial distribution of fuel is determined using the spray cone angle and a certain penetration depth. Verification by Chmela et al. [8] shows good results. A drawback of the proposed method, is that spray angle and nozzle exit velocity are not assessed easy.

A different approach is taken by Tauzia et al. [30]. The method is based on the calculation of a representative mixing time τ_{mix}. The different phases identified are presented in Figure 2.3. In total three equations (for τ_i, P_1 and P_2) govern the evolution of the mixing time. The parameters of the equations are determined using a multi-linear regression method. The (relative large amount of) parameters (C, X, Y, Z, U, V and W) necessary, are different for each equation. For the two engines parametrized in their rapport, in each equation only one parameter differs (C) and all others are equal for both engines. Influence of the following parameters was taken into account: boost pressure, inlet air temperature, swirl, oxygen concentration at the inlet, injection timing, injection velocity, injection duration, injection nozzle area and engine speed and load.
Validation results against CFD-simulations and actual test engines are good. The rate of injection is an input to the model, which is not always accurately measured.

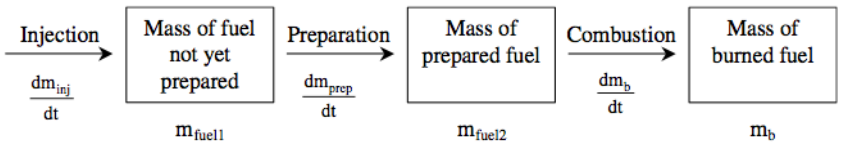

Figure 2.3: Model principle from Tauzia et al. [30] (taken from Tauzia et al. [30])

The concept of apparent combustion time (ACT) is used by Arrègle et al. [1] to form a link between injection rates and combustion. A parameter is sought that only relies on instantaneous cylinder conditions. In Figure 2.4 the definitions are introduced. The three zones are: (I) pre-mixed combustion phase, (II) diffusion combustion phase and (III) late combustion phase. Based on turbulent jet theory, the flame length (FL) and mixing time (t_{mix} - time required to reach stoichiometric conditions in the flame front) are calculated. The apparent combustion time is assumed to have the form: $\rho^a u_0^b [O_2]^c \phi^d$. Applying this to all packages of fuel, resulted in an expression for the ACT:

$$ACT(i) = K \left[\overline{\rho_a^{0.5} u_0 [O_2]^{0.5}} \phi_0^{-1} \right]_{POI(i) \rightarrow POC(i)}^{-1} \tag{2.23}$$

where ϕ is the nozzle diameter. Validation shows good agreement between simulations and measurements. The model shows how instantaneous parameters influence the heat release rate and only one parameter (K) is required for calibration. The model is further improved to also include the effects when the injection is finished Arrègle et al. [2].

Although a first principle approach is favored throughout this thesis, here a different philosophy is followed. The measured pV-signal will be converted into a heat release rate, using an anti-causal model proposed by Ding [10]. This means that in the model no information regarding the fuel spray and ignition delay is available and part of the predictive capability of the model is sacrificed. On the other hand pV-measurements can easily be performed on existing engines. Building a model that can predict emissions based on measurements is an objective. Therefore the advantage of not introducing parameters, which cannot be easily assessed, at the cost of some local information is accepted. So, pV-measurement is smoothed and converged to

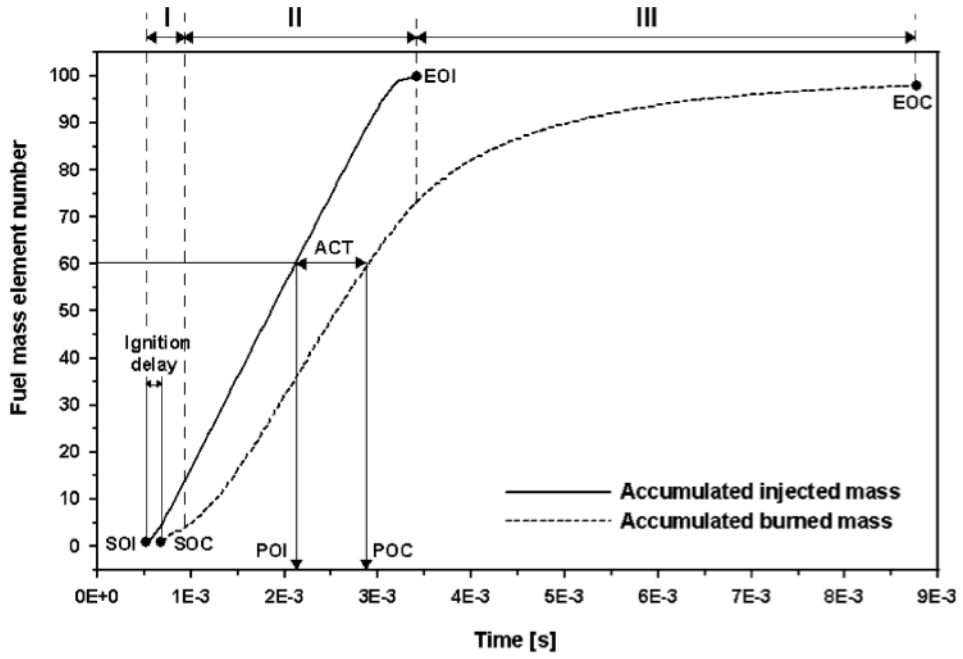

Figure 2.4: Parameter definitions for the ACT (taken from Arrègle et al. [1])

a (Vibe-function based) HRR using a single-zone MVFP model. The simulation model will not provide details regarding the fuel spray, but also no additional uncertainty is introduced by injection parameters.

2.3. Emission formation

Emissions can be categorized in different ways. The division based on origin from Stapersma [28] is followed here. Air related emissions come from species present in air, such as nitrogen (N_2) and argon (Ar). These species pass through the engine (almost) unchanged. For part of the oxygen (O_2) in the air this is also the case. Fuel related emissions come from the complete combustion of a fuel. Complete oxidation of hydrocarbons results in carbon dioxide (CO_2) and water (H_2O). Diesel fuel can also contain sulphur, resulting in sulphur trioxide (SO_3), or fuel bound nitrogen (FBN), resulting in nitrogen dioxide (NO_2). Water is the only product of complete combustions that is harmless. The last category is the cylinder process related emissions. These products result from incomplete combustion in the diesel engine process and comprise of carbon (C) normally called soot or smoke, carbon monoxide (CO), gaseous (unburned) hydrocarbons and particulate matter (PM). A class apart according to Stapersma [28] are nitrogen oxides (NO_x - comprising of nitrogen oxide(NO), nitrogen dioxide (NO_2) and nitrous oxide (N_2O)), since these are unintended combustion products. These products result from the (rather stable compared to FBN) nitrogen contained in air.

The formation of pollutants is mainly dependent on the air-fuel equivalence ratio and the temperature coupled with it Merker et al. [19]. A overview is presented in Figure 2.5.

2.3.1. Nitrous oxides

Nitric oxide can be formed via different mechanisms or routes that involve nitrogen from air: the thermal mechanisme, the prompt mechanism and the N_2O-intermediate mechanism Turns [31]. The reactions described in this subsection are from Turns [31].
Thermal NO is also often referred to as Zel'dovich NO, after Y.B. Zel'dovich who postulated the mechanism Warnatz et al. [33]. The activation energy of the mechanism is high (specially N.1 - 319050 kJ/kmol), therefore the reactions only occur at higher temperatures (as a rule of thumb the thermal mechanism is unimportant below 1800K). This is why a single zone model is not suitable for NO_X emission prediction, since average temperatures are substantially lower.

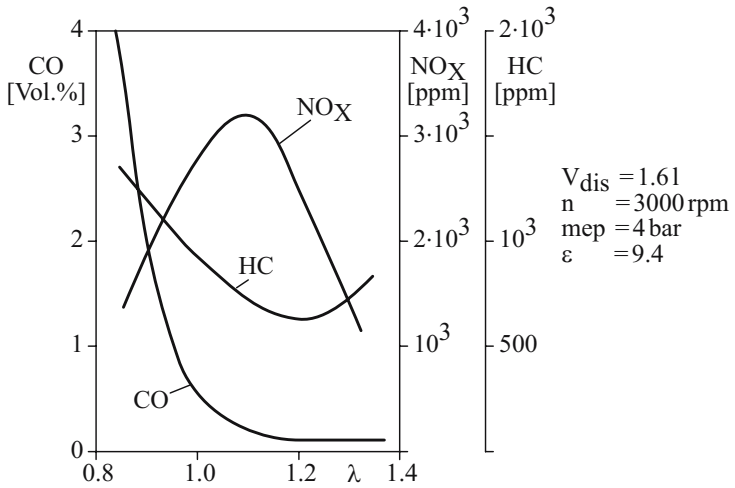

Figure 2.5: Pollutant formation contingent upon the equivalence ratio (taken from Merker et al. [19])

The Zel'dovich mechanism consists of two reactions Turns [31]:

$$O + N_2 \Longleftrightarrow NO + N \tag{N.1}$$

$$N + O_2 \Longleftrightarrow NO + O \tag{N.2}$$

which can also be extended by adding the reaction

$$N + OH \Longleftrightarrow NO + H \tag{N.3}$$

The three-reaction set is also referred to as the extended Zel'dovich mechanism. The process of combustion and the (extended) Zel'dovich mechanism can be uncoupled in processes where fuel combustion is completed before NO formation becomes significant. Further assuming NO concentrations to be much less than equilibrium concentration, allows for neglecting the reverse reactions. The rate equation simplifies to Turns [31]:

$$\frac{d[NO]}{dt} = 2k_{N,1f}[O]_{eq}[N_2]_{eq} \tag{2.24}$$

where $k_{N,1f}$ is the forward reaction coefficient of reaction N.1:

$$k_{N,1f} = 1.8 \cdot 10^{11} \exp\left[-38370/T(K)\right].$$

The mechanism of prompt or Fenimore NO was postulated by C.P. Fenimore (1979), who noted that the [NO] did not approach zero above a hydrocarbon flat flame as the probe approached the flame from the downstream side, as predicted by the Zel'dovich mechanism Warnatz et al. [33]. The general scheme of the Fenimore mechanism is that hydrocarbon radicals react with molecular nitrogen to form amines or cyano compounds. The amines and cyano compounds are then converted to intermediate compounds that ultimately form NO Turns [31]:

$$CH + N_2 \Longleftrightarrow HCN + N \tag{N.4}$$

$$C + N_2 \Longleftrightarrow CN + N \tag{N.5}$$

where (N.4) is the primary path and the rate limiting step. The following chain sequence is valid for equivalence ratios below 1.2. For richer mixture other routes open up and the chemistry involved becomes much more complex.

$$HCN + O \Longleftrightarrow NCO + H \tag{N.6}$$

$$NCO + H \Longleftrightarrow NH + CO \tag{N.7}$$

$$NH + H \Longleftrightarrow N + H_2 \tag{N.8}$$

$$N + OH \Longleftrightarrow NO + H \tag{N.9}$$

The reaction of CH with the nitrogen of the air, forming hydrocyanic acid (HCN), which reacts further to NO, is depicted in Figure 2.6. Although the reaction of FBN is shown, the kinetics are quite similar Warnatz et al. [33].

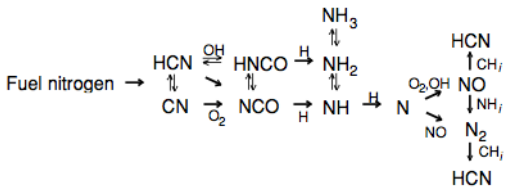

Figure 2.6: Reaction scheme for the NO production from fuel nitrogen (taken from Warnatz et al. [33] - original Glarborg et al. (1986))

The nitrous oxide (N_2O) -intermediate mechanism is important in fuel-lean low temperature conditions (mainly seen in gas turbines):

$$O + N_2 + M \Longleftrightarrow N_2O + M \tag{N.10}$$

$$H + N_2O \Longleftrightarrow NO + NH \tag{N.11}$$

$$O + N_2O \Longleftrightarrow NO + NO \tag{N.12}$$

where M may be any molecule and is frequently referred to as a third body. Lean conditions can suppress the formation of CH and, hence, lead to less Fenimore NO and low temperatures suppress the Zel'dovich NO. These circumstances lead to the N_2O route being the major source of NO formation Warnatz et al. [33]. For combustion in a diesel engine, these circumstances are not likely to occur.

2.3.2. Unburned hydrocarbons

The chemistry involved with the formation of unburned hydrocarbons in diesel engines is complex. The following sources are the most important for HC formation in a diesel engine Merker et al. [19]: at the periphery of the spray the mixture composition lies outside the ignition area (too lean); at the inner spray area the mixture composition is too rich; extinguishment of the diffusion flame by rapid pressure and temperature decreases during expansion; the fuel adhering to the wall is not completely oxidized due to insufficient temperature; and "after-injection" due to renewed opening of the nozzle needle after injection finish (from this result extremely large fuel drops, which can only evaporate and combust slowly).

2.3.3. Soot

It is widely accepted that the further growth of polycyclic aromatic hydrocarbons (PAH) leads to the formation of soot Merker et al. [19]. An overview of soot formation models is given by Xi and Zhong [34] and presented in Figure 2.7. A simple model of soot formation is given by Nishida and Hiroyasu (1989). Both the formation and oxidation of soot are modeled with an empirical formulation. The amount of soot is the difference between formation and oxidation Merker et al. [19]

$$\frac{dm_{P,f}}{dt} = A_f m_{f,g} p^{0.5} \exp\left[-\frac{6.313}{T}\right] \tag{2.25}$$

$$\frac{dm_{P,ox}}{dt} = A_{xo} m_P x_{O_2} p^{1.8} \exp\left[-\frac{7.070}{T}\right] \tag{2.26}$$

Name	Content	Variables solved	Chemistry model	Reference
Hiroyasu's model (1983)	$\frac{dm_s}{dt} = \left(\frac{dm_s}{dt}\right)_{formation} - \left(\frac{dm_s}{dt}\right)_{oxidation}$	Mass of soot	Equilibrium	[63–67]
Moss' model (1988, 1994)	$\frac{d}{dt}\left(\frac{f_N}{N_A}\right) = \left(\dot{W}_{f_N}\right)_{nucleation} - \left(\dot{W}_{f_N}\right)_{coagulation}$ $\rho_s \frac{df_V}{dt} = \left(\dot{W}_{f_V}\right)_{growth} + \left(\dot{W}_{f_V}\right)_{nucleation} - \left(\dot{W}_{f_V}\right)_{oxidation}$	Soot volume fraction and particle number density	Flamelet library	[70]
Tesner's model (1971)	$\frac{dn}{dt} = n_0 + (f-g)n - g_0 Nn$ $\frac{dn}{dt} = (a - bN)n$	Concentration of radical nuclei and soot particles	–	[72–77]
Lindstedt's model (1994)	1. Soot inception: $C_2H_2 \xrightarrow{\dot{R}_{1,1}} 2C_s + H_2$ $C_6H_6 \xrightarrow{\dot{R}_{1,2}} 6C_s + 3H_2$ 2. Soot mass growth: $C_2H_2 + nC_s \xrightarrow{\dot{R}_2} (n+2)C_s + H_2$ 3. Soot oxidation: $C_s + \frac{1}{2}O_2 \xrightarrow{\dot{R}_3} CO$ 4. Particle coagulation: $nC_s \xrightarrow{\dot{R}_4} (n)C_s$	Soot mass fraction and particle number density	292 step kinetics	[79–82]
Detailed models (1990)	Detailed PAH kinetics and soot particle dynamics	Species mass fractions; soot number, size and volume fraction	Detailed kinetics of acetylene pyrolysis; PAH growth	[84–91]

1) m_s is the soot mass; 2) f_N is the soot number density, f_V is the soot volume fraction, ρ_s is the density of soot particles (assumed to be 1800 kg/m^3). N_A is Avogadro's number ($6.023 \cdot 10^{23}$ mol^{-1}); 3) n and N are the number densities of radical nuclei and soot particles, respectively. f and g are branching and termination coefficients, respectively. g_0 is the rate of loss of nuclei due to collisions with soot particles, and a and b are the rate coefficients.

Figure 2.7: Overview of published models of diesel soot formation (taken from Xi and Zhong [34])

$$\frac{dm_P}{dt} = \frac{dm_{P,f}}{dt} - \frac{dm_{P,ox}}{dt} \tag{2.27}$$

The model is adapted by Lipkea and DeJoode (1994) and incorporated in the two-zone combustion model proposed by Rakopoulos et al. [22]. Effects that are presumed to influence soot formation, such as (turbulent) mixing rates and the availability of free radicals are not taken into account in this formulation. More detailed (CFD) simulations (e.g., Cheng et al. [7] with 70 species and 313 reactions) improve understanding of the occurring phenomena, however effort is still necessary in order to understand fundamental aspects of particle formation and oxidation to an adequate extent Merker et al. [19]. Other ways to predict soot emissions to a good accuracy based on measurement, include the use of artificial neural networks (e.g., Ghazikhani and Mirzaii [14] or the use of non-linear autoregressive models with exogenous inputs (NLARX) (e.g., Deng et al. [9]).

2.4. In-cylinder models

As mentioned in the introduction, the in-cylinder process is mainly covered by the conservation equations. In this subsection the definition or division of the cylinder volume will be discussed. After that, some theories for the calculation of heat loss and friction will be presented.

2.4.1. Single zone models

In a single zone model, the cylinder volume is treated as one zone. Parameters are spatial averages which represent the state within the cylinder. The volume occupied by liquid fuel is neglected, since it is in general very small. The heat released by combustion is modeled using a method described in section 2.2. An example of such a model can be found in Ding [10], where the implementation is clearly described. Merker and colleagues also present a brief but thorough single zone model Merker et al. [19].

2.4.2. Two zone models

In this subsection two two-zone models will be briefly described based on Merker et al. [19]. For further information the original text from Merker and colleagues or the summery by Galindo Lopez [13] is recommended.

Hohlbaum divides the cylinder volume in two zones: (I) contains only unburned mixture (fuel and air) and (II) contains incompletely oxidized fuel. In zone 2 secondary oxidation takes place for which reaction kinetic models are required. NO formation occurs in zone 2 following the Zel'dovich mechanism. The pressure is assumed to be the same in both zones (which hardly introduces any error given the speed of sound at the expected pressure inside a cylinder). The two zones are separated by a flame front, which has no mass and is infinitesimal thin. Primary oxidation takes place in the flame front until OHC-equilibrium. Air is allowed to go from zone 1 to zone 2. A drawback according to Merker et al. [19] is the lack of physical depth of the model. Therefore the model requires more or less arbitrary assumptions regarding the development of the AFR in different zones and the ratio of heat loss of the two zones.

Another way to define the zones is suggested by Heider. In the reaction zone (I) the energy conversion takes place. The air fuel ratio is assumed to be constant in this zone. The mass of this zone is fixed by the HRR. The remaining volume is represented by zone 2, which contains the remaining unburned mass. In case of the Heider model, results of a single zone model are required. An implementation of the Heider model is performed by Galindo Lopez [13]. In this work a third zone is introduced, which holds the liquid fuel (so fuel evaporation is also modeled). Three model parameters are introduced, which must be calibrated using a single zone model. Using only imep to calibrate the model parameters proved not to be sufficient. The three model parameters introduced are: λ_{ent} to account for the possibility that the composition of the bulk zone is not pure fresh air, S_{HH} defined as the quotient between the stoichiometric gas flow leaving the flame zone and the stoichiometric gas production rate, and S_{mass} defined as the ratio between the initial mass of the flame zone and the trapped mass at IC.

2.4.3. Multi-zone models

A variety of zones can be defined. In this section a six-zone model suggested by Xue and Caton [35] will be described. The choice to describe a six-zone model is quite arbitrary, but this model clearly shows advantage of multiple zones, without becoming overly complex. In Figure 2.8 the different zones and in Figure 2.9 the temporal evolution of the zones are given.
Zone 1 consist of liquid fuel and zone 2 consists of fuel vapor. Air is entrained from the bulk (zone 6). Auto-ignition begins to occur volumetrically throughout zone 3, where the air fuel ratio is around 0.25 - 0.5. Zone 4 contains fuel-rich combustion products, which begins to grow toward the injector and spray tip (the pre-ignition zone (zone 3) becomes smaller). Incomplete combustion products are generated at intermediate temperatures (1600 - 1800K). After the initially premixed combustion, a diffusion flame (zone 5) forms at the jet periphery. The model requires six empirical constants to be calibrated (4 ignition delay parameters, 1 parameter related to the lift-off length and 1 entrainment multipier). The simulation results agree well with measurements performed. However, the simulated HRR shows some deviation from the measured HRR.

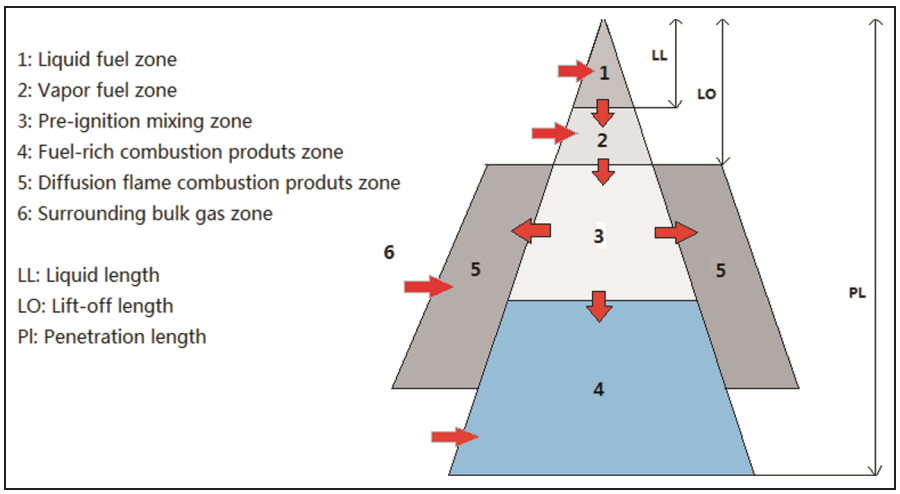

Figure 2.8: Schematic diagram of the zone description (taken from Xue and Caton [35])

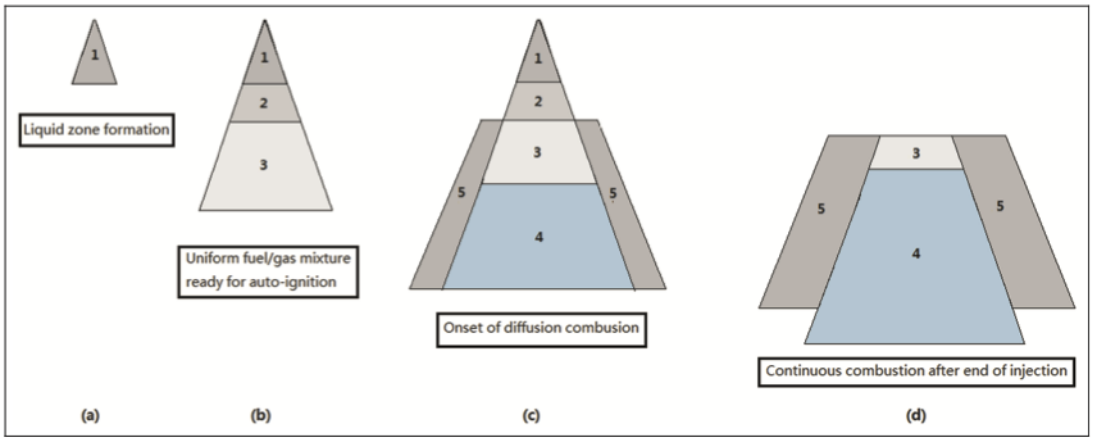

Figure 2.9: Temporal sequence of schematics showing the fuel spray jet evolution (taken from Xue and Caton [35])

2.4.4. Package models

A division of the cylinder can also be made based on the fuel injected. Next to the cylinder volume, the injected fuel is divided in packages (basically zones). Each fuel packages is followed from injection until completely burned (the existence of a package ends when package λ is equal to the bulk λ). Figure 2.10 displays the development of the diesel fuel jet. The number of packages chosen by Hernandez et al. [16] is 20, which

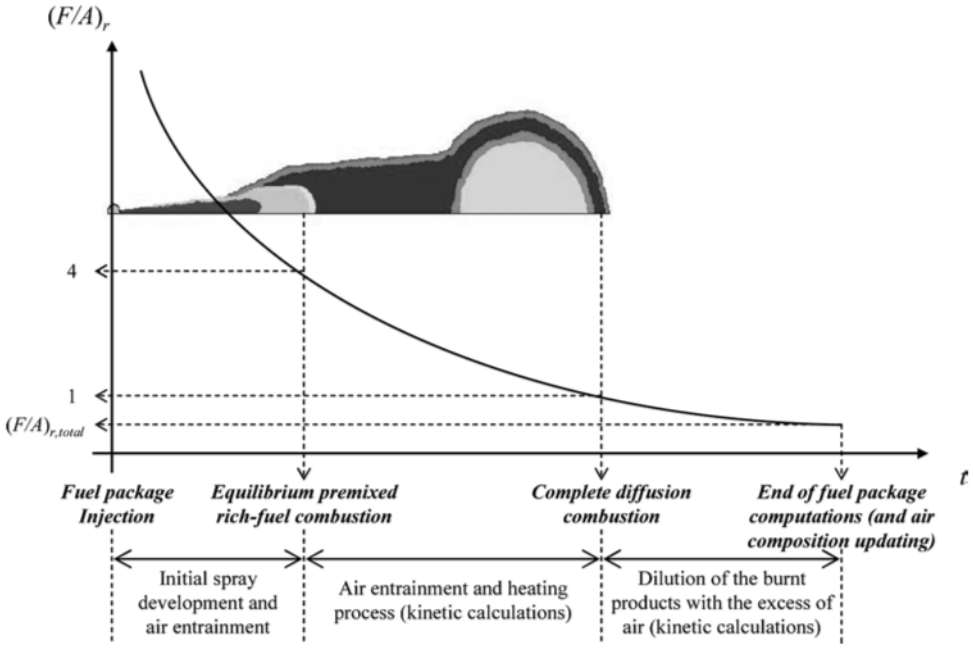

Figure 2.10: Development of the diesel fuel jet and different processes considered in the model (taken from Hernandez et al. [16])

is a trade-off between computational time and accuracy. NO-concentration varies significantly between the different packages. The model calculates the composition based on 27 species and 59 reactions. Agreement of the model with measurements is acceptable and the model has predictive capabilities for optimization. However, deviations occur at higher injection pressures.

For the development of a simulation model that predicts emissions, a formulation is favored with the least possible calibration parameters at sufficient accuracy. Although not all phenomena (such as spray de-

velopment) are captured in a two-zone model, sufficient detailed temperature and composition information is available for emission calculation. The small amount of calibration parameters makes a two-zone model most suitable for the modeling purpose.

2.4.5. Cooling and lubrication

Cooling and lubrication play an important role in diesel engine operation. The intermittent character of the diesel engine allows for high local temperatures (in excess of 2000K). Materials used in engines cannot cope with these temperatures and need cooling. The average cylinder wall temperature is around 500 - 600 K. During air intake, heat is released from the cylinder wall to the entering air (negative effect on specific power). During most part of compression and combustion, heat flow is out of the cylinder (loss). Heat transfer is influenced both by the changing area and the changing heat transfer coefficient. The cylinder wall shows a temperature gradient and the driving force (temperature gradient) fluctuates significantly within a cycle.

Part of the heat in the cylinder is released to the lubrication oil. This can be through the piston crown to the lub oil cooled underside of the crown or through the piston rings, through the lub oil film to the cylinder wall. Stapersma [28] gives an overview of the most common prediction methods for the heat transfer coefficient α in a cylinder: Sitkei [1962], Annand [1963] and Woschni [1964]. Woschni is applied on a crank-angle base for the 6 point Seiliger diagram [Stapersma, 2001]. Baldi et al. [5] uses the correlation proposed by Woschni to calculate the heat transfer coefficient and from that based on a constant wall temperature and an average cylinder temperature (from the internal energy of the fluid), the heat loss to the walls.

2.4.6. Mechanical losses

Mechanical losses in a diesel engine come from friction and mechanical driven pumps. The difference between the (thermodynamic) work done on all pistons and the work available from the crank shaft (or more common the break power), is the mechanical loss. In the DE-A3 model a 50-50% rule is applied. Meaning mechanical losses are matched at nominal/full-load condition and 50% of the losses is taken as a constant value and the other 50% linear with the engine rotational speed. The DE-B model uses Chen and Flyn to calculate mechanical losses. This empirical relation is dependent on both speed (mean piston $c_m \simeq n$) and the maximum cylinder pressure. Implementation in the DE-A4 model of Chen and Flyn is not easy, since maximum cylinder pressure is not known at pre-processing; therefore complicating the model. Difference between Chen and Flyn and the 50-50% approach seems little [Volbrandt, 2015].

2.4.7. Conclusions on model selection

The choice to use a two-zone model is made while formulating the research question. The objective is to have a first principle mean value simulation model able to predict NO-formation. Both Heider and Hohlbaum have suggested a model formulation to predict NO.
For this thesis the Hohlbaum formulation is preferred, since it does not require single-zone calculations as an input. The implementation of Galindo Lopez [13] showed that three additional parameters are required, which cannot be uniquely determined using the imep. Much of the predictive capability of the model is lost and NO_X measurements are required to fully calibrate the model. However, it might be possible to calibrate the parameters in the Heider formulation by using the full pressure signal instead of the (time-averaged) imep.
In this thesis the Hohlbaum formulation is favored over a Heider formulation. The modeling effort of Hohlbaum aims at predicting NO-emissions and the conclusion of his work is that the agreement between measured and calculated results is pretty good. The assumption of linearity for the air flow passing the flame front is identified by the author as a point to be improved, whereby a more physical base for the assumptions is desirable. By including the gas properties - based on an equation of state - in the model formulation, more knowledge regarding the size of each zone might be found. Knowing that the combined volume of both zones must be equal to the cylinder volume, might give a more accurate description of the air flow passing the flame front. A different path to explore can be to include the results of a single zone calculation in order to gain more insight in the flows in the two-zone model.

Temperature has significant influence on NO formation. Therefore, a model to calculate the heat flow from the gasses in the cylinder to the cylinder walls, crown and piston is required. Although Ding [10] experienced some trouble using the correlation proposed by Woschni, this is the preferred method, since many authors

used it with succes. In implementation the method of Woschni will be applied and if possible validated.

2.5. The gas path

2.5.1. Air flow

A diesel engine requires sufficient air to ensure good/full combustion. The air excess ratio λ is the ratio between the available air in the cylinder and the stoichiometric required amount of air. The air excess ratio influences the (quality of the) combustion process, the emissions and cylinder temperatures (a measure for mechanical loading and thus an indication of required maintenance). Quantitative correct modeling/prediction of the air flow (and thus the air excess ratio) is an important aspect of any diesel engine simulation model. The volume flow of air in a 4-stroke diesel engine is mainly determined by piston displacement (removing flue gas and 'sucking in' fresh air) and the pressure difference over the inlet and outlet receiver in combination with the valve overlap (scavenging). In a 2-stroke engine (not having an inlet and exhaust stroke) scavenging is dominant. The mass flow of air into the cylinder is determined by the volume flow and the inlet receiver / cylinder inlet conditions ($\rho = f(p,h)$) [This is correct for the piston displacement part; but not entirely sure if this is also true for scavenging - valve equation is mass flow based]. Turbo machinery is described in the next subsection and the cylinder process is already covered in the previous subsection. This section focusses on the modeling of all other components in the air flow path.

From inlet to cylinder the air comes through: the inlet filter, inlet duct, compressor, intercooler, inlet receiver and inlet valve opening. In the cylinder fuel is added and combustion takes place. On the way out the flue gas comes through: exhaust valve opening, exhaust receiver, turbine and silencer. The inlet filter results in a relative small pressure drop (general < 2%). The pressure drop can be modeled using a fixed value (this can also be zero, when it is neglected) or with a relation based on the valve equation ($\Delta p = f(\dot{m}^2)$).

The inlet duct can vary considerable in size depending on engine and application (e.g., Air Defense and Command Frigate (ADCF) with long ducts through several decks and an Ocean-going Patrol Vessel (OPV) with intake in the engine room (also different ambient conditions)). The inlet duct has some resistance, but this is often combined with the inlet filter resistance. Heat can be exchanged between air and surroundings, but in general heat exchange is small (since temperature differences are small). Dynamic effects can occur with load/speed changes, until a new equilibrium is found. The influence of the inlet duct on overall dynamic performance of a diesel engine is estimated to be small, since the pressure difference with the ambient is small.

The intercooler(s) main function is to cool the air after the compressor, increasing its density. The design of the cooler will result in flow resistance. Nowadays it is common to have a high temperature (HT) and low temperature (LT) cooling circuit in an engine. A cooler can be modeled using two flowing media and the area and overall heat transfer coefficient UA as matching parameter. An other option is to define the heat exchangers effectiveness ϵ.

The inlet receiver is a volume, which is usually located near hotter parts of the engine. This can result in some heat exchange. The temperature of the air at the trapped condition is not equal to the inlet receiver temperature (Stapersma [25]). Measuring the temperature of air leaving the inlet receiver is not easy, when the system boundary is at the inlet valve(s). During load or speed changes of the engine, this volume can play a role in the dynamic behavior of the engine. Friction in this volume is relative small (compared to the intercooler and the inlet valve(s)) and generally included in other parts of the model.

The inlet and exhaust valve are resistances in the flow. For a large part of the cycle the valves are fully closed. Opening is determined by the engine design (e.g. shape of the camshaft). In general there is some valve overlap, allowing for (positive) scavenging. In case there is no positive pressure difference over the engine, flue gas might flow back to the inlet receiver. This is an unwanted situation and in practice will not happen (often). Friction can be modeled with a valve-equation type of calculation. For crank-angle models the actual (time dependent) effective area is required. For mean value models a single effective area for scavenging can be calculated. The trapped mass is in that case calculated from the volume and trapped conditions (p, h). Both inlet and exhaust valve gain temperature during the closed part of the cycle and the exhaust valve even more from the flue gas flowing by. Cooling of the valves comes mainly from the flow of air (for exhaust valve only the scavenging air).

The outlet receiver shows many similarity with the inlet receiver. Heat transfer is from the flue gas to the surroundings. The conditions in the exhaust receiver can be determined by assuming 'Zinner-blowdown' (Stapersma [26]). Plug flow is then assumed from the cylinder to the exhaust receiver. Corrections for a pulse system can be included in the Zinner-blowdown.

The silencer will add a small resistance to the flow, which results in a small pressure drop. In case of flue gas cleaning systems, the pressure drop can be larger. Also dynamic aspects can play a role (fouling of filters will be on a very different time-scale compared to the other processes in the engine). Systems that make use of the heat in the flue gas, may as well increase the pressure drop.

2.5.2. Turbo machinery

Turbo machinery contributes to the diesel engine performance in two ways. The entering air is pressurized, increasing the air density and allowing for more fuel injection at constant air excess ratio. The specific power of the diesel engine is increased [at a small expense in efficiency]. The second contribution of turbo machinery to the diesel performance is creating a positive pressure difference over the cylinders. The resulting scavenging flow improves foul gas disposal from the cylinder and cools the exhaust valve.

The increase in pressure is developed by means of a compressor. The compressor can be driven by a turbine in the exhaust flue gas flow. The main advantage of such a system is that it runs on waste-energy. Performance is enhanced without a penalty on fuel consumption. This system is usually referred to as a turbocharger. The compressor can also be driven by power take off from the crank shaft. A mechanical coupling with a fixed transfer ratio is used, making the compressor speed proportional to the engine speed. This system is usually referred to as a supercharger. Since the system takes power from the engine, specific fuel consumption is increased (or efficiency decreased). Another option is to drive the compressor by an electric motor. Compressor speed can than be controlled independent from the engine speed. In 2-stroke engines at part-load an electric driven compressor is used to maintain a positive pressure difference over the engine (Stapersma [26]).

Most common in diesel engines is the turbocharger. All relevant phenomena (with exception of the electro motor) of the other configurations are included in this system. A disadvantage of a turbocharger is the performance at lower engine speed. To increase performance at lower speed nowadays more exotic configurations are used (e.i. sequential turbocharging, bleed-off, variable geometry).

The turbocharger can be modeled in different ways. The most familiar in name is the 'Buchi-equation' (DE A5-model), which gives a balance between turbine and compressor power. Manufacturers provide characteristics for compressors and turbines. The compressor and turbine characteristic relate (corrected) mass flow, (corrected) shaft speed, (corrected) power and the isentropic efficiency for compressor or turbine, respectively. In the model proposed by Baldi et al. [5] turbocharger speed and pressure ratio are considered inputs and corrected mass flow and isentropic efficiency are calculated by interpolation from a map. For both the compressor and turbine the torque is calculated using the enthalpy difference over the component. By integration of the difference in torque, the rotational speed of the turbocharger is calculated with the turbocharger inertia as time constant. Schulten [24] already proposed a similar approach for the compressor, using the performance map to determine the isentropic efficiency and volume flow from the pressure ratio over the compressor. A generic turbine map is used to model the turbine Under the assumption of Ideal Gas, the temperature and torque are calculated. The inlet pressure can also be calculated based on the energy in the exhaust gasses, using Q_{51} from the Seiliger formulation (DE A3-model). Recent measurements have shown that the Buchi-equation is more accurate than the formulation using Q_{51} Barsingerhorn et al. [6].

2.6. Relating crank-angle based models to MVFP DE-models

As mentioned before, mean value first principle models require less computational time than crank-angle based models, while still capturing most of the physical phenomena. Emission formation is large based on local quantities (AFR and temperature) and is not readily implemented in a MVFP DE-model. A combination of a MVFP and a crank-angle based model is proposed by Baldi et al. [5]. The model is a MVFP model supplemented with a crank-angle based single-zone model for the closest part of the cylinder process. Calculation time proved to be only slightly larger than a MVFP model, while accuracy was adequate.

A different approach is taken by Ding [10], who uses a crank-angle based model to determine the Seiliger parameters based on measurements. The fit of the Seiliger parameters can be done using different optimization criteria, resulting in a different (load/speed dependent) parameter definition. Although parameters are not uniquely defined, trends in the variation of Seiliger parameters at part-load emerge, increasing understanding of MVFP DE-models at part load.

A method of implementing NO_x emission in a mean value diesel engine model is presented by Asprion et al.

[3]. Both a polynomial look-up map is created based on an empirical NO_x formation model and a physics based NO_x formation model Asprion et al. [4] are used. Calculation times are in the order of magnitude of a MVFP DE-model and results are acceptable. Emission measurements are required for model calibration by means of a nonlinear minimization function based on the predicted NO_X formation. Although this method is physic based and also shows good results in dynamic operating conditions, a drawback is the requirement of NO_X emissions for model calibration.

2.7. Conclusions

In the introduction (Section 2.1) the basic conservation laws are introduced and the phenomena occurring in a diesel engine (DE) are described. Next, in Section 2.2 mathematical and physical based models to describe the heat release rate are presented. The HRR is seen as an intermediate description, that allows to use the output from measurements (pV-signal) as an input ($\dot{Q}$) for the model simulations. Therefore for the heat release rate, the first principle philosophy is abandoned. The two main advantages are that no physical parameters (which are not easily assessed) are introduced and it allows for smoothing the pressure signal (Ding [10]).
In Section 2.3 emission theory is presented. For NO_X formation the (extended) Zel'dovich method is most relevant given the temperatures and pressures in a diesel engine. For soot formation a formation-oxidation model can be used. A detailed description of soot formation requires much more complex models (CFD), which lie outside the scope of this thesis. The formation of SO_X and CO_2 will be tracked based on fuel properties and full conversion.
From the models presented in Section 2.4, a two-zone model is preferred. The advantage of a two-zone model is that sufficient accurate local temperature and composition information is produced at lowest possible increase in complexity. Furthermore the amount of parameters introduced is limited. The Hohlbaum description is favored over the Heider description, because no single-zone model is required and the Heider implementation proposed by Galindo Lopez [13] looses predictive capability because of the three additional parameters (which cannot be uniquely defined) introduced.
The gas path is described in Section 2.5. The purpose is to introduce the other phenomena occurring in a diesel engine and present the commonly seen modeling approaches.
Methods to relate a crank-angle model to a mean value first principle model are briefly introduced in Section 2.6. The aim is to relate emission to a theoretical cycle (Seiliger process), since this is the most common description in MVFP-models (used at DUT). Since this might very well not be possible to sufficient accuracy, implementation of a look-up map might provide an alternative.

3

Simulation model

3.1. Introduction

The developed simulation model consists of several sub-models. The model is a 2-zone representation of the combustion process in a diesel engine cylinder. A sketch of the system under consideration will be used to introduce state variables and heat- and mass-flows. Before describing the sub-models in more detail, the overall model-relations are presented. For each sub-model relevant phenomena, hypothesis, assumptions and model equations will be described, where possible accompanied by a short validation of the sub-model.

3.2. Model overview

3.2.1. Model aim

The aim of the model is to predict NO-emissions. The formation of NO is (mainly) determined by four factors: temperature, gas composition (in a diesel engine defined by the air excess ratio $\lambda(t)$), pressure and residence time. Residence time is a consequence of engine design and operating conditions, such as valve timing, injection profile and engine speed. Pressure is a measured variable (and of less influence). The composition of flue gas is a measured variable. The flue gas composition is a time averaged variable and gives no detail regarding the creation of destruction of species over time in the cylinder. Temperature is of relative large influence on NO-formation. The average cylinder temperature of a diesel engine - as calculated using a single zone model - is too low to adequately predict NO-formation. The two zones in a 2-zone model will have a different temperature and composition; one temperature being significantly lower than the other, where NO is formed. A good prediction of NO-formation requires a model that adequately predicts temperature and composition in the zone(s) where NO is formed. This explains the necessity of taking heat loss to the cylinder wall and crown and piston into account. Also modeling the fuel injection as a function of time is important. Crank-angle is generally used to define fuel injection and valve timing. As shown describing the piston movement both are closely related.

Two overviews of the cylinder volume are sketched in Figure 3.1. The left part shows a single zone model and the right part a 2-zone model. The choice of in-cylinder model/representation, does not affect the flows entering and leaving. The mass flow (of air) entering the cylinder f_E is determined by the pressure difference over the intake valve(s) and the valve position. The mass flow (of flue gas) leaving the cylinder f_L is determined by the exhaust valve position and the pressure difference over the valve. The heat loss to the cylinder crown and -walls and piston $\dot{Q}_{\text{loss,tot}}$ is driven by a temperature difference between the gas and the surface and the heat transfer coefficient. In case of the two zone model the heat loss is split into two; creating a loss in zone I $\dot{Q}_{\text{loss},I}$ and a loss in zone II $\dot{Q}_{\text{loss},II}$ (where $\dot{Q}_{\text{loss,tot}} = \dot{Q}_{\text{loss},I} + \dot{Q}_{\text{loss},II}$).

The gas in zone I has an enthalpy h_I and the gas in zone II an enthalpy h_{II}. Two mass flows are possible between zone I and zone II. The first flow f_F leaves zone I through the flame front. The flame front contains no mass. In the flame front primary combustion takes places and the equilibrium products enter zone II as $f_{\dot{F}}$. The mass flow entering zone II is slightly larger than the flow leaving zone I due to fuel addition in the flame front.

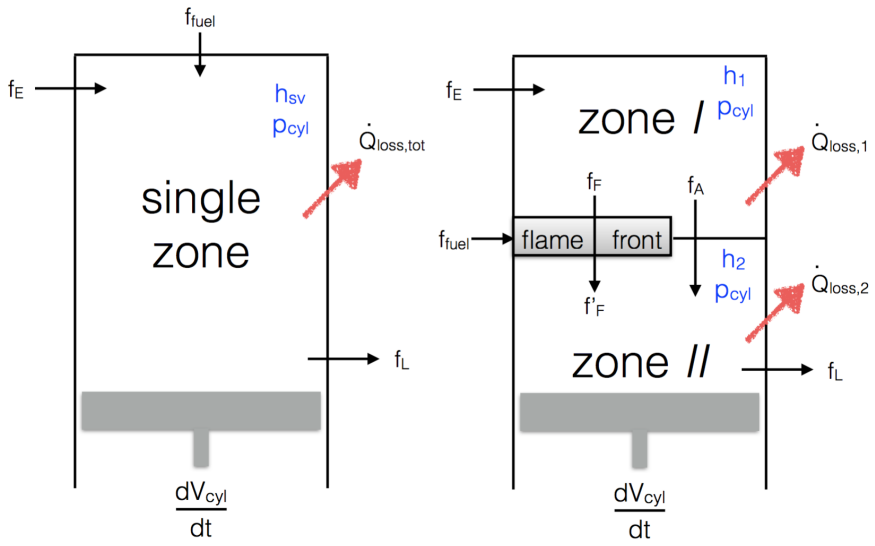

Figure 3.1: The state variables and mass- and heat flows in a single zone model (left) and in a 2-zone model (right)

The second flow f_A passes the flame front. This flow is not involved in the primary combustion process, but does influence the air excess ratio in zone II, where secondary combustion takes place.

3.2.2. Modeling considerations

A model is a representation of reality. Many models of diesel engines already exist, as is illustrated in the chapter literature overview. Differences in models can come from the assumptions and hypothesis. For each sub-model these wil be discussed in the next section, describing the sub-models. Another source of differences between models comes from the choice of state variables and the implementation of the equation of state.
The specific enthalpy is chosen as state variable. For a closed (control) volume, this might not be the obvious state variable. This choice is made based on two considerations. First, the diesel engine is not a closed system. Air flows continuously through the engine. Even a single cylinder is an open system part of the time. A formulation based on specific enthalpy resembles the formulation used in other parts of the engine, such as the compressor and turbine. Implementation in a total diesel engine model would be easier by an enthalpy based formulation. The model can be used to simulate the full engine cycle (i.e., 720 ° crank-angle).
The aim of this model is to predict NO-emissions. Formation of NO occurs during the closed part of the cylinder process. In this 2-zone model formulation the transfer of mass from zone I to zone II is regarded as a flow. An enthalpy based formulation enables this more easily.

The second modeling consideration is the strict separation of the conservation equations and the equation of state. The equation of state is implemented using FluidProp. All properties of the gas are calculated based on the three state variables specific enthalpy h, pressure p and composition y. The equation of state used is the Ideal Gas Law. Only in the derivation of the system of equations for the OHC-equilibrium the assumption of an Ideal Gas Mixture is made explicitly and marked with $\overset{\text{IGM}}{=}$.
The Ideal Gas approximation is common within diesel engine simulation models and holds well. The relative deviation is less than 6 % in the most unfavorable condition and less than 2 % in most realistic conditions in the cylinder (Stapersma [29]). Nonetheless, other equations of state are possible and might prove more accurate for the system under consideration. For a system containing hydrocarbons at elevated pressures, but not containing chloride an appropriate choice is Peng-Robinson or Soave-Redlich-Kwong with van der Waals one fluid mixing rules [23].

3.2.3. Zone definitions

The two zones in the model and flows between the zones are defined as suggested by Hohlbaum. zone I only contains fresh air. zone II initially has no volume or only a small volume containing air. zone I and zone II are separated by a flame front. The flame front itself is infinitesimal thin and contains no mass. Air from zone I and fuel enter the flame front. The amount of air that enters the flame front is determined by the fuel flow and the air fuel ratio. The air fuel ratio in the flame front is assumed to be constant and a tuning parameter of the model. Reaction in the flame front are relative fast. Chemical equilibrium between O, H, and C containing species is assumed to be instantaneously. Species in equilibrium are N_2, O_2, CO_2, H_2O, Ar, O, CO, H, H_2 and OH. This chemical equilibrium is referred to as OHC-equilibrium in this document. As suggested by Merker et al. [18] molecular nitrogen is assumed to be inert through the flame front. Therefore there will be no thermal or prompt NO formation in the flame front.
The air excess ratio λ in the flame front is smaller than unity and set to a value in accordance with premixed combustion $\lambda \simeq 0.7$, as suggested by Hohlbaum. The air excess ratio in the flame front is a tuning parameter for the model and will be varied during the matching of the model to measurements.
The choice of an air excess ratio smaller than unity results in incomplete combustion in the flame front. The mass flow of air entering the flame front from zone I f_F is smaller than the mass flow of OHC-equilibrium products entering zone II f_F'. Air and fuel convert adiabatically into combustion products at the adiabatic flame temperature. The heat required to evaporate the fuel is relative small and not taken into account. Therefore, the entering and leaving enthalpy are equal.

Air from zone I can also 'by-pass' the flame front and directly enter zone II. The mass flow of air from zone I to zone II is denoted f_A. The direct addition of air to zone II reflects the mixing of burned mixture and air introduced by diffusion and turbulence. The composition of zone II changes over time, due to the two incoming flows f_{fuel} and f_A. Zone II is assumed to be perfectly mixed and OHC-equilibrium achieved instantaneously. Due to the flow of air passing the flame front the air excess ratio in zone II is larger than the air excess ratio in the flame front. The combustion occurring in zone II is referred to as secondary combustion.

Two observations allow model simplification. First, the content of zone II is assumed to be perfectly mixed and an equilibrium condition between species is achieved immediately. This implies that the composition in zone II is based on pressure and enthalpy, which determine the temperature of which equilibrium-constants are a strongly dependent; and the number of O, H, C, N and Ar atoms in the volume. Equilibrium is based on what is in the zone and not the form in which it enters.
The second observation is that an adiabatic flame is assumed. This means no enthalpy change within the flame front. Therefore, no equilibrium calculations are required in the flame front. Specifying the amount of fuel and air that enters zone II and taking into account the heat loss in zone II is sufficient to calculate the equilibrium condition in zone II.

The air flow entering zone II consists of two parts. First, a part that is defined by the amount of fuel injected and the air excess ratio λ in the flame front. The second part of the air flow comes from the assumptions regarding the zones in the model. Assuming little mass in zone II at the start of combustion and (almost) all mass in zone II at the moment the exhaust valve opens, requires a mass flow from zone I to zone II. The mass flow passing the flame front is initially kept constant, as suggested by Hohlbaum.

The state of the gas in zone I is determined by the pressure p_{cyl}, the specific enthalpy h_1 and the composition y_1. The state of the gas in zone II is determined by the pressure p_{cyl}, the specific enthalpy h_2 and the composition y_2. The pressure p_{cyl} in zone I and zone II are equal.

3.2.4. Sub-models

Figure 3.2 gives an overview of the sub-models used. The two zones in the cylinder are formed by the sub-models labelled zone I and zone II. In each sub-model the volume, enthalpy and composition are calculated, based on the (measured) pressure, and flows leaving and entering each zone.
The mass flow of air f_E enters the cylinder from the inlet receiver. The composition of the entering flow y_E is determined by the air composition. The air flow enters zone I at an enthalpy h_E dictated by the inlet receiver temperature and heat pick-up from the inlet port. The pressure upon entering the cylinder is equal to the cylinder pressure (there is a pressure difference over the inlet valve).
Mass flow of flue gas f_L leaves the cylinder from zone II. The composition of this gas y_L is determined by OHC-equilibrium and NO-formation in zone II. The zones in the model are assumed to be perfectly mixed.

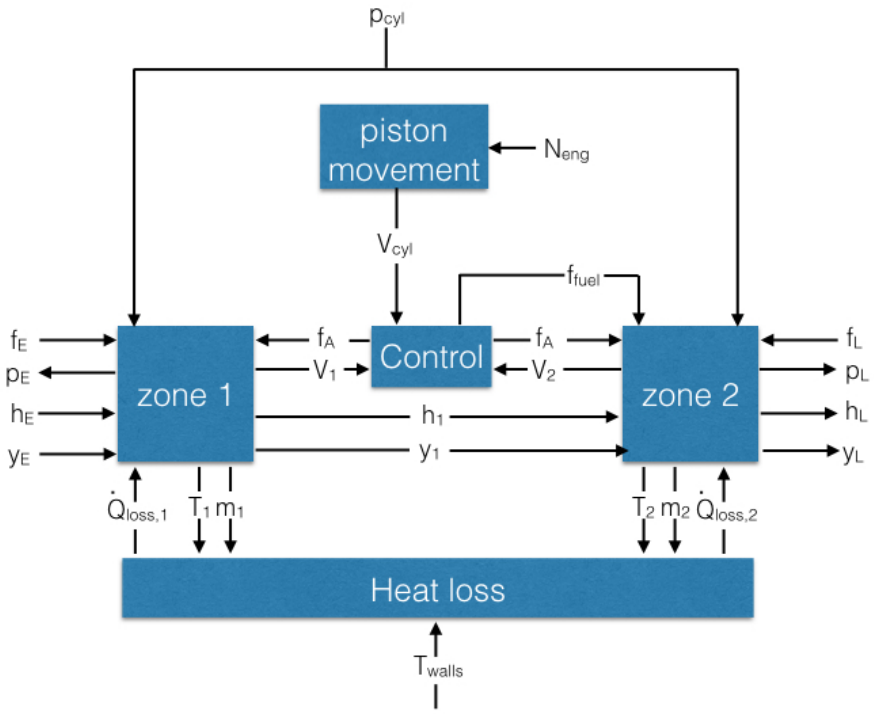

Figure 3.2: Overview of sub-models and the main variables in the model

The enthalpy of the leaving gas h_L is equal to the enthalpy of zone II. The pressure of the leaving gas is equal to the cylinder pressure (this is before the exhaust valve, which acts as an flow resistance).
During the closed part of the cylinder process, in which NO is formed, both the entering and leaving mass flow of air will be zero (i.e., inlet and exhaust valve are closed).
The cylinder volume V_{cyl} is calculated in the piston movement sub-model. The volume change is dictated by the fixed cylinder geometry and the engine speed N_{eng}. The combined volume of zone I and zone II must be equal to the cylinder volume. To achieve this, the amount of fuel added through the flame front, to zone II is controlled. When the combined volume of zone I and zone II is smaller than the cylinder volume, the fuel flow f_{fuel} is increased. A limit to this control mechanism is that the fuel flow cannot be negative. Therefore, an underestimation of the losses in the cylinder, will result in a difference between the cylinder volume and the combined volume of zone I and zone II.
Losses to the cylinder walls and -crown and piston are calculated in the heat loss sub-model. The empirical formulation from Woshni is used to calculate the heat transfer coefficient α_{HT}. To determine the ratio of heat loss between zone I and zone II the formulation proposed by Hohlbaum ($\frac{\dot{Q}_{\text{loss},1}}{\dot{Q}_{\text{loss},2}} = \left(\frac{m_1}{m_2}\right)^2 \frac{T_1}{T_2}$) is used.
The temperatures of the different surfaces serve as an input for the model, but are kept constant during the simulations.

3.3. Sub-model description

The sub-models for the volumes of zone I and zone II are volume elements. The composition of the gas in these volume elements is calculated in a composition sub-model. The sub-model interfacing zone I and zone II is a resistive model. The OHC-equilibrium sub-model is used in the single volume en zone II sub-model as well as in the flame front. The NO-formation model is used in the zone-2 sub-model.

3.3.1. Volume element - single phase storage module

Relevant phenomena, hypothesis and assumptions

The volume element contains a fluid in the gaseous fase. The composition of the gas can change, due to in- and outflow. Secondary combustion takes place in zone II and is represented by occurring reactions, which will also change the gas composition within the volume. Heat exchange between the volume and its surrounding is possible, as well as work by volume change.

The volume element can store mass, but has no flow resistance (the pressure is equal within the volume). Within the volume conservation of mass and conservation of energy are obeyed. The volume is assumed to be perfectly mixed. The (spatial) average value of the state parameters is assumed to give a good representation of the state of the gas.

Model equations

The model equations of the volume element are based on conservation of mass, the energy equation and specie balances. The derivation of model equations is in line with the suggestion made by P. Colonna [20]. An overbar represents a lumped (spacial averaged) parameter.

Conservation of mass

The average density in a volume is given by:

$$\overline{\rho} = \frac{m}{V} \tag{3.1}$$

Conservation of mass within the cylinder dictates that the difference between incoming and leaving mass flows is accumulated within the volume.

$$\frac{dm}{dt} = f_{\text{in}} - f_{\text{out}} \tag{3.2}$$

where m is the mass within the volume, f_{in} and f_{out} the entering and leaving mass flow, respectively.

$$\frac{dm}{dt} = \frac{d\overline{\rho}V}{dt} = \frac{d\overline{\rho}}{dt}V + \overline{\rho}\frac{dV}{dt} \tag{3.3}$$

Combining equation 3.2 and 3.3 gives an expression for the rate of change of average density:

$$\frac{d\overline{\rho}}{dt} = \frac{1}{V}\left[f_{\text{in}} - f_{\text{out}} - \overline{\rho}\frac{dV}{dt}\right] \tag{3.4}$$

The state variables are specific enthalpy and pressure, therefore $\rho = f(h,p)$. The composition in a volume (and therefore total number of moles) can change, due to the occurring chemical reactions or in- and outflow, therefore $\rho = f(h,p,N_i)$. Within the volume elements the composition is tracked using the composition sub-model. The amount of each specie is calculated. The (change in) number of moles N_i of each species is used within the volume element, but the composition of the gas in terms of mole fraction y is the output variable used for interaction with other sub-models. The time rate change of density is:

$$\frac{d\rho}{dt} = \left(\frac{\delta\rho}{\delta h}\right)_{p,N_i}\frac{dh}{dt} + \left(\frac{\delta\rho}{\delta p}\right)_{h,N_i}\frac{dp}{dt} + \sum_{i=1}^{\mathcal{N}}\left(\frac{\delta\rho}{\delta N_i}\right)_{p,h,N_{j\neq i}} \tag{3.5}$$

for a system with $\mathcal{N}$ species. Introducing a symbol for all partial derivative terms on the RHS and applying the terms on the average volume properties:

$$\xi = \left(\frac{\delta\overline{\rho}}{\delta\overline{h}}\right)_{p,N_i} \tag{3.6}$$

$$\psi = \left(\frac{\delta\overline{\rho}}{\delta p}\right)_{\overline{h},N_i} \tag{3.7}$$

$$\chi = \left(\frac{\delta\overline{\rho}}{\delta N_i}\right)_{p,\overline{h}} \tag{3.8}$$

Combining both expressions for the rate change of (average) density results in a differential equation for the pressure (state parameter p):

$$\frac{dp}{dt} = \frac{1}{\psi}\left[\frac{1}{V}\left(f_{\text{in}} - f_{\text{out}} - \overline{\rho}(\overline{h}, p)\frac{dV}{dt}\right) - \xi\frac{d\overline{h}}{dt} - \chi\frac{dN_i}{dt}\right] \tag{3.9}$$

In the two zone model, the volume of the two zones (zone I and zone II) is unknown. based on conservation of mass an expression for the change in volume can be found:

$$\frac{dV}{dt} = \frac{1}{\overline{\rho}}\left(\left[f_{\text{in}} - f_{\text{out}}\right] - V\xi\frac{d\overline{h}}{dt} - V\psi\frac{dp}{dt} - V\chi\frac{dN_i}{dt}\right) \tag{3.10}$$

Conservation of energy

To find an expression for the change of enthalpy within the volume, the conservation of energy is used. The volume exchanges energy with its surroundings by means of mass flows entering and leaving the volume, heat exchange through walls, shaft work or compression work done on the gas.

$$\frac{dU}{dt} = f_{\text{in}}f_{\text{in}} - f_{\text{out}}f_{\text{out}} + \dot{Q} - \dot{W}_s - p\frac{dV}{dt} \tag{3.11}$$

The terms represent (from left to right): dU/dt: energy change in the volume; $f_{\text{in}}h_{\text{in}}$: inflowing enthalpy; $f_{\text{out}}h_{\text{out}}$: outflowing enthalpy; $\dot{Q}$: heat input; $\dot{W}_s$: shaft work and pdV/dt: work due to volume change.

Remembering that $\overline{u} = U/m$ and $H = U + pV$ gives:

$$U = m\overline{u} = m\left[\overline{h} - \frac{\overline{p}}{\overline{\rho}}\right] = \overline{\rho}V\left[\overline{h} - \frac{p}{\overline{\rho}}\right] = \overline{\rho}V\overline{h} - V\overline{p} \tag{3.12}$$

thus:

$$\frac{dU}{dt} = \frac{d\left(\overline{\rho}V\overline{h} - \overline{p}V\right)}{dt} = \frac{d\overline{\rho}}{dt}V\overline{h} - \overline{\rho}\overline{h}\frac{dV}{dt} + \overline{\rho}V\frac{d\overline{h}}{dt} - \overline{p}\frac{dV}{dt} - V\frac{dp}{dt} \tag{3.13}$$

Combining both equations for the energy change in the volume dU/dt gives:

$$f_{\text{in}}h_{\text{in}} - f_{\text{out}}h_{\text{out}} + \dot{Q} - \dot{W}_s - p\frac{dV}{dt} = V\overline{h}\frac{d\overline{\rho}}{dt} - \overline{\rho}h\frac{dV}{dt} + \overline{\rho}V\frac{d\overline{h}}{dt} - p\frac{dV}{dt} - V\frac{dp}{dt} \tag{3.14}$$

Rearranging to bring the change in enthalpy to LHS (the pdV/dt terms cancel out):

$$\overline{\rho}V\frac{d\overline{h}}{dt} = f_{\text{in}}h_{\text{in}} - f_{\text{out}}h_{\text{out}} + \dot{Q} - \dot{W}_s - V\overline{h}\frac{d\overline{\rho}}{dt} - \overline{\rho}\overline{h}\frac{dV}{dt} + V\frac{dp}{dt} \tag{3.15}$$

As done before, density is expressed as a function of the state variables pressure p and specific enthalpy h. The earlier defined partial derivatives ξ and ψ are used:

$$\overline{\rho}V\frac{d\overline{h}}{dt} = f_{\text{in}}h_{\text{in}} - f_{\text{out}}h_{\text{out}} + \dot{Q} - \dot{W}_s - V\overline{h}\left(\xi\frac{d\overline{h}}{dt} + \psi\frac{dp}{dt} + \chi\frac{dN_i}{dt}\right) - \overline{\rho}\overline{h}\frac{dV}{dt} + V\frac{dp}{dt} \tag{3.16}$$

Combining terms:

$$\left(\overline{\rho}V + V\overline{h}\xi\right)\frac{d\overline{h}}{dt} = f_{\text{in}}h_{\text{in}} - f_{\text{out}}h_{\text{out}} + \dot{Q} - \dot{W}_s - \left(V - V\overline{h}\psi\right)\frac{dp}{dt} - \overline{\rho}\overline{h}\frac{dV}{dt} - V\overline{h}\chi\frac{dN_i}{dt} \tag{3.17}$$

Resulting in an expression for the change in enthalpy:

$$\frac{d\overline{h}}{dt} = \frac{f_{\text{in}}h_{\text{in}} - f_{\text{out}}h_{\text{out}} + \dot{Q} - \dot{W}_s - V\left(1 - \overline{h}\psi\right)\frac{dp}{dt} - \overline{\rho}\overline{h}\frac{dV}{dt} - V\overline{h}\chi\frac{dN_i}{dt}}{V\left(\overline{\rho} + \overline{h}\xi\right)} \tag{3.18}$$

The following assumptions are made regarding the air flows:

- fresh air enters in zone I
- combustion products leave zone II
- mass transfer from zone I to zone II can be through the flame front (f_F) in which OHC-equilibrium is reached, and
- mass transfer from zone I to zone II can be passing the flame front (f_A - only air)

The expression for enthalpy can be calculated for both zones; each zone has its own temperature, but the pressure is assumed to be equal in both zones. For zone I:

$$\frac{d\overline{h}_I}{dt} = \frac{f_E h_E - f_F \overline{h}_I - f_A \overline{h}_I + \dot{Q}_{\text{loss},I} - V_I \left(1 - \overline{h_I}\psi_I\right)\frac{dp}{dt} - \overline{\rho}_I \overline{h}_I \frac{dV_I}{dt} - V_I \overline{h}_I \chi_I \frac{dN_{i,I}}{dt}}{V_I \left(\overline{\rho}_I + \overline{h}_I \xi_I\right)} \tag{3.19}$$

and for zone II:

$$\frac{d\overline{h}_{II}}{dt} = \frac{f_F' h_F^* + f_A \overline{h}_I - f_L \overline{h}_{II} + \dot{Q}_{\text{loss},II} - V_{II} \left(1 - \overline{h}_{II}\psi_{II}\right)\frac{dp}{dt} - \overline{\rho}_{II} \overline{h}_{II} \frac{dV_{II}}{dt} - V_{II} \overline{h}_{II} \chi_{II} \frac{dN_{i,II}}{dt}}{V_{II} \left(\overline{\rho}_{II} + \overline{h}_{II} \xi_{II}\right)} \tag{3.20}$$

The mass flow entering zone II through the flame front f_F' is calculated based on the amount of fuel entering the cylinder f_{fuel} and the model tuning parameter λ_F in the resistive element. The enthalpy of this flow h_F is based on the assumption of an adiabatic flame temperature and equal to the enthalpy in zone I $\overline{h}_I$. The amount of air passing the flame front f_A is also calculated in the resistive element. Losses are calculated in the heat loss model, based on the empirical Woschni formulation. The (change in) volume of zone I and zone II is calculated based on the flows and pressure in the resistive element.
The enthalpy of the single zone model is calculated using:

$$\frac{d\overline{h}_{SV}}{dt} = \frac{f_E h_E - f_L \overline{h}_{SV} + \dot{Q}_{\text{loss, tot}} - V\left(1 - \overline{h}_{SV}\psi_{SV}\right)\frac{dp}{dt} - \overline{\rho}_{SV} \overline{h}_{SV} \frac{dV}{dt} - V \overline{h}_{SV} \chi_{SV} \frac{dN_i}{dt}}{V\left(\overline{\rho}_{SV} + \overline{h}_{SV} \xi_{SV}\right)} \tag{3.21}$$

The change in leaving enthalpy is set equal to the change in average enthalpy ($\frac{dh_L}{dt} = \frac{d\overline{h}}{dt}$). This usually gives the most stable simulation result. For a diesel engine at the moment the exhaust valve opens, the leaving enthalpy is equal to the average enthalpy (mainly consisting of zone II at this point in time). Therefore this implies the cylinder is perfectly mixed.

The solving system of equations is:

$$\begin{aligned}
\frac{dV}{dt} &= \frac{1}{\overline{\rho}}\left(\left[f_{in} - f_{out}\right] - V\xi\frac{d\overline{h}}{dt} - V\psi\frac{dp}{dt} - V\chi\frac{dN_i}{dt}\right) \\
\frac{d\overline{h}}{dt} &= \frac{f_{in}\overline{h}_{in} - f_{out}\overline{h}_{out} + \dot{Q}_{\text{loss}} - V\left(1 - \overline{h}\psi\right)\frac{dp}{dt} - \overline{\rho}\overline{h}\frac{dV}{dt} - V\overline{h}\chi\frac{dN_i}{dt}}{V\left(\overline{\rho} + \overline{h}\xi\right)} \\
V &= \int \frac{dV}{dt}dt \\
\overline{h} &= \int \frac{d\overline{h}}{dt}dt \\
\xi &= \left(\frac{\delta\overline{\rho}}{\delta\overline{h}}\right)_{p,N_i} = f(p, \overline{h}, [N_1 ... N_{\mathcal{N}}]) \\
\psi &= \left(\frac{\delta\overline{\rho}}{\delta p}\right)_{\overline{h},N_i} = f(p, \overline{h}, [N_1 ... N_{\mathcal{N}}]) \\
\overline{\rho} &= f(p, \overline{h}, [N_1 ... N_{\mathcal{N}}]) \\
T &= f(p, \overline{h}, [N_1 ... N_{\mathcal{N}}]) \\
h_{out} &= \overline{h}
\end{aligned}$$

The specific inputs, outputs and parameters for zone I and zone II are presented in Table 3.1.

	zone 1	zone 2
flow entering	air from inlet receiver f_E	air from zone 1 f_A and fuel injected f_F
flow leaving	air to zone 2 f_A	air to exhaust receiver f_L
inputs	f_E (zero from IC to EO) h_E (based on IR conditions) f_A(based on assumption) $\dot{Q}_{\text{loss},I}$ (Woshni and Hohlbaum) p (from measurements) $\chi_I \frac{dN_{i,I}}{dt}$ (from composition submodel)	f_L (zero from IC to EO) f_A (based on assumption) f_F (controlled variable using $\frac{dV_I}{dt} + \frac{dV_{II}}{dt} = \frac{dV_{cyl}}{dt}$ $\dot{Q}_{\text{loss},II}$ (Woshni and Hohlbaum) p (from measurements) $\chi_{II} \frac{dN_{i,II}}{dt}$ (from composition submodel)
outputs	T_I	T_{II}
parameters		
initial conditions	V_I $\overline{h}_I$ $N_{i,I}$	V_{II} $\overline{h}_{II}$ $N_{i,II}$

Table 3.1: Overview of inputs, outputs and variables of the sub-models for zone I and II

Preliminary validation

In order to validate the volume element simulations are performed. The gas composition used is that of air, since it is well known and it is well approximated by ideal/perfect gas assumption. For now, the composition is kept constant. The FluidProp library 'Gasmix' is used, which applies an Ideal Gas EoS.

All qualitative checks of simulation results are satisfactory. Bringing more mass or heat into the volume, results in higher pressure and enthalpy. Removing gas from the volume at constant pressure, does not change the temperature of the gas in the volume. Reducing the volume, results in higher pressure and enthalpy.

Adiabatic compression

Over a simulation period of 10 s, the volume is reduced from $V(t=0) = 1m^3$ with a speed of $dV/dt = -0.05m^3s^{-1}$. The initial pressure is $p(t=0) = 2{\cdot}10^5 Pa$ and the initial enthalpy is $h(t=0) = 0Jkg^{-1}$ ($T = 386K$). The mass and heat flows are set to zero. The mass contained in the volume is $m = \frac{pV}{RT} = 1.81kg$, where $R_{air} = 287JK^{-1}kg^{-1}$. At the final volume $V(t=10s) = 0.5m^3$ the pressure can be estimated using $pV^n =$ constant, where $n = \gamma = 7/5$. The calculated final pressure is 5.28 bar and compares well with the simulated final pressure of 5.24 bar. The simulated final temperature of 506 K compares well with the final temperature calculated based on the ideal gas law of 508 K.

Heat addition at constant volume

Over a simulation time of 10 s, heat is added to the gas while maintaining the volume constant (at $1m^3$). The initial pressure is 1 bar. The expected change in temperature of the gas is $\frac{Q}{mc_{v,air}} = \frac{100}{0.90{\cdot}0.724} = 153K$. There is some deviation between the calculated final temperature of 539 K and the simulated temperature of 536 K. The reason lies in the perfect gas assumption in manual calculations combined with the value for the isochoric heat capacity obtained at the initial temperature (as a comparison: obtaining $c_{v,air}$ at the final temperature would result in a final (calculated) temperature of 534 K). Based on the Ideal Gas law calculated final pressure is 1.385 bar and simulated final pressure 1.389 bar.

Heat addition at constant pressure

Over a simulation time of 10 s, heat is added to the gas while maintaining the pressure constant (at $1bar$). The initial volume is $1m^3$. The expected change in temperature of the gas is $\frac{Q}{mc_{p,air}} = \frac{100}{0.90{\cdot}1.013} = 110K$. Again the calculated final temperature of 496 K and the simulated final temperature of 494 K show some deviation, but this is mainly due to the perfect gas assumption and the selection of the isobaric heat capacity at the initial temperature, while performing the manual calculation.

Comparison with Ding [10]

The volume change module is used to simulate the same engine as done by Ding (Ding [10]) (MAN). The simulated motored pressure is in the same order of magnitude as presented by Ding (75 bar vs 70 bar). The difference can be explained by the fact that heat loss is not yet simulated in the current model. Simulated

temperature (1020K) is also higher than the temperature presented by Ding (920K).

The heat input is also simulated for full load conditions of the MAN engine. Simulated peak pressure (90 bar) is slightly lower than the pressure presented by Ding (95 bar). However parameter estimation for the Vibe-function is very crude at this point and the medium considered is air.

3.3.2. Composition model

Relevant phenomena, hypothesis and assumptions

The composition tracked in the composition model by accounting the total number of each specie in a volume. The total number of mole can change by flow entering the volume, flow leaving the volume and by chemical reactions. Flows are defined by the mass flow f, the composition in mole fraction of each specie $y_i = \frac{N_i}{N_{\text{tot}}}$ and the specific enthalpy h.

A general overview of the composition model is presented in Figure 3.3. The occurring chemical reactions are designated secondary combustion (in the Figure 'sec. comb.') and are calculated using the OHC-equilibrium model. The secondary combustion process is the mixing of the incomplete combustion products with the air in zone II (which passed the flame front). The available oxygen will result in an (almost complete) combustion of the fuel. Reactants are removed from the volume and the reaction products are added to the volume. The reactions are assumed to occur instantaneous.

The change in density of the gas due to the chemical reaction is calculated based on the change in gas composition. The actual density during the closed part of the cycle is imposed by the trapped mass and the movement of the piston. The chemical reaction will have an effect on the pressure and enthalpy of the gas in the volume. The term $\frac{d\rho}{dt}$ connects the composition model to the volume element. In term, serve the pressure p and enthalpy h as inputs for the composition model, in order to calculate gas properties.

Figure 3.3 illustrates the situation in zone II. In zone I occurs no reaction. In the single volume there is no flame front and thus no change in density due to the reactions in the flame front. The reason that the change in density from reactions in the flame front is 'added' to those in zone II, lies in the assumption that the flame front holds no mass and has no volume. Changes in density cannot be accounted for there. The assumptions regarding the flame front, do not prevent that chemical conversion occurs which has a result on density, which must be accounted for. Since the reaction products enter zone II immediate, the change in density from the flame front is accounted for in zone II.

Model equations

The incoming and leaving mass flows are converted into molair flows:

$$\dot{N}_{i,k} = y_{i,k} \frac{f_k}{M_{k,\text{gas}}} \tag{3.22}$$

for the i-th specie in the k-th flow. The change in composition due to the occurring reaction is calculated in the OHC-equilibrium. The flows in zone I are $k = [f_E f_A]$ and in zone II $k = [f_{fuel}, f_A, f_L]$. The change in a specie due to a chemical reaction is:

$$\left.\frac{dN_i}{dt}\right|_{\text{reaction}} = K_{\text{reaction}} \left(N_{i,\text{OHC-equilibrium out}} - N_{i,\text{volume}}\right) \tag{3.23}$$

where $N_{i,\text{volume}}$ is the number of mole of the specie in the volume and $N_{i,\text{OHC-equilibrium out}}$ the number of mole of a specie from the OHC-equilibrium. The parameter K_{reaction} holds the dimension [1/s]. It can be interpreted as 'number of times the content of the cylinder passes through the OHC-equilibrium calculation per second'. The parameter is set to $K_{\text{reaction}} = 10^5$ [1/s].

The total number of mole of each specie is calculated using:

$$N_i = \int \left(\left.\frac{dN_i}{dt}\right|_{\text{reaction}} + \sum_{k=1}^{\mathscr{F}} \dot{N}_{i,k} \right) dt \tag{3.24}$$

for all the $\mathscr{F}$ flows entering and leaving the volume the volume.

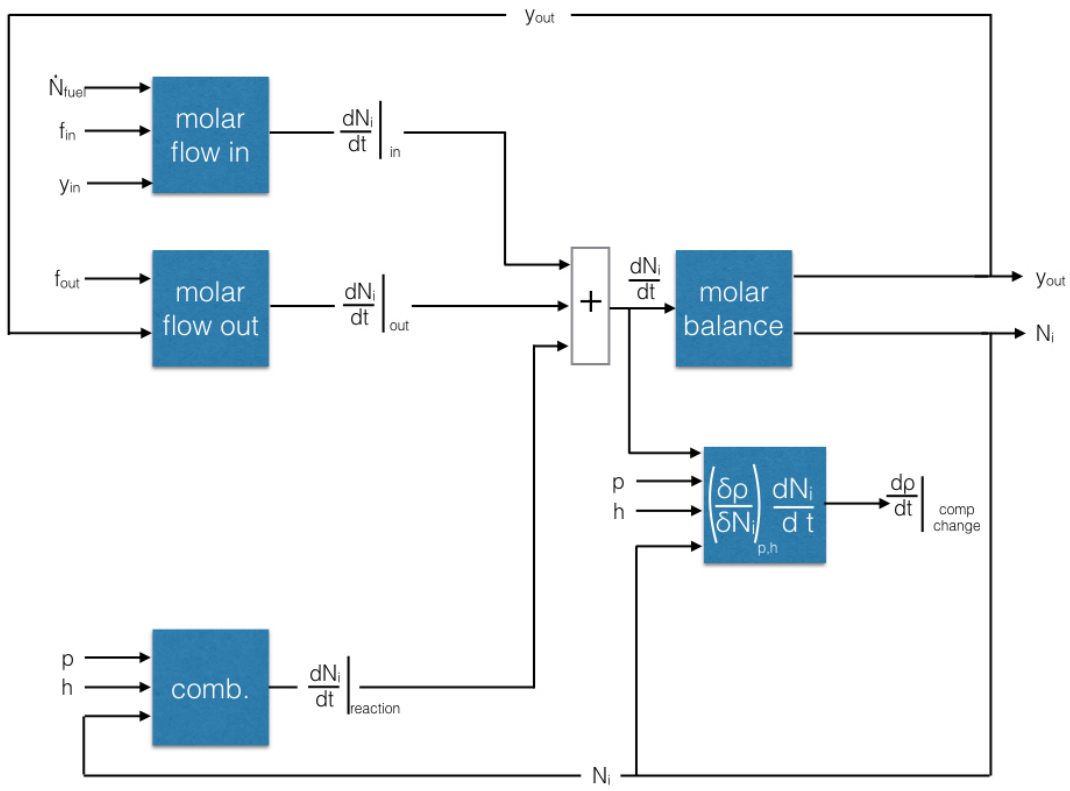

Figure 3.3: Overview of the composition change sub-model

The effect of a small change in the amount of one specie δN_i on the density is calculated while keeping the amount of the other species constant:

$$\left(\frac{\delta\rho}{\delta N_i}\right)_{p,h,N_{j\neq i}} = \frac{\rho\left(p,h,\frac{N_1}{N_{\text{tot}}+\delta N_i}\cdots\frac{N_i+\delta N_i}{N_{\text{tot}}+\delta N_i}\cdots\frac{N_{\mathcal{N}}}{dN_{\text{tot}}+\delta N_i}\right)-\rho\left(p,h,\frac{N_1}{N_{\text{tot}}}\cdots\frac{N_i}{N_{\text{tot}}}\cdots\frac{N_{\mathcal{N}}}{dN_{\text{tot}}}\right)}{\delta N_i} \tag{3.25}$$

where N_{tot} is the total amount of species in the volume. The change in density over time due to the reaction in the flame front and due to the OHC-equilibrium reaction in zone II is calculated using:

$$\left.\frac{d\rho}{dt}\right|_{\text{composition change}} = \sum_{i=1}^{\mathcal{N}}\left(\frac{\delta\rho}{\delta N_i}\right)_{p,h,N_{j\neq i}}\left[\left.\frac{dN_i}{dt}\right|_{\text{reaction}}+\left.\frac{dN_i}{dt}\right|_{\text{flow}}\right] \tag{3.26}$$

3.3.3. In-cylinder flows during combustiion

Relevant phenomena, hypothesis and assumptions

The cylinder volume is divided into two zones: zone I and zone II. The combined volume of both zone I and zone II should equal the cylinder volume. The amount of fuel injected is used as a controlled variable to accomplish this. When the combined volume of zone I and zone II are smaller than the cylinder volume, more fuel is injected.

The flow of air from zone I to zone II f_A is the combination of two assumptions:

1. Primary combustion occurs at an air excess ratio of $\lambda = 0.7$. This part of the air flow is directly dependent on the fuel flow into zone II.
2. At start of combustion (SOC) zone I contains (almost all) gas and zone II is (almost) empty. When the exhaust valve opens (EO) zone I is empty and zone II holds all gas. This part of the air flow is (for now) considered to be constant.

Model equations

The amount of fuel added is controlled based on the difference between the cylinder volume and the combined volume of zone I and zone II:

$$\dot{N}_{\text{fuel}} = \begin{cases} k_{FC}\left(V_I+V_{II}-V_{cyl}\right), & \text{if } V_{cyl}\geq V_I+V_{II} \\ 0, & \text{otherwise} \end{cases} \tag{3.27}$$

where k_{FC} is a gain, which controls the fuel flow. The amount of air accompanying the fuel through the fictional flame front at a certain air excess ratio λ is:

$$f_{A,FF} = C_{fuel}\cdot\lambda\dot{N}_{\text{fuel}} \tag{3.28}$$

where there is C_{fuel} kg of air required to burn 1 mole of fuel with the composition C_xH_y (for the fuel under consideration in this thesis (F-76): $C_{fuel} = 0.0706$ [kg air / mole fuel]). The total amount of air flowing from zone I to zone II is the flow associated with the flame front, combined with a flow of air bypassing the flame front $f_{A,\text{bypass}}$. The air flow bypassing the flame front is defined to meet the assumptions regarding the mass of zone I and zone II at SOC and EO.

$$f_A = f_{A,FF}+f_{A,\text{bypass}} \tag{3.29}$$

inputs	V_I, V_{II}, V_{cyl}
outputs	$\dot{N}_{\text{fuel}}$, f_A
parameters	k_{FC}, C_{fuel}, $f_{A,\text{bypass}}$
initial conditions	-

3.3.4. Piston movement model

Relevant phenomena, hypothesis and assumptions

The piston movement models is valid for a trunk piston engine. The movement of the piston is determined by the length of the crank and the connecting rod.

Model equations

The volume change is modeled according to Stapersma (Stapersma [27]). The ratio between the crank and the connection rod is defined as:

$$\lambda_{CR} = \frac{R_{CR}}{L_{CR}} = \frac{L_S/2}{L_{CR}} \tag{3.30}$$

The engine speed input is given in revolutions per minute (RPM), which is common in manufacturers documentation. The angular speed of the engine (in [rad/s]) is:

$$\frac{d\alpha}{dt} = 2\pi N_{eng}/60 \tag{3.31}$$

The stroke volume calculated using:

$$V_S = \pi \left(\frac{D_B}{2}\right)^2 L_S \tag{3.32}$$

The volume change is given by:

$$\frac{dV}{dt} = \frac{1}{2} V_S \left[\sin\alpha + \lambda_{CR}\left(\frac{\sin\alpha\cos\alpha}{\sqrt{1-\lambda_{CR}^2\sin^2\alpha}}\right)\right]\frac{d\alpha}{dt} \tag{3.33}$$

inputs	N_{eng}
outputs	$dV/dt, \alpha, d\alpha/dt$
parameters	L_S, L_{CR}, D_B
initial conditions	$\alpha(t=0)$

The solving system of equations is:

$$\frac{dV}{dt} = \frac{1}{2} V_S \left[\sin\alpha + \lambda_{CR}\left(\frac{\sin\alpha\cos\alpha}{\sqrt{1-\lambda_{CR}^2\sin^2\alpha}}\right)\right]\frac{d\alpha}{dt}$$
$$V_S = \pi \left(\frac{D_B}{2}\right)^2 L_S$$
$$\frac{d\alpha}{dt} = 2\pi N_{eng}/60$$
$$\lambda_{CR} = \frac{R_{CR}}{L_{CR}} = \frac{L_S/2}{L_{CR}}$$

3.3.5. Heat loss model

Model equations

The empirical formulation for the heat loss according to Woschni is implemented. The total heat loss is given by:

$$\dot{Q}_{loss} = \sum \alpha_{HT} A_i (T_{gas} - T_i) \tag{3.34}$$

where i represents the different parts of the engine (e.g., cylinder liner, piston and cylinder crown). Actual temperatures will be time variant and a gradient will be present. In the simulation, the wall temperatures are assumed to be constant and the average gas temperature is assumed to be representative in the calculation of heat losses. The work of Ding [10] is used as a reference for implementation. The heat transfer coefficient between gas and wall is given by:

$$\alpha_{HT} = C_1 \frac{1}{D_B^{0.214}} \frac{p^{0.786}}{T^{0.525}} \left(C_3 c_m + C_4 \frac{p - p_0}{p1} \frac{V_S}{V_1} T_1\right)^{0.786} \tag{3.35}$$

The suffix 0 denotes the 'no fuel' or motored condition and the suffix 1 represent the 'trapped condition' - i.e.,

the state at IC. The pressure in the empirical formulation is in [bar]. The coefficients in the model are:

$$C_1 = 130 \qquad \text{estimated by Ding} \tag{3.36}$$

$$C_3 = 6.18 + 0.417\frac{w_t}{c_m} \qquad \text{for the Gas Exchange} \tag{3.37}$$

$$C_3 = 2.28 + 0.308\frac{w_t}{c_m} \qquad \text{for compression and expansion} \tag{3.38}$$

$$C_4 = 0.00324\ [\text{m s}^{-1}\text{K}^{-1}] \qquad \text{for Direct Injection engines} \tag{3.39}$$

where the estimate of $w_t/c_m = 10$ for the MAN-engine at the NLDA is taken from Ding. The mean piston speed c_m is calculated using:

$$c_m = 2L_S N_{eng}/60 \tag{3.40}$$

with the engine speed N_{eng} in [RPM]. The stroke volume is calculated using the bore diameter D_B and the stroke length L_S.

inputs	p, T, p_{IR}, N_{eng}, α, valve position, A_i, T_i, T_{gas}
outputs	$\dot{Q}_{loss}$
parameters	D_B, L_S, V_1, T_1, C_1,w_t/c_m,C_4, $p_0 = f(p_{IR})$
initial conditions	-

In the 2-zone model a division is made between the loss in zone I and the loss in zone II. The solution proposed by Hohlbaum is adapted:

$$\frac{\dot{Q}_{\text{loss},1}}{\dot{Q}_{\text{loss},2}} = \left(\frac{m_1}{m_2}\right)^2 \frac{T_1}{T_2} \tag{3.41}$$

where the two flows equal the total heat loss $\dot{Q}_{\text{loss},1} + \dot{Q}_{\text{loss},2} = \dot{Q}_{\text{loss, tot}}$. Since the division in two flows does not influence the total amount of heat lost.

3.3.6. OHC-equilibrium

Relevant phenomena, hypothesis and assumptions

The OHC-equilibrium is reached fast (compared to other phenomena in the cylinder). The equilibrium condition is a function of temperature, pressure and initial composition. Elements included in the balance are: H_2, O_2, H_2O, CO_2, CO, OH and radicals H and O. The system does not contain any mass. The conversion of reactants to products is assumed to occur instantaneous. Inputs of the system are the pressure p, temperature T and composition. Parameters in the model are the air composition and the fuel composition. The output of the system is the composition of reaction products (either in mole-fraction or species mole number). The behavior of the gas can be accurately described by an ideal gas approximation.

Model equations

The five independent chemical reactions involved in the OHC-equilibrium are determined using the procedure proposed by Denbigh. The independent reactions are chosen in such a way that the equilibrium constant is given (as a function of temperature) in Sandler, table 13.1-2. The reactions are:

$$2O \Longleftrightarrow O_2 \tag{RXN.13}$$

$$2H \Longleftrightarrow H_2 \tag{RXN.14}$$

$$H_2 + \frac{1}{2}O_2 \Longleftrightarrow H_2O \tag{RXN.15}$$

$$CO + \frac{1}{2}O_2 \Longleftrightarrow CO_2 \tag{RXN.16}$$

$$OH + \frac{1}{2}H_2 \Longleftrightarrow H_2O \tag{RXN.17}$$

The incoming flows are air and fuel. Air is [for now, later include Argon and water] assumed to consist of oxygen O_2 and nitrogen N_2. Nitrogen does not participate in the reactions. Fuel is assumed [for now, later include sulphur] to be a combination of carbon and hydrogen C_xH_y. Fuel is decomposed to components in the OHC-system. The carbon is introduced in the system as carbon-monoxide CO, which is the carbon containing species with the lowest formation enthalpy in the system. The oxygen-atom required is coming from the oxygen O_2 in the air. The hydrogen from the fuel is introduced as a hydrogen radicals H.

The initial number of moles of oxygen, nitrogen and fuel are $N_{O_2,0}$, $N_{N_2,0}$ and $N_{C_xH_y,0}$, respectively. Reactions can occur both forward and reverse. The molar extend of reaction X_j (unit [mol]) is introduced for each independent chemical reaction. The stoichiometric coefficient for species i in the jth reaction is ν_{ij}. The number of moles of species i is than given by:

$$N_i = N_{i,0} + \sum_{j=1}^{\mathscr{M}} \nu_{ij} X_j \tag{3.42}$$

where the summation is over the set of $\mathscr{M}$ independent chemical reactions. The suffix 0 denotes the initial number of moles.

specie	Initial mole number	Final mole number
O_2	$N_{O_2,0} - \frac{1}{2}xN_{X_xH_y,0}$	$N_{O_2,0} - \frac{1}{2}xN_{X_xH_y,0} + X_1 - \frac{1}{2}X_3 - \frac{1}{2}X_4$
N_2	$N_{N_2,0}$	$N_{N_2,0}$
H_2O	0	$X_3 + X_5$
CO_2	0	X_4
O	0	$-2X_1$
H	$yN_{C_xH_y,0}$	$yN_{C_xH_y,0} - 2X_2$
H_2	0	$X_2 - X_3 - \frac{1}{2}X_5$
CO	$xN_{C_xH_y,0}$	$xN_{C_xH_y,0} - X_4$
OH	0	$-X_5$
Total		Σ

where Σ is the final total number of moles and is given by:

$$\Sigma = N_{O_2,0} + N_{N_2,0} + \frac{1}{2}xN_{C_xH_y,0} + yN_{C_xH_y,0} - X_1 - X_2 - \frac{1}{2}X_3 - \frac{1}{2}X_4 - \frac{1}{2}X_5$$

The number of moles of a specie cannot be negative ($N_i \geq 0$), resulting in the following restrictions to the molar extend of reaction:

$$\begin{aligned}
X_3 + X_5 &\geq 0 && \text{since} && N_{H_2O} \geq 0 \\
X_4 &\geq 0 && \text{since} && N_{CO_2} \geq 0 \\
X_1 &\leq 0 && \text{since} && N_O \geq 0 \\
2X_2 &\leq yN_{C_xH_y,0} && \text{since} && N_H \geq 0 \\
X_2 - X_3 - \tfrac{1}{2}X_5 &\geq 0 && \text{since} && N_{H_2} \geq 0 \\
X_4 &\leq xN_{C_xH_y,0} && \text{since} && N_{CO} \geq 0 \\
X_5 &\leq 0 && \text{since} && N_{OH} \geq 0 \\
X_1 - \tfrac{1}{2}X_3 - \tfrac{1}{2}X_4 + N_{O_2,0} + \tfrac{1}{2}xN_{C_xH_y,0} &\geq 0 && \text{since} && N_{O_2} \geq 0
\end{aligned}$$

The equilibrium constant $K_{a,i}$ is known for each of the independent chemical reactions as a function of temperature. The activity coefficient a_i is determined using the ideal gas mixture equation of state $a_i = \frac{y_i p}{p_{ref}}$. A more appropriate equation of state for elevated pressures for a vapor mixture that contains hydrocarbons, nitrogen, oxygen carbon dioxide and/or other inorganic gasses, is Peng-Robinson or Soave-Redlich-Kwong

with van der Waals one-fluid mixing rules ([23]).

$$K_{a,1} = \frac{a_{O_2}}{{a_O}^2} \overset{\text{IGM}}{=} \frac{y_{O_2}}{{y_O}^2}\frac{p_{\text{ref}}}{p} \tag{3.43a}$$

$$K_{a,2} = \frac{a_{H_2}}{{a_H}^2} \overset{\text{IGM}}{=} \frac{y_{H_2}}{{y_H}^2}\frac{p_{\text{ref}}}{p} \tag{3.43b}$$

$$K_{a,3} = \frac{a_{H_2O}}{a_{H_2}{a_{O_2}}^{\frac{1}{2}}} \overset{\text{IGM}}{=} \frac{y_{H_2O}}{y_{H_2}{y_{O_2}}^{\frac{1}{2}}}\left(\frac{p_{\text{ref}}}{p}\right)^{\frac{1}{2}} \tag{3.43c}$$

$$K_{a,4} = \frac{a_{CO_2}}{a_{CO}{a_{O_2}}^{\frac{1}{2}}} \overset{\text{IGM}}{=} \frac{y_{CO_2}}{y_{CO}{y_{O_2}}^{\frac{1}{2}}}\left(\frac{p_{\text{ref}}}{p}\right)^{\frac{1}{2}} \tag{3.43d}$$

$$K_{a,5} = \frac{a_{H_2O}}{a_{OH}{a_{H_2}}^{\frac{1}{2}}} \overset{\text{IGM}}{=} \frac{y_{H_2O}}{y_{OH}{y_{H_2}}^{\frac{1}{2}}}\left(\frac{p_{\text{ref}}}{p}\right)^{\frac{1}{2}} \tag{3.43e}$$

where $y_i = \frac{N_i}{\Sigma}$ and the reference pressure $p_{\text{ref}} = 1\text{bar}$. Expressed in the molar extent of reaction this gives:

$$\frac{y_{O_2}}{{y_O}^2} = \frac{N_{O_2,0} - \frac{1}{2}xN_{C_xH_y,0} + X_1 - \frac{1}{2}X_3 - \frac{1}{2}X_4}{4X_1^2}\Sigma \tag{3.44a}$$

$$\frac{y_{H_2}}{{y_H}^2} = \frac{X_2 - X_3 - \frac{1}{2}X_5}{(yN_{C_xH_y,0} - 2X_2)^2}\Sigma \tag{3.44b}$$

$$\frac{y_{H_2O}}{y_{H_2}{y_{O_2}}^{\frac{1}{2}}} = \frac{X_3 + X_5}{(X_2 - X_3 - \frac{1}{2}X_5)(N_{O_2,0} - \frac{1}{2}xN_{X_xH_y,0} + X_1 - \frac{1}{2}X_3 - \frac{1}{2}X_4)^{\frac{1}{2}}}\Sigma^{\frac{1}{2}} \tag{3.44c}$$

$$\frac{y_{CO_2}}{y_{CO}{y_{O_2}}^{\frac{1}{2}}} = \frac{X_4}{(xN_{C_xH_y,0} - X_4)(N_{O_2,0} - \frac{1}{2}xN_{X_xH_y,0} + X_1 - \frac{1}{2}X_3 - \frac{1}{2}X_4)^{\frac{1}{2}}}\Sigma^{\frac{1}{2}} \tag{3.44d}$$

$$\frac{y_{H_2O}}{y_{OH}{y_{H_2}}^{\frac{1}{2}}} = \frac{X_3 + X_5}{(-X_5)(X_2 - X_3 - \frac{1}{2}X_5)^{\frac{1}{2}}}\Sigma^{\frac{1}{2}} \tag{3.44e}$$

The sets of equations 2 and 3 can (theoretical) be solved for the 5 unknown in the system ($[X_1 ... X_5]$), obeying the boundaries for the variables. First [based on the recommendation from docent numerieke wiskunde NLDA) a standard Matlab solver is used. The problem is reformulated to a minimum search, since Matlab does not contain a constrained zero-finding algorithm.

$$\epsilon_{\text{tot}} = \sum_{j=1}^{5} {\epsilon_j}^2 \tag{3.45}$$

where ϵ_j is the difference between the LHS and RHS for the j-th equation in the set of equations [2].

Satisfying solutions are only found at higher temperatures. For lower temperatures, the constrained minimum search does not find a minimum near zero. Investigating the system of equations at low temperature ($T = 1300\text{K}$), shows that the equilibrium constants are large. There will hardly be any O or H radicals, since Ka is in the order of magnitude of 10^{13} and 10^{11} for reactions 1 and 2, respectively. The other three equilibrium constants are significantly smaller ($\approx 10^7$), but still (very) large. Since the equilibrium constants are the same order of magnitude, their influence on the equilibrium-point will more or less be equal. The definition of the error ϵ_{tot} implies that a small deviation from the equilibrium point, results in an error several orders of magnitude larger than the optimum. Even a small/the smallest possible step-size in the variables $[X_1 ... X_5]$ does not guaranty a satisfying solution. More over, since the error at a small deviation from equilibrium becomes large, no quantitive measure for the accuracy of the solution is available. Therefore this approach is not deemed suitable for the problem at hand.

A different approach to the problem is provided by ir. H. Knoll. Using the four conservation of species equations and five balance equations a set of 9 equations is obtained. By substitution a single expression for the amount of H_2 is found. The 1-dimensional zero-finding problem is solved for the amount of H_2 and the

other compositions are calculated from that. Results are good for an air excess ratio smaller than 1. However from an air excess ratio of 1 and up, numerical problems arise, since the fraction of H_2 becomes (very) small. Since the fractions of CO_2 and H_2O are expected to be significant in most situations the same approach as suggested by ir. H. Knoll is used, but now solving for the amount of CO_2. This approach also gives numerical difficulties in situations where (almost) no CO is present (at lower temperature and $\lambda \geq 1$). In these specific cases a solution is found by assuming full conversion to CO_2 and no CO present in the system, reducing the number of equation by 2.

Starting with the general reaction equation for the conversion of 1 kmol fuel with air into reaction products.

$$\begin{aligned} &C_xH_y + \lambda(x+\frac{y}{4})(_2{+}3.76N_2) \rightarrow \\ &\quad \rightarrow aCO + bCO_2 + cO_2 + dH_2O + eO + fN_2 + gH_2 + hH + iOH \end{aligned} \tag{RXN.18}$$

In total there are 9 unknown variables ($[a...i]$). Conservation of species dictates:

$$x = a + b \qquad \text{conservation of } C \tag{3.46a}$$
$$y = 2d + 2g + h + 1 \qquad \text{conservation of } H \tag{3.46b}$$
$$3.76\lambda(x+\frac{y}{4}) = f \qquad \text{conservation of } N_2 \tag{3.46c}$$
$$2\lambda(x+\frac{y}{4}) = a + 2b + 2c + d + e + i \qquad \text{conservation of } O \tag{3.46d}$$

The mole fraction of a specie is the number of mole of a specie divided by the total number of mole in the system. The total number of reactants is assumed to be n. The set of equilibrium equations [2] can be expressed in the unknowns $[a...i]$.

$$K_{a,1} = \frac{y_{O_2}}{{y_O}^2}\frac{p_{\text{ref}}}{p} = \frac{[c/n]}{[e/n]^2}\frac{p_{\text{ref}}}{p} \tag{3.47a}$$
$$K_{a,2} = \frac{y_{H_2}}{{y_H}^2}\frac{p_{\text{ref}}}{p} = \frac{[g/n]}{[h/n]^2}\frac{p_{\text{ref}}}{p} \tag{3.47b}$$
$$K_{a,3} = \frac{y_{H_2O}}{y_{H_2}{y_{O_2}}^{\frac{1}{2}}}\left(\frac{p_{\text{ref}}}{p}\right)^{\frac{1}{2}} = \frac{[d/n]}{[g/n][c/n]^{\frac{1}{2}}}\left(\frac{p_{\text{ref}}}{p}\right)^{\frac{1}{2}} \tag{3.47c}$$
$$K_{a,4} = \frac{y_{CO_2}}{y_{CO}{y_{O_2}}^{\frac{1}{2}}}\left(\frac{p_{\text{ref}}}{p}\right)^{\frac{1}{2}} = \frac{[b/n]}{[a/n][c/n]^{\frac{1}{2}}}\left(\frac{p_{\text{ref}}}{p}\right)^{\frac{1}{2}} \tag{3.47d}$$
$$K_{a,5} = \frac{y_{H_2O}}{y_{OH}{y_{H_2}}^{\frac{1}{2}}}\left(\frac{p_{\text{ref}}}{p}\right)^{\frac{1}{2}} = \frac{[d/n]}{[c/n][g/n]^{\frac{1}{2}}}\left(\frac{p_{\text{ref}}}{p}\right)^{\frac{1}{2}} \tag{3.47e}$$

Rearranging this equation and introducing five auxiliary constants to improve the readability.

$$e^2 = cC_I \qquad \text{with } C_I = \frac{n}{K_{a,1}}\frac{p_{ref}}{p} \tag{3.48a}$$
$$h^2 = gC_{II} \qquad \text{with } C_{II} = \frac{n}{K_{a,2}}\frac{p_{ref}}{p} \tag{3.48b}$$
$$g^2c = d^2C_{III} \qquad \text{with } C_{III} = \frac{n}{K_{a,3}^2}\frac{p_{ref}}{p} \tag{3.48c}$$
$$a^2c = b^2C_{IV} \qquad \text{with } C_{IV} = \frac{n}{K_{a,4}^2}\frac{p_{ref}}{p} \tag{3.48d}$$
$$i^2g = d^2C_V \qquad \text{with } C_V = \frac{n}{K_{a,5}^2}\frac{p_{ref}}{p} \tag{3.48e}$$

By substitution the set of equations is reduced to two equation expressed in the variables b and d. Using $a = x - b$

$$a^2c = b^2C_{IV} \Rightarrow c = \left(\frac{b}{x-b}\right)^2 C_{IV} \tag{3.49}$$

This result is used to find an expression for g:

$$g^2 = \frac{d^2}{c} C_{III} = g^2 c = d^2 C_{III} = \frac{d^2}{\left(\frac{b}{x-b}\right)^2 C_{IV}} C_{III} \Rightarrow g = \frac{d}{\frac{b}{x-b}} \frac{\sqrt{C_{III}}}{\sqrt{C_{IV}}} \tag{3.50}$$

The result is again used to express h in the variables b and d:

$$h = \sqrt{gC_{II}} = \sqrt{\frac{d}{\frac{b}{x-b}} \frac{\sqrt{C_{III}}}{\sqrt{C_{IV}}} C_{II}} \tag{3.51}$$

The same can be done for e:

$$e = \sqrt{cC_I} = \sqrt{\left(\frac{b}{x-b}\right)^2 C_{IV} C_I} \tag{3.52}$$

and from the conservation of H it follows that:

$$i = y - 2d - 2g - h = y - 2d - 2\left(\frac{d}{\frac{b}{x-b}} \frac{\sqrt{C_{III}}}{\sqrt{C_{IV}}}\right) - \left(\sqrt{\frac{d}{\frac{b}{x-b}} \frac{\sqrt{C_{III}}}{\sqrt{C_{IV}}} C_{II}}\right) \tag{3.53}$$

Now, to summarize the results so far, the set of 9 equations and 9 unknown is, by substitution, reduced to 2 equations expressed in the variables b and d. The reduced set of equations is (from the conservation of O and the last equilibrium equation):

$$\begin{aligned} c &= \lambda(x - \frac{y}{4}) - \frac{1}{2}a - b - \frac{1}{2}d - \frac{1}{2}e - \frac{1}{2}i \qquad (3.54a) \\ &= \left(\frac{b}{x-b}\right)^2 C_{IV} = \\ &\lambda(x - \frac{y}{4}) - \frac{x-b}{2} - b - \frac{1}{2}d - \frac{1}{2}\sqrt{\left(\frac{b}{x-b}\right)^2 C_{IV} C_I} - \frac{1}{2}y - 2d - 2\left(\frac{d}{\frac{b}{x-b}} \frac{\sqrt{C_{III}}}{\sqrt{C_{IV}}}\right) - \left(\sqrt{\frac{d}{\frac{b}{x-b}} \frac{\sqrt{C_{III}}}{\sqrt{C_{IV}}} C_{II}}\right) \\ d^2 &= \frac{1}{C_V}\left[y - 2d - 2g - h\right]^2 g \qquad (3.54b) \\ &= \frac{1}{C_V}\left[y - 2d - 2\frac{d}{\frac{b}{x-b}} \frac{\sqrt{C_{III}}}{\sqrt{C_{IV}}} - \sqrt{\frac{d}{\frac{b}{x-b}} \frac{\sqrt{C_{III}}}{\sqrt{C_{IV}}} C_{II}}\right]^2 \frac{d}{\frac{b}{x-b}} \frac{\sqrt{C_{III}}}{\sqrt{C_{IV}}} \end{aligned}$$

The objective now is to express d as a function of c. To simplify the manipulation of equation, two auxiliary variables are introduced:

$$C_1 = \sqrt{\frac{1}{C_V}} \tag{3.55a}$$

$$C_2 = \sqrt{\frac{1}{\frac{b}{x-b}} \frac{\sqrt{C_{III}}}{\sqrt{IV}}} \tag{3.55b}$$

resulting in

$$d = C_1\left[y - 2d - 2dC_2^2 - \sqrt{dC_2^2 C_{II}}\right]\sqrt{d}C_2 \tag{3.56}$$

Bringing all terms to RHS:

$$C_1\left[y\sqrt{d}C_2 - 2d\sqrt{d}C_2 - 2d\sqrt{d}C_2^3 - dC_2^2\sqrt{C_{II}}\right] - d = 0 \tag{3.57}$$

Rearranging terms gives:

$$\left(-2C_1C_2 - 2C_1C_2^3\right)\sqrt{d}^3 + \left(-C_1C_2^2\sqrt{C_{II}} - 1\right)\sqrt{d}^2 + \left(C_1C_2y\right)\sqrt{d} = 0 \tag{3.58}$$

Dividing by $\sqrt{d}$ drops out the (unwanted) solution $d = 0$ and leaves a second-order equation to solve. The variable d can be expressed in the variable c (recalling C_2 to be a function of only b):

$$\sqrt{d_{1,2}} = \frac{-B_d \pm \sqrt{B_d^2 - 4A_d C_d}}{2A_d} \tag{3.59}$$

where

$$A_d = -2C_1C_2 - 2C_1C_2^3$$
$$B_d = -C_1C_2^2\sqrt{C_{II}} - 1$$
$$C_d = C_1C_2y$$

A single equation with one unknown variable b is obtained, which can be solved. From that, using equations [8] to [12] and [18], the other variables can be calculated. However, the total number of reactants n (embedded in the constants $[C_I...C_V]$ is not known in forehand. Rather than substituting all results in the constants $[C_I...C_V]$ (and making them variables), a numerical solution is chosen. The number of reactants is estimated (based on full conversion to CO_2 and H_2O, and by iteration updated until the number of reactants is constant ($|n_j - n_{j-1}|$ < required accuracy ($5 \cdot 10^{-6}$), with j the number of iterations). The solution converges well, and required simulation time is short enough to allow for this iteration [for now at least].

The solution for b - the amount of CO_2 - can theoretically lie between 0 (no CO_2) and x (all carbon in conversed to CO_2). A satisfying solution using this approach is found at high temperature (more dissociation) and in situations with an air excess ratio smaller than 1. In other situations (i.e., low temperature and $\lambda \geq 1$) the solution lies very close to full conversion to CO_2. In cases where the parameter b is not found accurately enough (residu > threshold), the search is (stepwise) refined in the area of complete conversion. This approach gives satisfying results over a wider range of temperatures and air excess ratios.
However, at a certain point (in the $\lambda - T$-domain) the amount of CO_2 is so close to full conversion, that numerical problems arise (mathematically: $(x - b) \rightarrow 0$). To overcome numerical difficulties, when the amount of CO is insignificant [lower than threshold], it is assumed that all carbon is conversed to CO_2 and no CO is present. With three variables known (a, b and f), the total set of 9 equations reduces to 6 equations (with 6 unknown variables): the carbon and nitrogen balance and the equilibrium equation for $CO - CO_2$ drop out.

Following the same procedure for the reduced set of equations as above, starts with the following set of equations:

$$y = 2d + 2g + h + i \qquad \text{conservation of } H \tag{3.60a}$$
$$2\lambda(x + \frac{y}{4}) - 2x = 2c + d + e + i \qquad \text{conservation of } O \tag{3.60b}$$
$$e^2 = cC_I \qquad \text{with } C_I = \frac{n}{K_{a,1}}\frac{p_{ref}}{p} \tag{3.60c}$$
$$h^2 = gC_{II} \qquad \text{with } C_{II} = \frac{n}{K_{a,2}}\frac{p_{ref}}{p} \tag{3.60d}$$
$$g^2c = d^2C_{III} \qquad \text{with } C_{III} = \frac{n}{K_{a,3}^2}\frac{p_{ref}}{p} \tag{3.60e}$$
$$i^2g = d^2C_V \qquad \text{with } C_V = \frac{n}{K_{a,5}^2}\frac{p_{ref}}{p} \tag{3.60f}$$

Again, by substitution, two equations - now dependent on the variables c and d - are formulated:

$$2\lambda(x + \frac{y}{4}) - 2x = 2c + d + \sqrt{c}\sqrt{C_I} + d\sqrt{C_V}\sqrt{\sqrt{\frac{c}{d^2C_{III}}}} \tag{3.61a}$$
$$y = 2d + 2\sqrt{\frac{d^2C_{III}}{c}} + \sqrt{\sqrt{\frac{d^2C_{III}}{c}}C_{III} + \sqrt{\frac{d^2C_V}{\sqrt{\frac{d^2C_{III}}{c}}}}} \tag{3.61b}$$

The first equation from the set is rewritten as:

$$\begin{aligned} 2\lambda(x+\frac{y}{4})-2x &= 2c+d+\sqrt{c}\sqrt{C_I}+d\sqrt{C_V}\sqrt{\sqrt{c}\frac{1}{\sqrt{C_{III}}}\frac{1}{d}} \\ &= 2c+d+\sqrt{c}\sqrt{C_I}+\sqrt{d}\sqrt{C_V}\sqrt{\sqrt{c}\frac{1}{\sqrt{C_{III}}}} \end{aligned} \tag{3.62}$$

Bringing all terms to the RHS, leaves a second-order equation of $\sqrt{d}$:

$$\sqrt{d}^2+\left(\sqrt{C_V}\sqrt{\sqrt{c}\frac{1}{\sqrt{C_{III}}}}\right)\sqrt{d}+\left(2c+\sqrt{c}\sqrt{C_I}-2\lambda(x+\frac{y}{4})-2x\right)=0 \tag{3.63}$$

Now, $\sqrt{d}$ can be solved for c, using:

$$\sqrt{d_{1,2}}=\frac{-B_d\pm\sqrt{B_d^2-4A_dC_d}}{2A_d} \tag{3.64}$$

where

$$\begin{aligned} A_d &= 1 \\ B_d &= \sqrt{C_V}\sqrt{\sqrt{c}\frac{1}{\sqrt{C_{III}}}} \\ C_d &= 2c+\sqrt{c}\sqrt{C_I}-2\lambda(x+\frac{y}{4})-2x \end{aligned}$$

From the set of equations [20] only the second remains, reducing the problem to a 1-dimensional zero-finding. Once the variable c is determined, the rest of the variables can be calculated. As was the case previously, n is assumed known - which is not the case - and must be determined by iteration.

Validation
In order to validate the results, first a qualitative check is performed. The equilibrium composition is calculated for different temperature, pressure and air excess ratio. Results are plotted with only one input variable varying, while keeping the other two constant. It is expected that the final composition is a smooth function of each of the three variables.
In figure 3.4 the final composition is presented at constant temperature and pressure for a varying air excess ratio. The amount of CO and OH decreases with increasing air excess ratio, as is expected. For an air excess ratio smaller than 1, almost al oxygen O_2 is conversed. At higher air excess ratios, oxygen is present in larger quantities in the final composition. The mole fraction of carbon-dioxide CO_2 and water H_2O decreases at air excess ratios larger than one. This does not mean there is less carbon-dioxide and water formed, but merely shows that more of the other species are present (nitrogen and oxygen, since more air is added to the same amount of fuel).

In figure 3.5 the final composition is presented at constant pressure and air excess ratio ($\lambda = 0.6$), for varying temperature. From low to medium temperature the equilibrium shifts towards the formation of water and carbon-monoxide, away from hydrogen and carbon dioxide. At higher temperatures (> 3300), dissociation results in H and O radicals, mainly at the expense of water formed. The same happens at an air excess ratio slightly larger than 1, as can be seen in figure 3.6. But now, dissociation leads to less CO_2 and less H_2O.

At a high temperature ($T = 4000$K) and an air excess ratio slightly above 1, the effect of pressure is investigated. At such a high temperature, the effect of dissociation is expected to be significant. This can be seen in figure 3.7. Increasing the pressure has the effect of reducing dissociation; this is in-line with expectations. At low temperatures ($T = 500$K) there is almost no dissociation and pressure effects are insignificant for the final composition, as can be seen in figure 3.8.

Calculations are performed for a wide range of the three variables. Each intersection of the resulting output-data, gives a composition that is a smooth function of each input variable. The effect of dissociation, which plays a significant role in the formation of NO, is seen at higher temperatures. The implementation is suitable for use from Simulink.

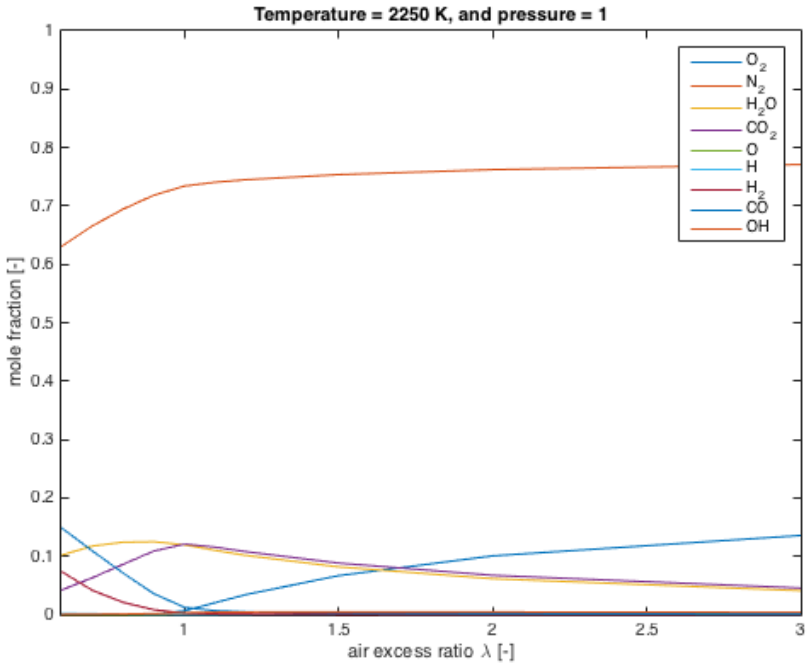

Figure 3.4: Composition at $T = 2250$K and $p = 1$bar

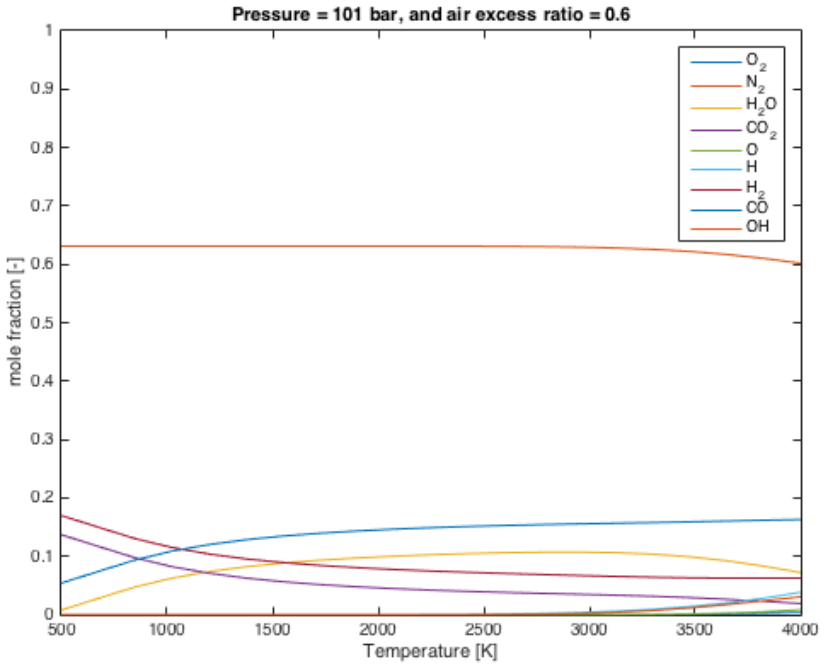

Figure 3.5: Composition at $\lambda = 0.6$ and $p = 101$bar

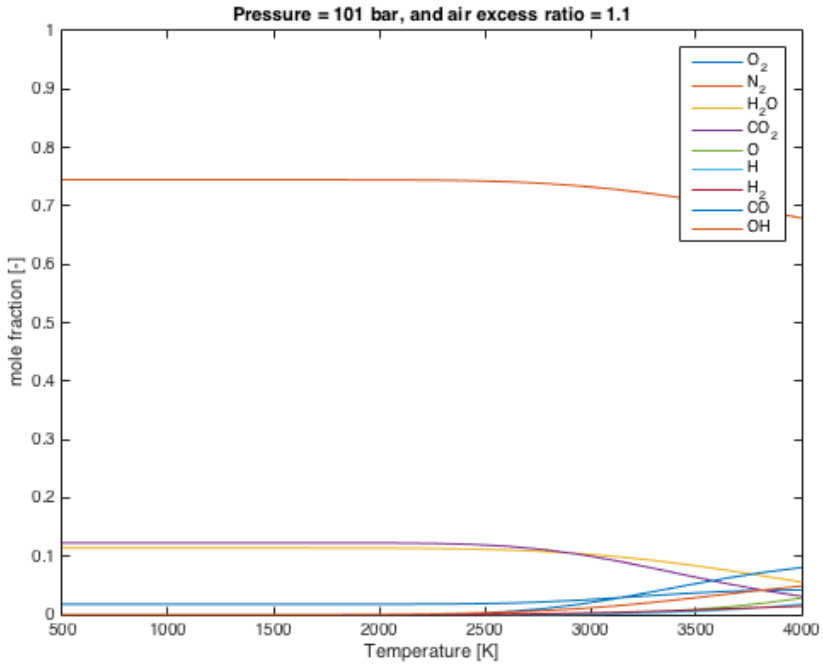

Figure 3.6: Composition at $\lambda = 1.1$ and $p = 101$bar

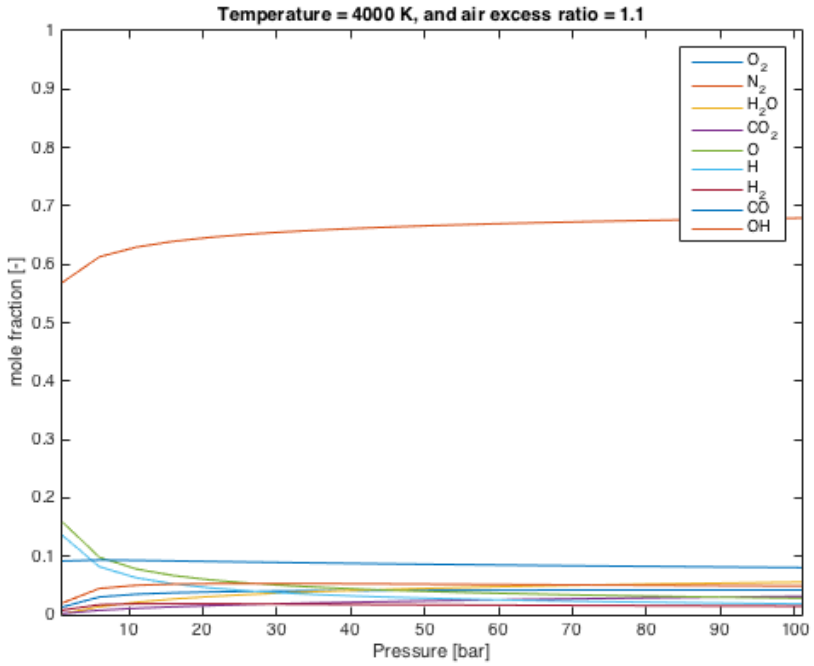

Figure 3.7: Composition at $\lambda = 1.1$ and $T = 4000$K

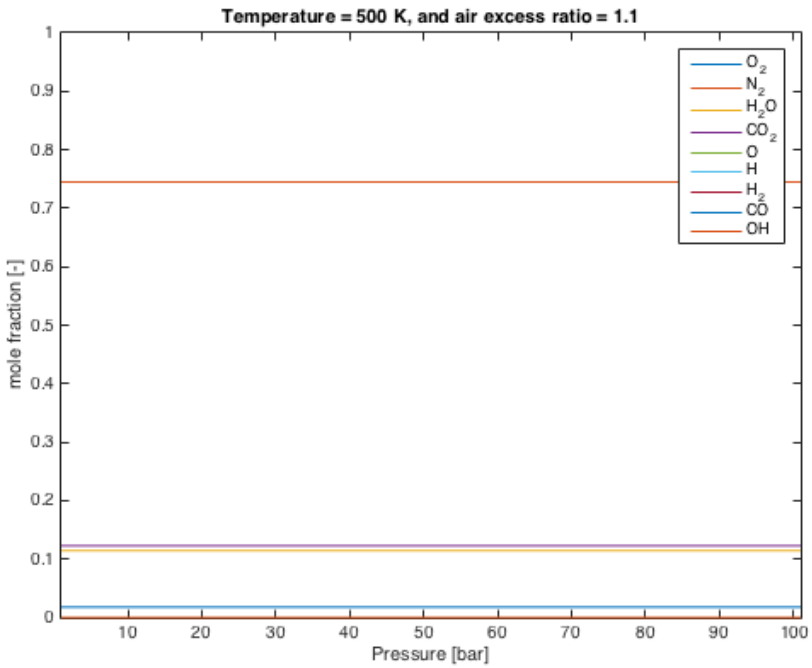

Figure 3.8: Composition at $\lambda = 1.1$ and $T = 500$K

3.3.7. NO-formation model

Relevant phenomena, hypothesis and assumptions

The extended Zel'dovich mechanism is used, under the assumption that OHC-equilibrium is achieved before NO-formation becomes significant. The NO-formation is decoupled from the OHC-equilibrium. The additional assumption that NO-concentrations are much less than there equilibrium values, the reverse reactions can be neglected.

Model equations

The rate of formation of NO is given by:

$$\frac{d[NO]}{dt} = k_{N,1f}[O][N_2] + k_{N,2f}[N][O_2] + k_{N,3f}[N][OH] - k_{N,1r}[NO][N] - k_{N,2r}[NO][O] - k_{N,3r}[NO][H] \quad (3.65)$$

The rate of formation of NO under the assumptions stated in this section, as explained in Chapter 2, is simplified to:

$$\frac{d[NO]}{dt} = 2k_{N,1f}[O]_{eq}[N_2]_{eq} \quad (3.66)$$

The concentration of $[NO]$ (unit $[kmol/m^3]$) can also change as a consequence of a volume change:

$$\frac{d[NO]}{dt} = \frac{d}{dt}\left(\frac{N_{NO}}{V}\right) = \frac{1}{V}\frac{dN_{NO}}{dt} + N_{NO}\frac{d\frac{1}{V}}{dt} \quad (3.67)$$

where the first term on the RHS represents the formation of NO and the second term on RHS represents the effect of volume change on the concentration. Now, only looking at the formation of NO:

$$\frac{1}{V}\frac{dN_{NO}}{dt} = 2k_{N,1f}[O]_{eq}[N_2]_{eq} = 2k_{N,1f}\frac{N_O}{V}\frac{N_{N2}}{V} \quad (3.68)$$

Dividing by the volume results in the expression for the formation of NO:

$$\frac{dN_{NO}}{dt} = 2k_{N,1f}N_O N_{N2}\frac{1}{V} \quad (3.69)$$

where the forward reaction rate coefficient $k_{N,1f} = 1.8 \cdot 10^{11} exp(-38370/T)$ is highly temperature dependent (unit: $[m^3/kmol-s]$ and temperature in [K]) Turns [31]. Further more NO-formation depends on the amount of O-radicals, N_2-atoms and the volume available. The total amount of NO formed is calculated based on integration:

$$N_{NO} = \int 2k_{N,1f} N_O N_{N2} \frac{1}{V} dt \tag{3.70}$$

Taking reverse reactions into account
The rate of formation of NO is only significant at high temperatures (>1800 K). The strong N_2 triple bond has a high dissociation energy of 941 kJ/mol. this effect, represented by the high activation energy, makes it the rate limiting step of the extended Zel'dovich mechanism. Oxidation of nitrogen atoms requires less energy and the rate of consumption of free nitrogen atoms becomes equal to the rate of formation. Therefore, a quasi steady state can be established.
When taking the reverse equation into account and assuming the formation of nitrogen atoms rate limiting, equation 3.65 reduces to [21]:

$$\frac{d[NO]}{dt} = 2[O] \frac{k_{N,1f} k_{N,2f} [N_2][O_2] - k_{N,1r} k_{N,2r} [NO]^2}{k_{N,1r}[NO] + k_{N,2f}[O_2] + k_{N,3f}[OH]} + 2 \frac{k_{N,1f} k_{N,3f} [N_2][OH][O] - k_{N,1r} k_{N,3r} [NO]^2 [H]}{k_{N,1r}[NO] + k_{N,2f}[O_2] + k_{N,3f}[OH]} \tag{3.71}$$

4

Measurements

4.1. Introduction

In order to validate the model, measurements are performed. As described in Chapter 2, the NO-formation strongly depends on the state of the gas in the cylinder. The model will only predict emissions accurately when the in cylinder process is captured adequately.

4.2. Measurement set-up

Measurements are performed on a four cylinder line engine MAN4L20/27, located at the Royal Netherlands Naval College, which is part of the Netherlands Defense Academy. The measurements are performed at different steady-state operating points. At each operating point, both the engine variables as well as the emissions are measured.

4.2.1. Engine

The maximum effective power of the engine is 340 kW at 1000 RPM. The main parameters of the engine are presented in Table 4.1. The valve timing is taken from the engine manufacturers manual. Before the measurements started, an attempt is made to measure the valve position as a function of the crank-angle. The available equipment made accurate measurement difficult. The deviation in measured values from the engine manual is large. The results are presented in Figure 4.1. The difference in exhaust valve opening is over 14 ° and in inlet valve closing over 18 °. In the lifetime of the engine the camshaft might be changed. No engine documentation, which indicates a change of camshaft, is found. The lack of accuracy in the measurement of the valve position, led to the choice of taking the values presented in the engine manual for the valve timing.

The measurement grid is defined to obtain results at constant engine speed as well as constant torque. Constant engine speed results in a constant residence time in the cylinder. Constant torque results in an almost constant heat input. The main reason that constant torque does not result in constant heat input, is the heat loss, which is also a function of engine speed. The measurement grid used is depicted in Figure 4.2.

Data acquisition is split in two parts. Most variables are considered to be time invariant at a steady-state operating point. Two signals are (highly) time-variant, namely the cylinder pressure and the pressure before the turbine. The cylinder pressure is an important matching parameter for the model. The pressure before

Table 4.1: Engine main characteristics

Parameter	
Model	MAN4L20.27
Number of cylinders	4
Bore	0.20 m
Stroke	0.27 m
Connection rod length	0.52 m
Compression ratio	13.4

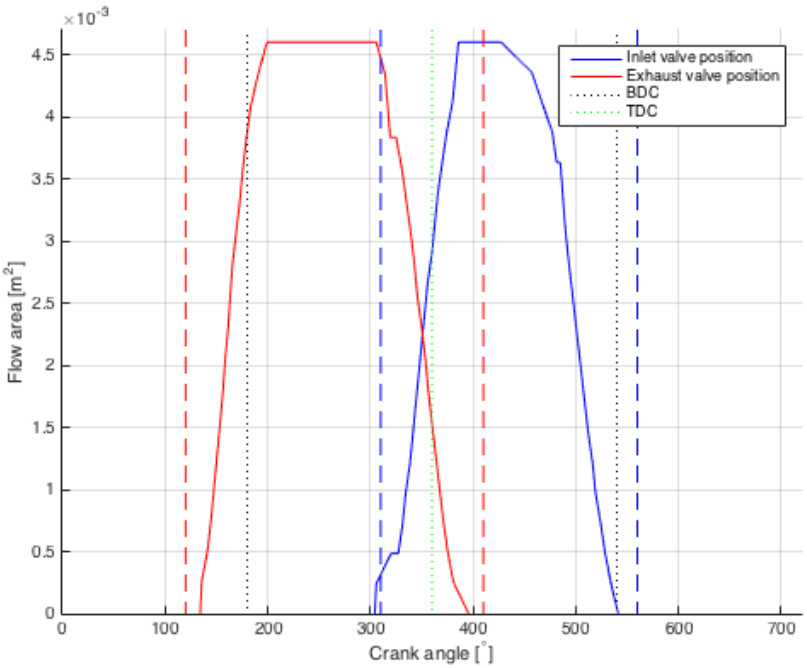

Figure 4.1: Valve timing: opening and closing from engine manual (dashed lines) and measured position (solid lines)

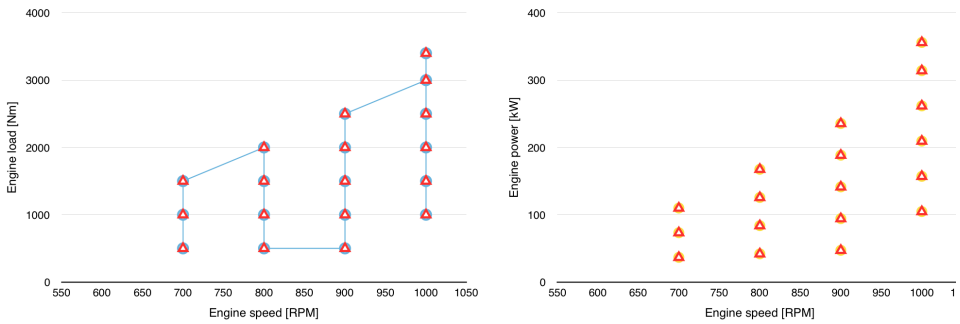

Figure 4.2: The measurement grid: Torque (left) and power (right) at different engine speeds

the turbine is variant, due to the pulse turbo charger configuration. The pressure before the turbine only becomes relevant when the valves are also part of the model.

The pressure in each of the four cylinders is measured over time. Data acquisition is limited to 150 000 data points at 50 075 Hz, which yields 18 to 25 complete cycles depending on engine speed. The pressure signal has to be transposed in two direction. The pressure sensors do not have a correct absolute value. The pressure signal has to be vertically sifted to the correct value.
Secondly, the TDC-sensor is not very accurate. The pressure signal has to be shifted horizontally to match the volume signal.

The vertical shift of the pressure signal can be computed in different ways. An option is to look at the compression just after IC. The gas composition in the cylinder is close to air. The gas temperature is approximately the same as the wall temperature. Therefore heat loss will be minimal and the process can be assumed to be adiabatic. With low velocities inside the cylinder, the process can be viewed as isentropic. In this case the polytropic exponent n is equal to the isentropic index k, which is known for an ideal gas ($k = 1.400$).
However, a more straight forward way of matching is used in this thesis. The vertical shift of the pressure signal is calculated using the assumption that just after BDC, when the piston speed is low, the cylinder pressure is equal to the inlet receiver pressure. The piston is moving in an upward direction, so flow velocities in and therefore pressure losses over the intake channel will be low. The average cylinder pressure between BDC and IC is matched to the measured inlet receiver pressure. The calculated average pressures between BDC and IC and the inlet receiver pressure are presented in Figure 4.3, along with the pressure signals.

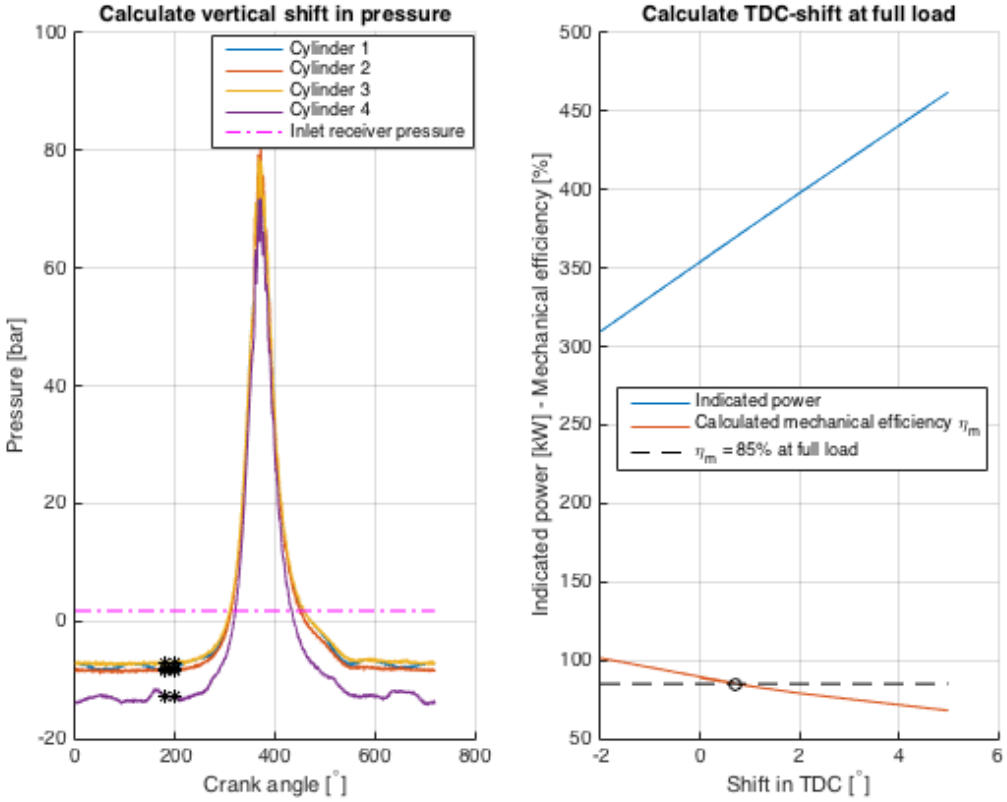

Figure 4.3: Pressure shift: Vertical to match p_{IR} between BDC and IC (left) and TDC-shift to match mechanical efficiency η_m at full load (right)

The TDC-shift, which is necessary to match the pressure signal to the volume signal, can be calculated in different ways. One option is the measure the cylinder pressure of one cylinder in the un-fueled condition.

Due to heat loss the highest cylinder pressure will be located just before TDC (approximately 0.5 degrees).
A different approach is taken. The mechanical efficiency is specified by the manufacturer for the full load condition. The indicated work can be calculated for different TDC-shifts. With known engine speed and number of cylinders this can be converted to indicated power. The power of the engine is measured at shaft (water brake). The ratio between brake power and indicated power is the mechanical efficiency.
The TDC-shift is calculated at 314 kW at 1000 RPM. The value for the TDC-shift of 0.7, which is found, is kept constant over the entire engine envelope. This value coincides with the value found by Ding for the same engine Ding [10]. Due to change in torque on the crankshaft, TDC-shift will be effected. However, effects are assumed to be minimal. The indicated power and associated mechanical efficiency are presented in Figure 4.3. A small shift in TDC has profound impact on the indicated power, explaining why the TDC-sensor accuracy is not sufficient.

With the TDC-shift fixed, the mechanical efficiency η_m can be calculated for all operating points under consideration. The results are presented in Figure 4.4. Mechanical efficiency decreases with engine speed and engine load. The first is explained by the fact that the mechanical efficiency increases with charge pressure [25]. The effect of engine load is partially explained by the increase in charge pressure, but also by the fact that the same mass has to be rotated while indicated power is less. Resulting in a relative (to the indicated power) larger mechanical loss.

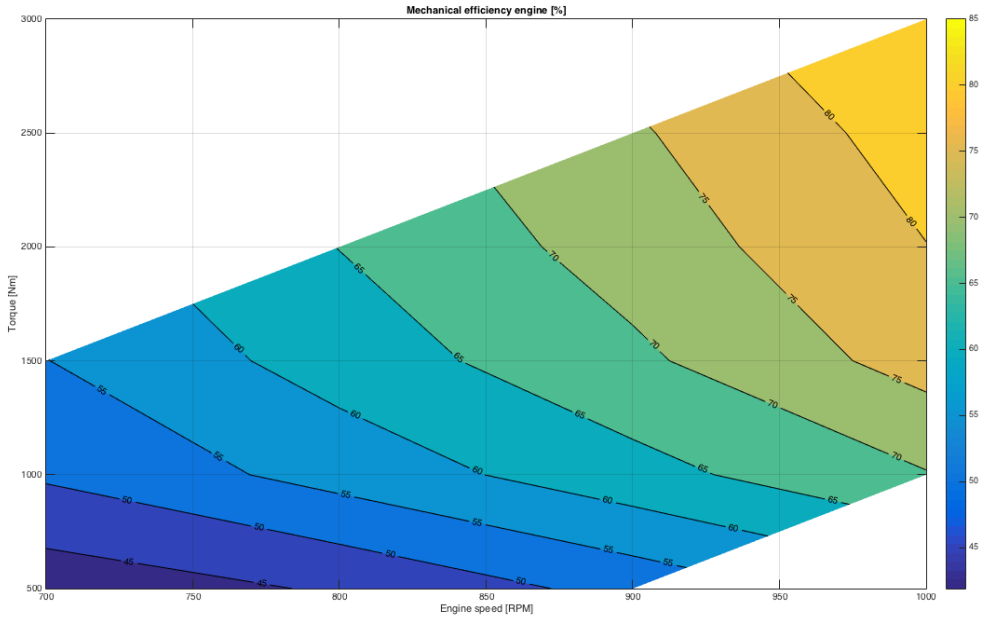

Figure 4.4: Mechanical efficiency calculated from measured brake power and indicated power from p-V measurement

In the pressure signal some high frequencies are observed. Two possible explanations are irregularities due to the combustion process and wave formation in the channel of the pressure sensor. Comparing different cycles of the same cylinder shows the higher order frequencies to overlap for different cycles, as can be seen in Figure 4.5 (left). Since there is some difference between the different cycles of one cylinder, the average value of all cycles measured is taken at each piston postion with a cycle. The cycle averaged pressure signals for all cylinders are compared. From Figure 4.5 (right) it can be observed that the higher order frequencies overlap as well. This overlap does not seem to be random, as would be expected from combustion irregularities. An explanation coming from the shape of the pressure sensor channel seems more appropriate.
A Fast Fourier Transformation (FFT) show the frequencies in the pressure signal. At the lower end of the frequency domain the engine speed and its higher orders are observed (Figure 4.6 (c)). The peak around 1100 Hz (Figure 4.6 (d)) is not associated with the engine speed and seems to have another source.

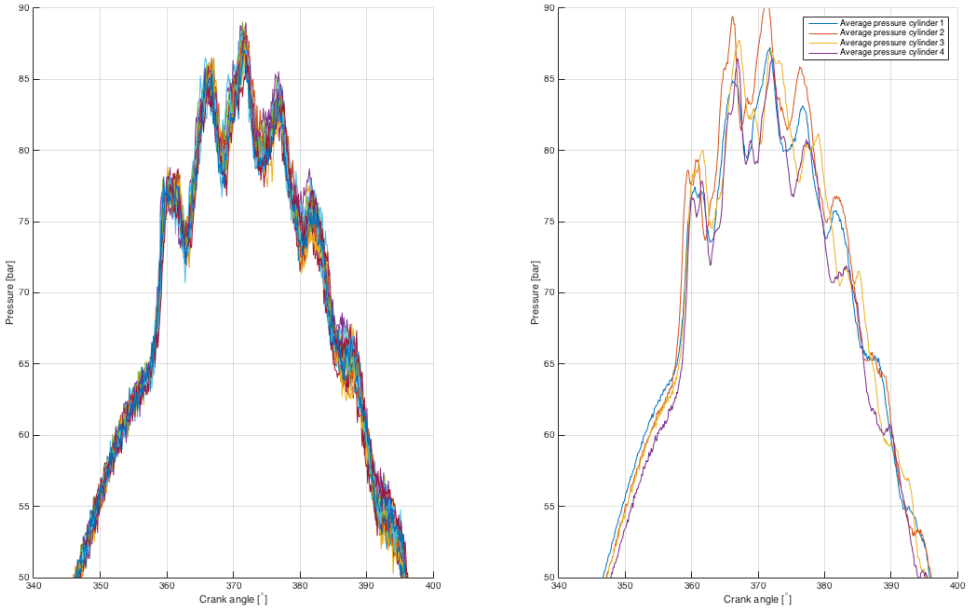

Figure 4.5: Measured pressure: different cycles of cylinder 1 (left) and average measured pressure of all four cylinders (right)

The higher order frequencies are undesirable, since the pressure signal acts as an input. Derivatives become large and can introduce instability in the simulation. Smoothing of the pressure signal can be done in several ways. Applying a low pass filter (LPF) on the FFT-data and converting back to the time domain is an option to filter out the higher order frequencies, as can be seen in Figure 4.6. A downside of this approach is that the indicated work is smaller in the filtered signal. The sharp increase in pressure at SOC is in the same frequency range as the disturbance and therefore also filtered out by the LPF. This is an undesirable side-effect.
An anti-causal model is suggested by Ding [10]. The average cylinder pressure of several cycles is taken as an input. While taking heat loss into account, the heat release rate is calculated and (multiple) Vibe-curves are fitted. Based on the Vibe-curves the pressure profile within the cylinder is calculated. The results obtained by Ding [10] look good.
Since developing an anti-causal model using the set of equations from the OHC-equilibrium is time consuming [and difficult], a more simple approach is taken. Compression and expansion are fitted linear in the log p-log V-diagram and the combustion (point 2 to 4 in the Seiliger diagram) using a 4^{th}-order polynomial.

During post-processing of the measured data, it was observed that the pressure of cylinder 4 - and to a lesser extend that of cylinder 1 - deviates significantly from the others, as can be seen in Figure 4.7 (a, b). The choice is made to first take the average of all cylinders, before smoothing. The average un-smoothed signal of all cylinders lies closely to the signals of cylinder 2 and cylinder 3 and is therefore expected to be representative. The effect of smoothing can be seen in both the log$p$-log$V$-diagram as well as in the p-ϕ-diagram in Figure 4.7 (d, c).

4.2.2. Emission measurement equipment

Emission measurements are performed using the Horiba PG-350E portable gas analyzer. The sampling is done using the M&C PSP4000. The measurement of NO is done using a Fluid Modulation and Chemiluminescence type Analyzer. The NO is oxidized using ozone O_3 to an exited state of NO_2^*. The (extremely fast

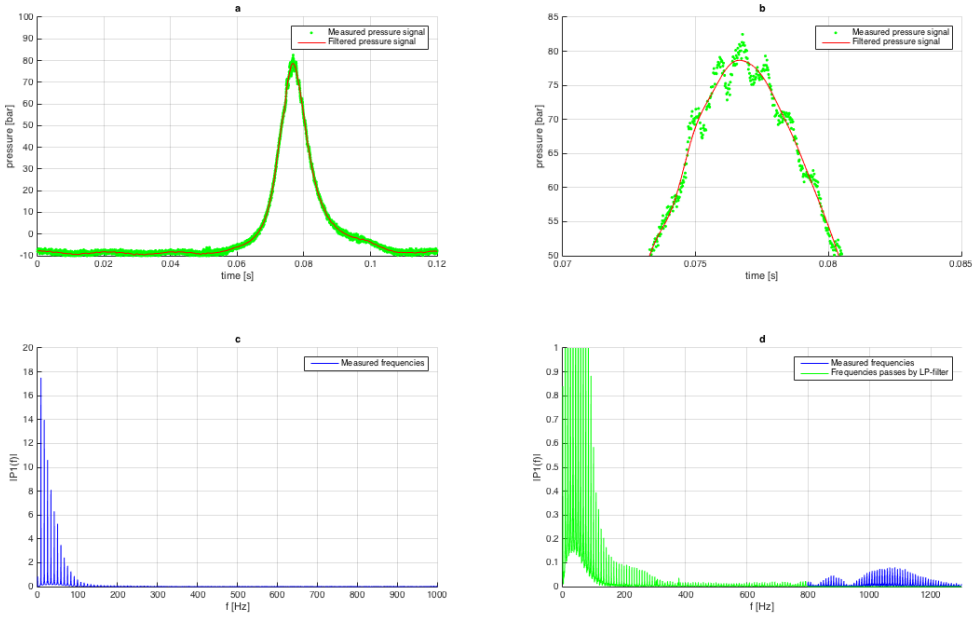

Figure 4.6: Frequency analysis using FFT: measured and filter signal (a), with zoom in at the peak pressure (b) and the frequencies in the signal (c) and a detail of the filter frequencies (d)

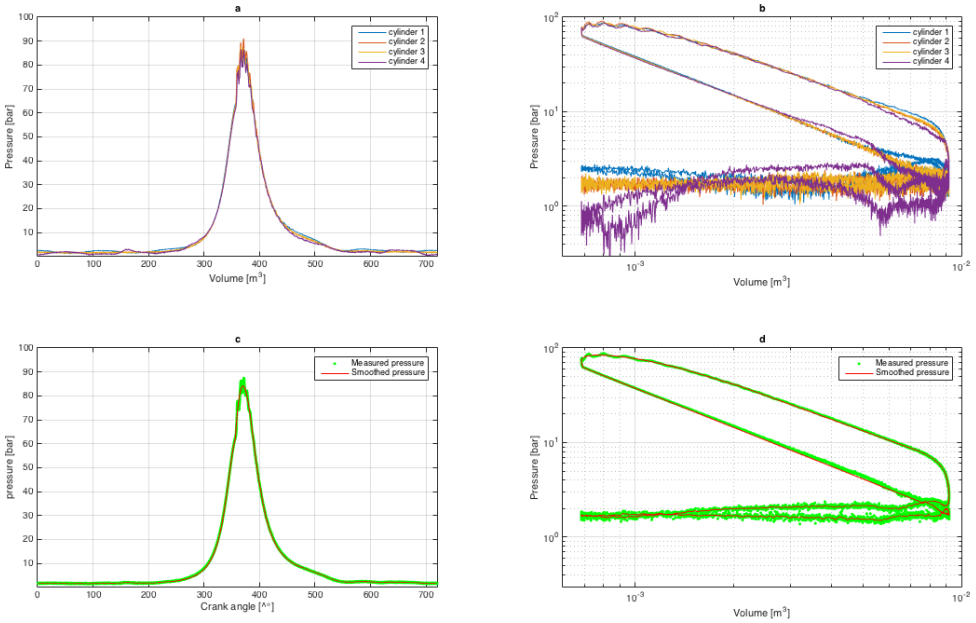

Figure 4.7: Pressure: measured signal versus crank-angle (a) and in log$p$-log$V$-diagram (b), and the average measured and smoothed signal versus crank-angle (c) and in log$p$-log$V$-diagram (d)

Table 4.2: Dry air composition

Component		Volume fraction [%]
Nitrogen	N_2	78.084
Oxygen	O_2	20.947
Argon	Ar	0.934
Carbondioxide	CO_2	0.035

Table 4.3: Antoine equation parameters for water valid for temperatures 304 K < T < 333 K

Parameter	Value
A	5.20389
B	1733.926
C	-39.485

occurring) change to its ground state radiates light.

$$NO + O_3 \rightarrow NO_2^* + O2$$
$$NO_2^* \rightarrow NO_2 + \text{light}$$

In the low concentrations of NO found in the flue gasses, the radiated light is proportional to the NO concentration. To measure NO_x, the NO_x is first converted to NO. The analyzer can at any time only measure NO or NO_x (switching takes approx. 20 sec).
The concentrations of CO and SO_2 are measured using a 'fluid modulation and infrared absorption'-type analyzer. Molecules consisting of different atoms can absorb infrared rays in a specific wavelength region. The absorption of infrared light corresponds with the concentration. The amount of transmitted light is attenuated by the amount absorbed and reaches the detector.

4.2.3. Atmospheric conditions

The temperature, pressure and relative humidity of the intake air is measured. The composition of dry air is presented in Table 4.2. The vapor pressure of water is calculated using the Antoine equation:

$$\log_{10} p_{sat} = A - \frac{B}{T + C} \tag{4.1}$$

where the temperature T is in Kelvin and the saturation pressure p_{sat} in bar. The coefficients are obtained from Linstrom and Mallard [17] and presented in Table 4.3. The volume fraction of water in air can be calculated based on the partial pressure of water in the air:

$$y_{H_2O} = \frac{p_{H_2O}}{p} = \frac{RH/100 \cdot p_{sat}}{p} \tag{4.2}$$

where RH is the measured relative humidity expressed in a percentage.

4.3. Results

4.3.1. Trapped conditions

The focus of the simulation is calculation of NO-formation. Therefore, the focus lies on the process between start of combustion (SOC) and exhaust valve opening (EO). To determine the state in the cylinder at SOC, simulations are performed with a single zone model. Until SOC there is no combustion, so the model is formulated to provide pressure as an output, which is matched to the measured pressure signal. The enthalpy of the air in the cylinder is calculated based on the inlet receiver temperature and corrected for heat pick-up during inflow. The condition of the gas in the cylinder at IC is denoted as the trapped condition.
The heat pick-up is modelled using the experimental equation from Zinner, using the parameters suggested by Ding [10]. The temperature of the gasses in the cylinder at IC is called the trapped temperature. The

trapped temperature T_{TR} is assumed to be equal to the induction temperature:

$$T_{TR} = T_{IR} + \frac{1}{6}(T_{INL} - T_{IR}) \tag{4.3}$$

where the temperature of the metal $T_{INL} = 513K$. The measured inlet receiver temperature and the calculated trapped temperature are presented in the top row of Figure 4.8.
The pressure inside the cylinder is assumed to be equal to the inlet receiver pressure at the moment the inlet valve closes. The inlet receiver pressure p_{IR} is presented in Figure 4.8. Knowing pressure, temperature and volume at IC, allows the calculation of the number of mole in the cylinder. Using the Ideal Gas Law gives $N = \frac{pV}{RT}$. Based on the composition of air, the mass in the cylinder can be calculated.
The mass flow air entering the engine is measured and presented in Figure 4.8 at right side of the middle row. The engine is a turbo-charged 4-stroke engine with a valve-overlap of 100°, so scavenging is expected. From the mass flow air entering the engine $\dot{m}_{in}$, a part is kept in the cylinder during the closed part of the cycle $\dot{m}_{fresh}$ and a part slips trough the cylinder $\dot{m}_{slip}$.

$$\dot{m}_{in} = \dot{m}_{fresh} + \dot{m}_{slip} \tag{4.4}$$

Defining the "slip" factor as proposed by Stapersma [25]:

$$s = \frac{\dot{m}_{slip}}{\dot{m}_{fresh}} \tag{4.5}$$

The slip factor s can be calculated under the assumption that the scavenging efficiency is high ($\eta_{sc} = 1$).
The cylinder is under this assumption completely filled with fresh air, so $m_{TR} = m_{fresh}$. As can be seen from Figure 4.8 left bottom, the calculated slip factor is not always positive. This could mean one (or more) of the assumptions regarding trapped pressure or temperature is incorrect. For the slip factor to become positive the trapped pressure must become lower than the inlet receiver pressure. This seems unlikely, since the piston is moving in an upward direction and so reducing cylinder volume.
The trapped temperature seems to be somewhat on the low end. Increasing the trapped temperature to a level where the slipflow is positive by employing the experimental equation from Zinner would require a metal temperature of 900 K, which is unrealistic. Another possibility is more heat pick-up during intake. The intake channel of the MAN is relatively short and cylinder cooling water is of an expected temperature (~ 80° C). The heat pick-up should be more than twice the amount suggested by the experimental equation, which seems unlikely for this engine.
Another explanation would be that the scavenging efficiency is not high. In fact the negative slip factor suggests back flow from the exhaust receiver. The turbo-charger on the MAN engine is a pulse-type originally matched to a 6 cylinder engine (opposed to the 4 cylinder engine it is mounted on). Where a pulse turbo-charger usually enhances part load performance in terms of filling efficiency, an adverse effect may occur here. The actual amount of back flow is less than suggested by the slip factor, since the flue gas temperature will be (much) higher than the induction air temperature.
At this point no further calculations are performed. It is noted that the assumption of high scavenging efficiency probably does not hold at low load due to back flow.

4.3.2. Fuel consumption and air excess ratio

The fuel flow to the engine is measured and the results are presented in Figure 4.9. The fuel flow is determined by supplying the engine fuel from a measurement tank on a scale and measuring weight and time required to consume the fuel. The engine has some leak flow of fuel, which is measured. In this leak flow will be some oil contamination. The leak flow is assumed to contain 75% fuel.
The optimum in specific fuel consumption (SFC) lies between 80 and 90% of the engine speed. An optimum is found at 900 RPM at 70% of the nominal engine power (340 kW). Based on the measurements an exact optimum is difficult to determine. The fuel flow is decreasing with engine speed at constant torque. Although correct, this is not intuitive. The bottom left part of Figure 4.9 shows the same fuel flow, but now as a function of engine power. Fuel flow increases almost linear with power. At the same power a lower engine speed is favorable for fuel consumption, indicating operation closer to the MCR-line gives a better fuel economy.

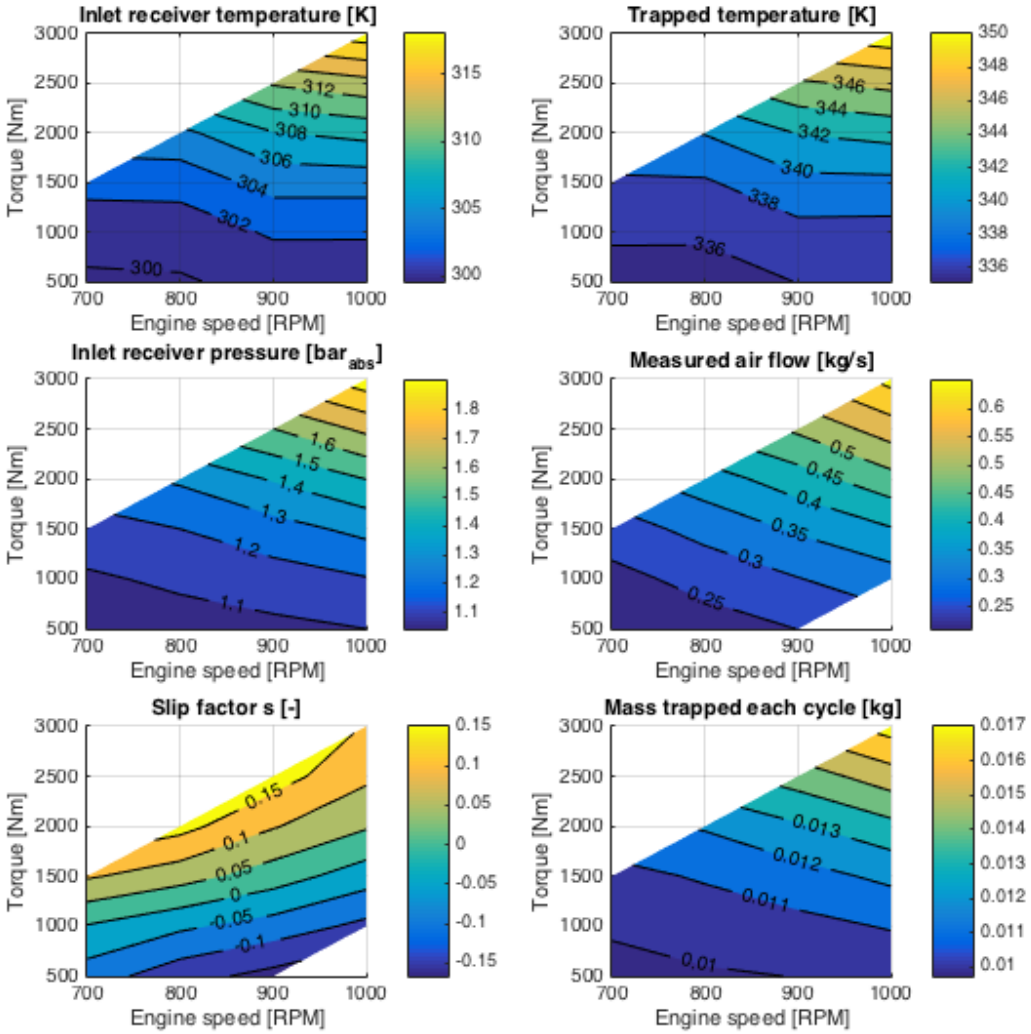

Figure 4.8: The inlet receiver temperature and absolute pressure of the air, trapped temperature, measured air flow, calculated slip factor and trapped mass

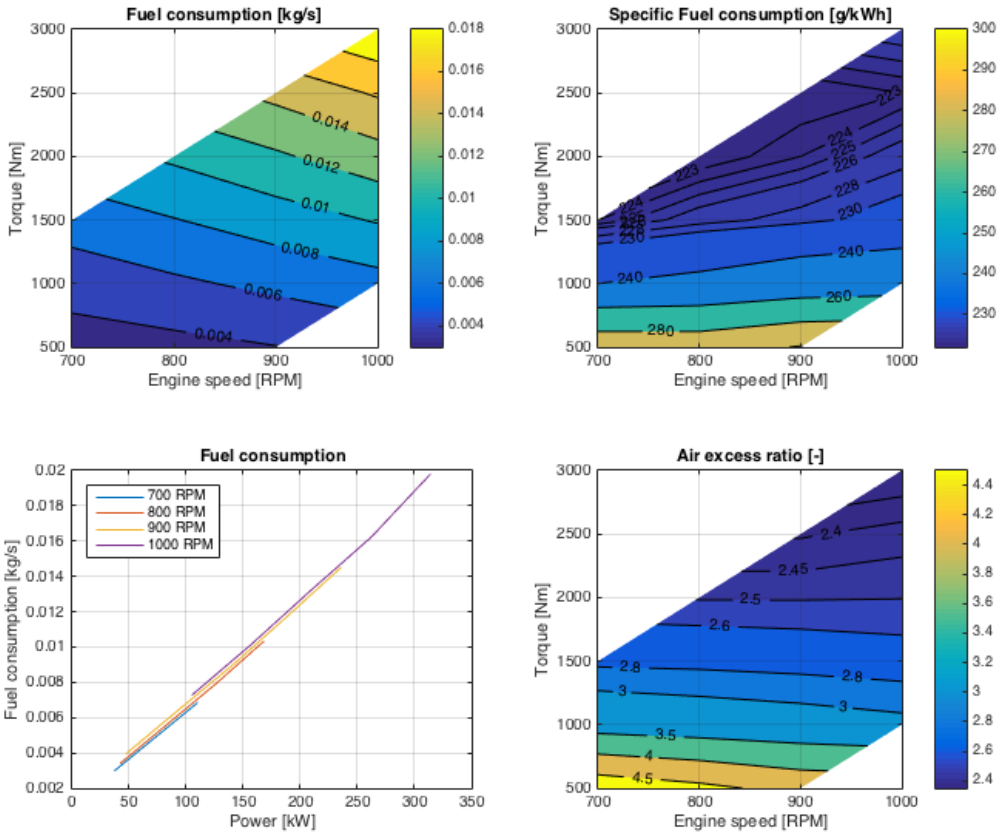

Figure 4.9: Fuel consumption (top left), specific fuel consumption (top right), fuel consumption as a function of power (bottom left) and air excess ratio (bottom right)

The overall air excess ratio λ is based on the measured air flow and fuel consumption and presented at the bottom right of Figure 4.9. The combined effect is a decrease of air excess with increasing load.

4.3.3. NO_x and NO emissions

Although the model aims at the prediction of NO, also NO_x is measured. Measurements in each operating point are performed three times. The results are within a 5% range. The measured values in PPMv are also made specific with respect to time and delivered energy. The results are presented in Figure 4.10.
The assumption that the NO_x-emission from a diesel engine mainly consists of NO, can now be quantified.

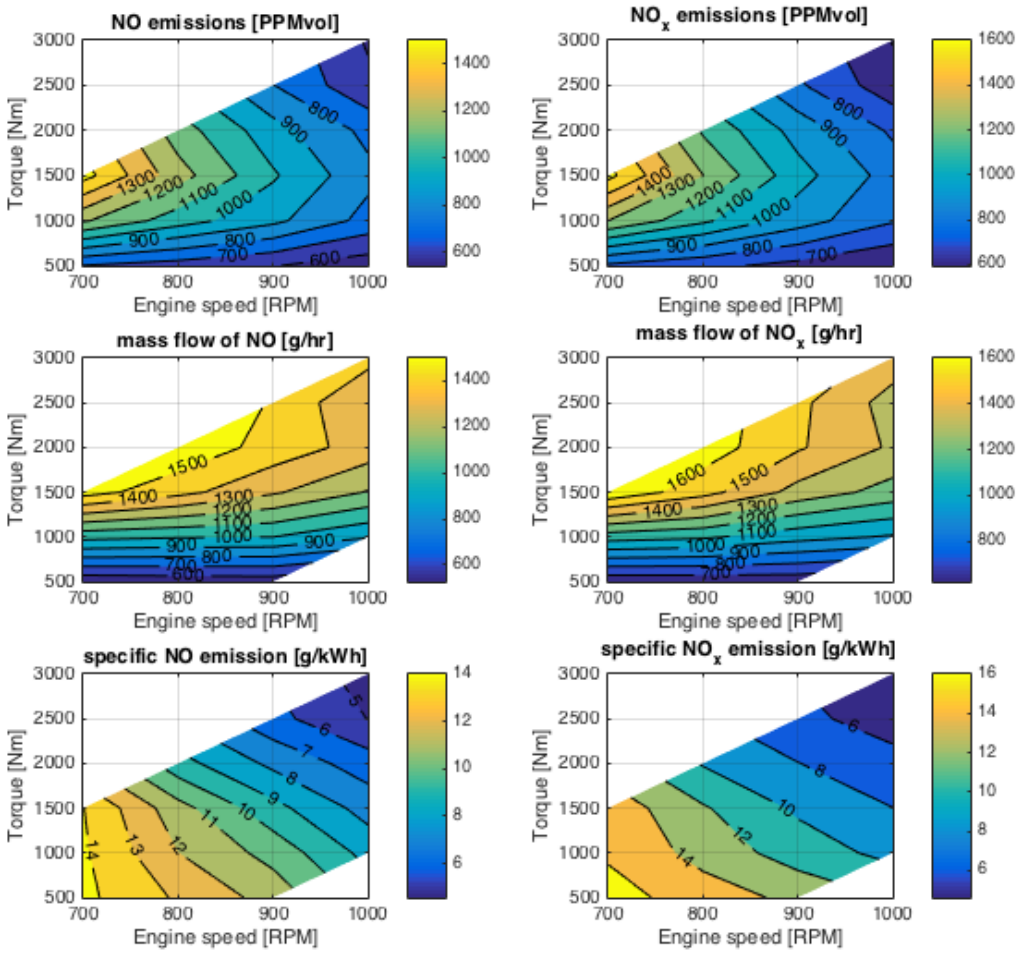

Figure 4.10: Measured NO (left column) and NO_x (right column) emissions in PPMV (top row), per hour (middle row) and specific emissions (bottom row)

From Figure 4.11 can be seen that the fraction of NO in NO_x is more than 90% based on volume. In the most frequently used power range - from a medium to a high power - the fraction is even larger (> 95%).

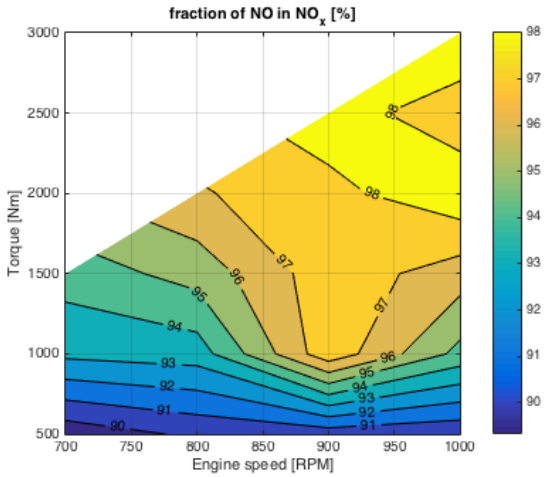

Figure 4.11: The measured volume fraction of NO in NO_x

5 Analysis

5.1. Introduction

In this chapter, the simulation model developed in Chapter 3 is matched with the measurements presented in Chapter 4. The original model formulated by Hohlbaum has a single tuning parameter: the air excess ratio in the flame front. Three of the original assumptions the model is based on prove relevant in this chapter:

- Zone I contains all mass at start of combustion and zone II no mass;
- Zone I contains no mass at exhaust valve opens and zone II contains all mass;
- The air flow passing the flame front is constant.

The first assumption determines the initial conditions for the simulation and will be discussed in the next section. Once the effect of the initial conditions on the simulation is discussed, an attempt is made to match the model using the air excess ratio as a tuning parameter. Since the tuning parameter proves insufficient to completely match the model to the measurements, the assumption regarding the air flow is examined in more detail in Section 5.4

5.2. Initial conditions

The initial conditions for the simulation are the enthalpy of the gas in the cylinder, the composition of the gas in the cylinder and the volume of zone I and II.
Two of the three required initial conditions for the simulation with the two zone model from SOC to EO, are known; the enthalpy comes from the pre-processing with the single volume model (see Appendix A) and the composition is taken to be air. This is not exactly true, since some residual gas will still be left in the cylinder. Based on the slip factor the approximation of the initial cylinder composition to be air, holds at higher loads, but at low loads a small error is introduced.

An initial condition which is more difficult to obtain is the initial volume of zone I and zone II. Hohlbaum suggested the assumption that zone II holds no mass at SOC. In order to investigate the influence of the initial volumes, simulations are performed with different initial volume of zone II.
Differences in results are significant in two areas of interest. First, the initial volume of zone II influences the temperature development of zone II. Temperature largely influences the formation of NO. Second, the calculated fuel consumption differs for different initial conditions for the volume of zone II. The effect of the initial volume of zone II is presented in Figure 5.1 for an operating point at 900 RPM and 1500 Nm torque.
Fuel consumption is a measured quantity. For example, at the operating point presented in Figure 5.1 there is 0.0631 mol of fuel injected in a cylinder each cycle. Therefore, at this specific operating point, an initial volume for zone II of 10%, gives a simulated fuel consumption that best matches the measured fuel consumption. The effect of the initial volume on fuel consumption in the simulation is the same in all points investigated. A small zone II results in more fuel consumption.
The increase in fuel consumption associated with a small initial volume of zone II is explained by the fact that the low air excess ratio in the small volume, has a smaller contribution to overall density than a larger

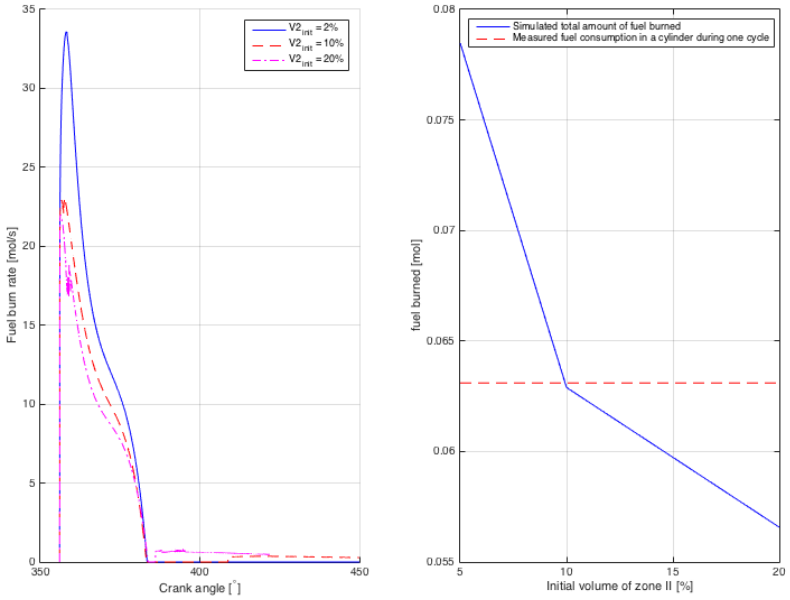

Figure 5.1: The burn rate of fuel (left) and the total amount of fuel burned (right) at 1500 Nm torque and 900 RPM

volume with a slightly higher air excess ratio.

The amount of fuel injected is calculated in a control loop based on the difference between the cylinder volume and the combined volume of zone I and zone II. The relative difference between he cylinder volume and the combined volume of zone I and zone II is presented in Figure 5.2. At a smaller initial volume of zone II, more fuel is injected, resulting in a larger combined volume of zone I and zone II. In order to 'match' the volumes, more heat should be lost during expansion. The extra fuel injected just after SOC, has to be dissipated in order to match the measured pressure and volume. As confirmed by fuel measurements, too small of an initial volume of zone II results in an over-estimation of fuel consumption. This leads to an energy increase within the volume, that is too large for the later part of the expansion process. This can be seen in Figure 5.2 (bottom left, green line) for an initial volume of zone II of 2% of the cylinder volume. A minimum initial volume of zone II is 5% of the cylinder volume is required to keep the combined volume of zone I and zone II within the cylinder volume.
The results for an initial volume of zone II of 5%,10% or 20% can give a relative difference less than 0.5%, which is satisfying. When the initial volume of zone II is chosen too large, the difference between the combined volume of zone I and zone II, also becomes larger. This is due to the fact that there are relative much molecules at a higher temperature, increasing the volume occupied by these molecules. The results for four different operating points are presented in Figure 5.2.

The estimation of the initial volume of zone II is done at each operating point based on measured fuel consumption. The measured and simulated fuel consumption is compared for four different operating points. The points are at 900 and 1000 RPM and at 2000 and 2500 Nm. In this part of the engine operating envelope the slip factor is positive. Simulations are performed for three different initial values for the volume of zone II. The relative difference in fuel consumption for these four operating points and three initial volumes is presented in Figure 5.3. The relative difference is defined as:

$$\text{relative difference} = \frac{\text{simulated value - measured value}}{\text{measured value}} \cdot 100\% \tag{5.1}$$

Although the trend is the same for the four operating points, no single value for the initial volume can be found that matches the simulated fuel consumption to the measured value.
As mentioned at the begin of this section, the temperature of the gas in zone II is also affected by the choice

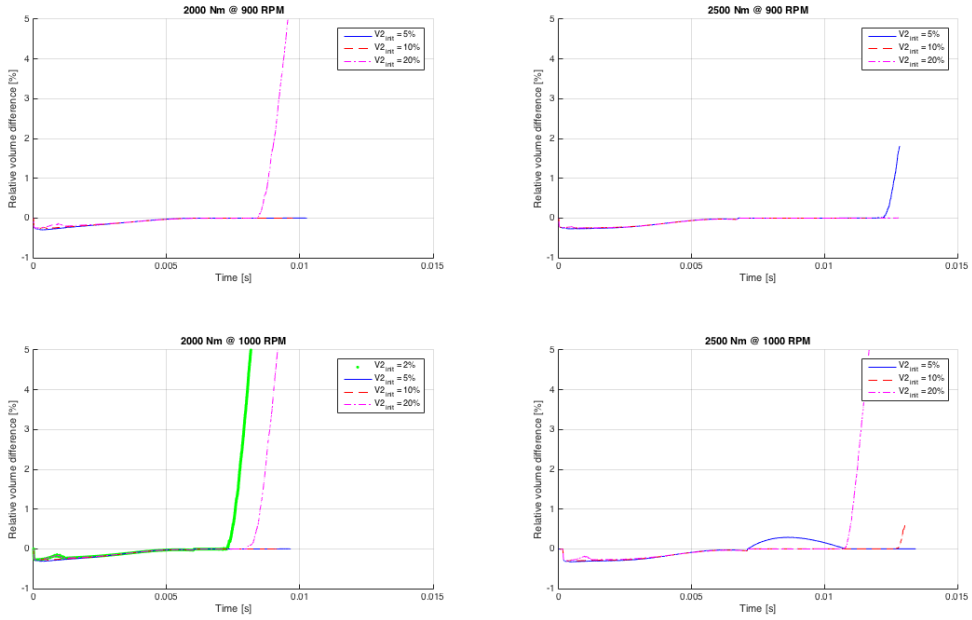

Figure 5.2: The relative difference between the cylinder volume and the combined volume of zone *I* and zone *II* for different initial volumes of zone *II*

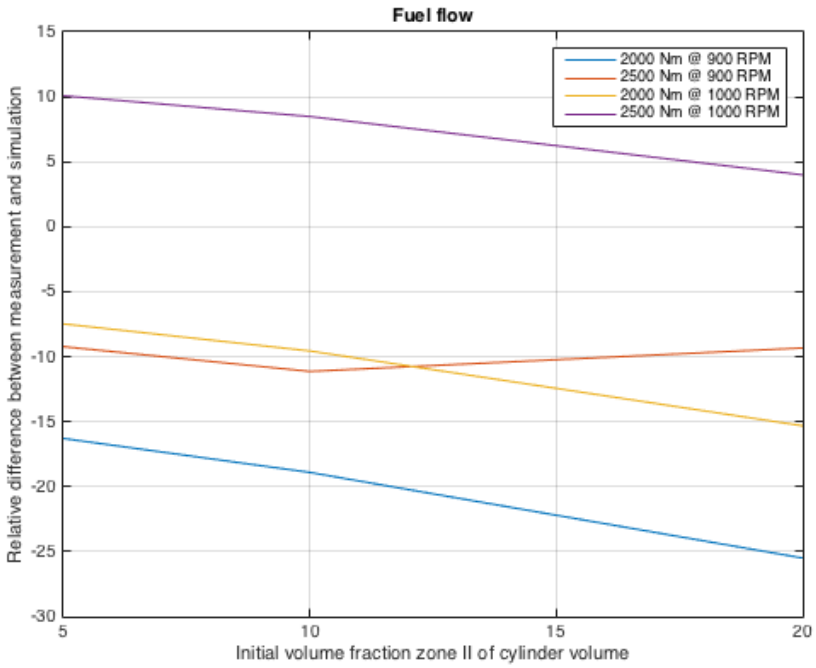

Figure 5.3: The relative difference between simulated and measured fuel consumption

of initial volume of zone II. In Figure 5.4 the temperatures of zone II are presented for three different initial volumes of zone II. The example presented is at the same operating point as described before: 900 RPM and 1500 Nm torque.
A larger initial volume of zone II results in significantly lower temperatures in zone II. As temperature strongly influences NO formation, the correct choice of the initial volume is of essence.

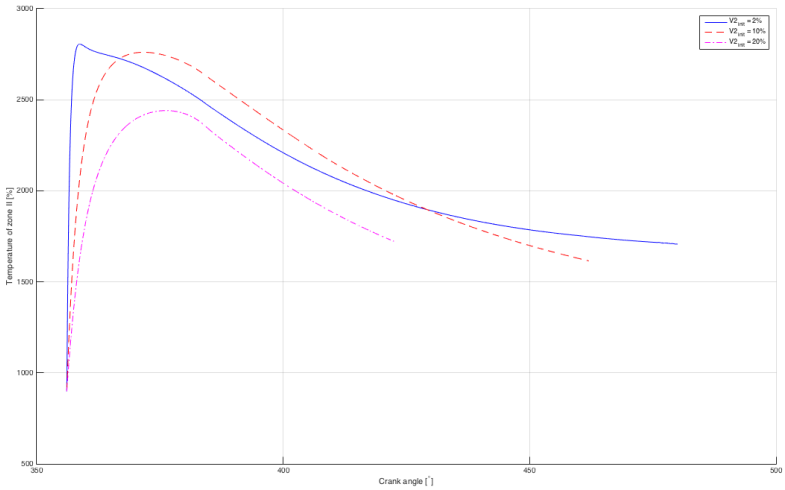

Figure 5.4: The temperature of zone II at 1500 Nm torque and 900 RPM

5.3. Tuning the air excess ratio in the flame front

The simulated temperature and composition are used to calculate the NO formation within zone II of the cylinder. The concentration of NO is calculated based on the total number of mol in the cylinder and corrected for the scavenge flow through the engine. The four operating points under consideration all have a positive slip factor and residual gas at IC is assumed to be negligible.
Details of the input to the NO-formation model are presented in Appendix D. The results for an air excess ratio of 0.7 in the flame front using only the forward reaction kinetics are presented in Figure 5.5 (left). The calculated emission are high compared to the measured emissions. When also considering the reverse reaction under the assumption of quasi steady-state, as described in Section 3.3.7, results are more in line with measurements. However, the relative deviation can still be large for some initial values of the volume of zone II.

There is an initial volume in which the simulated NO-emission matches the measured NO emission. However, since the fuel flow is not matched between simulation and measurement, results provide little insight.

Since it is not possible to match both the fuel consumption and the NO emissions with measurements using the same initial conditions, tuning is required. Until now, the air excess ratio in the flame front is kept constant at 0.7. By adjusting this parameter, the model can be tuned. In Figure 5.6 the results for three different values of the air excess ratio λ are presented. The air excess ratio does influence the amount of fuel injected. The relative difference between the measured and simulated fuel flow, does not show a combination of air excess ratio and initial volume of zone II, that will match the fuel flow exactly.
The calculated NO fraction in the flue gas is also influenced by the choice of the air excess ratio. Although there are combinations for the air excess ratio and the initial volume of zone II where the relative error in NO emissions is zero, no single combination can be identified as the correct solution. Especially, since the fuel flow is not correctly matched.

The simulated fuel flow into the cylinder is between 6 and 17% lower than the measured fuel flow. The evaporation of fuel is not modeled, as suggested by Hohlbaum. Modeling the evaporation of fuel would in-

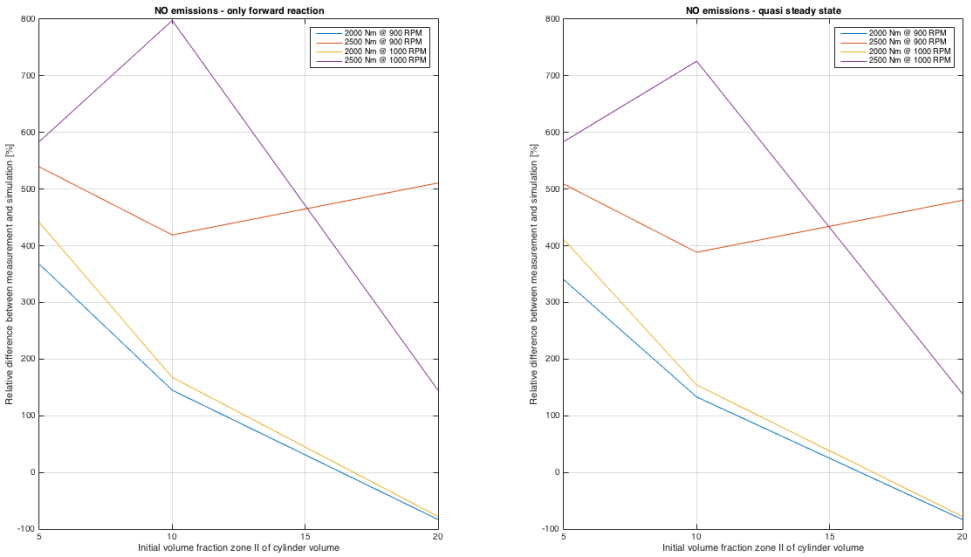

Figure 5.5: Relative difference between simulated and measured NO results for different initial volumes of zone II considering only the forward reaction kinetics (left) and under the quasi steady-state approximation (right)

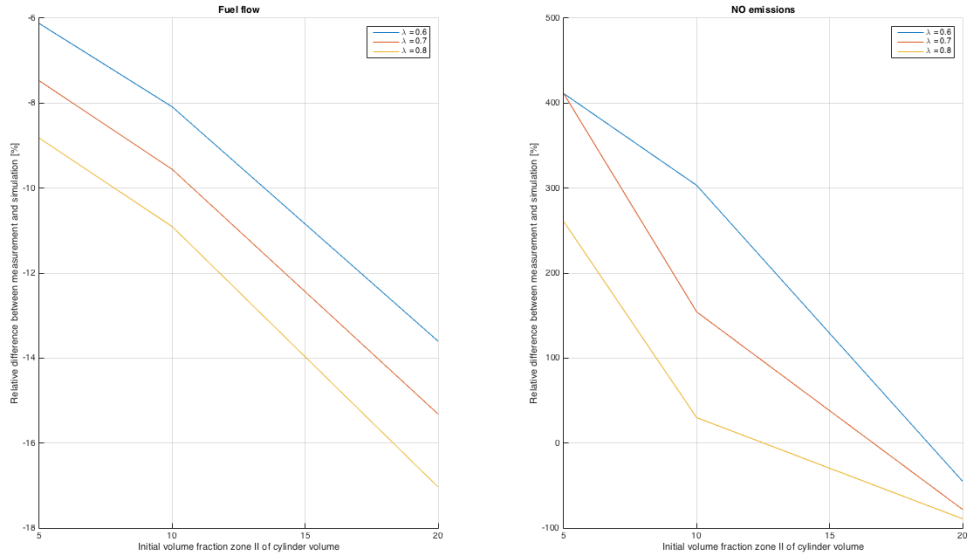

Figure 5.6: The relative difference between simulated and measured fuel flow (left) and NO fraction in the flue gas (right) for different air excess ratios in the flame front

clude two effects. Firstly, heat would be required to evaporate the fuel. The energy used to evaporate the fuel would lower the temperature in the cylinder. Secondly the fuel, especially when evaporated, would occupy volume.
The first effect would lead to more fuel addition, since fuel flow is a controlled variable. The second effect would reduce the fuel flow to the cylinder, also since the fuel flow is a controlled variable. The combined effect is difficult to estimate, but would certainly not increase calculated fuel consumption by 10 percent or more.
A lower temperature in zone II would decrease the NO-formation and bring it closer to the measured values. The fuel flow is best matched at a small initial volume of zone II and at a relative low air excess ratio in the flame front. For the NO-formation the opposite holds: a small initial volume of zone II and relative low air excess ratio, the matching shows a large deviation, where the simulated value is up to 4 times the measured value. Although NO-formation is strongly dependent on temperature, it is doubtful if inclusion of the evaporation of fuel would reduce the NO-formation by a factor 4.

5.4. Adapting the air flow passing the flame front

The air excess ratio as only tuning parameter provides too little possibilities to tune the model to correctly simulate fuel flow and NO-emissions. The air flow passing the flame front is assumed to be constant. As is explained in Appendix B, it is not possible to calculate the air flow passing the flame front based on the measurement data available. However, it is possible to modify the assumptions with respect to the air flow passing the flame front. The assumption that all gas is in zone II at EO is kept. So, at the time the exhaust valve opens, the cylinder is assumed to be perfectly mixed. The amount of air that passes the flame front from SOC to EO is determined by the initial volume of zone II, which also fixates the initial volume of zone I.
Next to a constant air flow passing the flame front, two different assumptions are evaluated. An air flow that is initial zero and linearly increases and an air flow that is initially at its maximum value and decreases linearly to zero at EO. Of course, many other shapes of the air flow profile are possible, but the purpose now is to see if there is a solution where the simulated fuel flow matches the measured fuel flow.

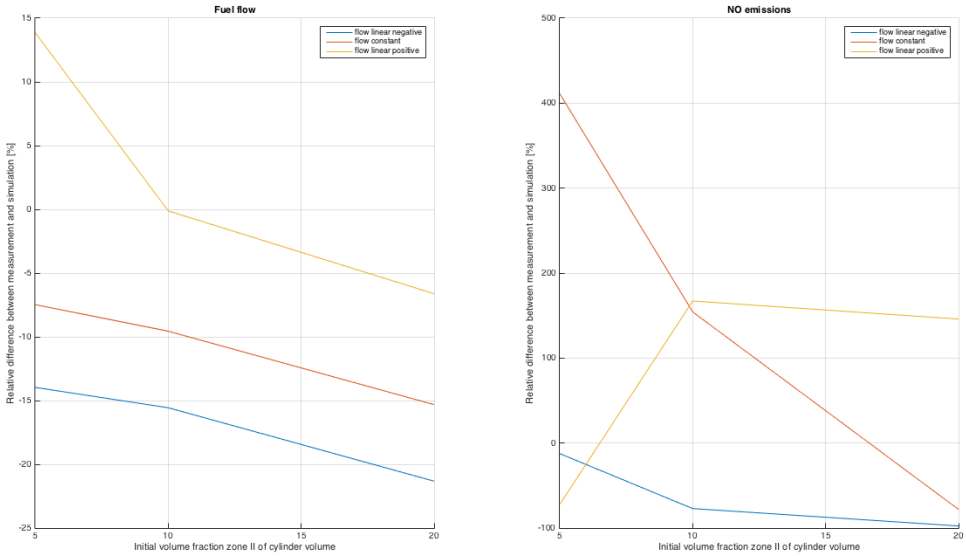

Figure 5.7: The relative difference between simulated and measured fuel flow (left) and NO fraction in the flue gas (right) for different profiles of the air flow passing the flame front

Figure 5.7 shows the results for the three assumed profiles for the air flow passing the flame front. The results for the fuel flow using a linear positive flow profile match the measured values at an initial volume of zone II of 10%. However, the NO emissions calculated are over twice the measured values.

5.5. Conclusions

Hohlbaum concludes his work stating *the agreement between measured and calculated results is pretty good* [18]. The results obtained by Hohlbaum are not reproduced by the model developed. The assumption that zone II holds no mass at SOC, results in to much fuel injected in the first part of the combustion process. This leads to an excess of energy within the volume and therefore a combined volume of zone I and zone II that is larger than the cylinder volume. An initial volume of zone II between 5 and 20% of the total cylinder volume, results in a relative volume difference between the combined volume of zone I and zone II and the cylinder volume of less than 0.5%, which is acceptable.

The air excess ratio in the flame front is a tuning parameter for the model. Using only this parameter it is not possible to match the simulated and measured fuel flow correctly. A difference between 6 and 17% remains depending on initial volume of zone II and the chosen air excess ratio in the flame front. The main downside is not only the relative difference, but also the inability to use the fuel flow to find the correct initial volume of zone II.

The evaporation of fuel is not modeled, as suggested by Hohlbaum. The evaporation of fuel would require heat, increasing fuel flow, but on the other hand fuel would occupy volume, reducing the fuel flow. The combined effect is difficult to estimate, but would not increase simulated fuel flow by 10 percent or more.

An adaption of the profile of the air flow passing the flame front makes it possible to match the simulated and measured fuel flow. The corresponding simulated NO-emission is larger than the measured value. Although an exact matching is not performed, there could be a flow profile of the air passing the flame front, that matches both fuel consumption and NO emissions.

6

Conclusions and recommendations

6.1. Introduction

The proposed model is intended to estimate NO-formation. Regulations on NO_x emissions have become more stringent in the past decades and are expected to do so even more in the future. Future regulations might also include transient restrictions on emissions. Efforts should be focussed on reducing emissions under real operating conditions. Simulation models can be useful to understand and predict emission behavior of engines.

Hohlbaum has suggested a model approach to predict NO emissions and claimed pretty good agreement between simulated and measured results [18]. The inclusion of gas properties by means of an equation of state was seen as an opportunity to reduce the uncertainty with respect to the air flow passing the flame front in the model.
The goal was to obtain an accurate estimation of NO-formation with as little as possible tuning parameters to simplify the matching process. The model is formulated based on state parameters which are also useful/commonly used in other components in a diesel engine, such as the compressor and turbocharger.

6.2. Conclusions

6.2.1. Model formulation

In the model two zones with spacial averaged temperatures and compositions are uses to represent the cylinder volume. The composition is calculated under the assumption the equilibrium is instantaneously reached. Composition, temperature and residence time at a higher temperature influence NO-formation. Obtaining a representative average temperature profile in the zone where combustion occurs is critical to accurately predict NO formation.

The chosen state variables are pressure p, specific enthalpy h and composition y. For a closed system internal energy u is generally used in model formulations. The advantage of using the enthalpy is simplifying the coupling of the in-cylinder model to the other flow models in the system, such as turbo-machinery and heat exchangers. The crank-angle based model would, opposed to models based on the Seiliger-process not need a distinction between the open and closed part of the process.
In this thesis only the closed part of the cycle is investigated and a formulation based on internal energy would also suffice. However, within the 2-zone model there are two distinct flows between zone I and zone II. The energy accompanying these flows is captured using the enthalpy.

The gas properties are calculated using a FluidProp library. The equation of state is thereby separated from the conservation equations. This choice allows a change of equation of state without alteration of the model. In this thesis the choice is made to use the Ideal Gas approximation, since it is most commonly used in diesel engine simulation models. A more appropriate choice for the gas mixture inside the cylinder is Peng-Robinson or Soave-Redlich-Kwong with van der Waals one fluid mixing rules [23].

A single zone sub-model is implemented. The results of the single zone model from IC to SOC are used to determine the initial values in the two zone model. The advantage of this formulation, next to the enthalpy as state variable, is the component balance. The component balance allows the calculation of gas properties based on composition. Due to the lower average temperature of the gasses in the cylinder, effects of dissociation will be less in the OHC-equilibrium. However, effects of a change in H/C-ration in the fuel can be simulated.

6.2.2. Differences with Hohlbaum

The starting point of this thesis was the model approach suggested by Hohlbaum. The additional use of an equation of state seemed an opportunity to also use the available measured time-dependent cylinder volume. The original formulation has only one tuning parameter: the air excess ratio in the flame front. Two possible improvements to the original model identified by Merker, are the division of the heat loss between zone I and zone II and the assumption of a constant flow passing the flame front [19].

The additional constraint that the combined volume of zone I and zone II must be equal to the cylinder volume, required a change in the original assumptions posed by Hohlbaum. The fuel added to the flame front is a controlled variable. By varying the fuel flow to the flame front, the combined volume of zone I and zone II is kept equal to the cylinder volume. The assumption that zone II holds no mass at the start of combustion, leads to an increase in fuel injection in the beginning of the combustion proces.This required fuel injection is larger than measured. The energy contained in this amount of fuel is more than required in the later part of the combustion process, resulting in deviation between simulated and measured variables.

The assumption that zone II holds no mass gives undesirable results and is dropped, introducing a new tuning parameter, the initial volume of zone II. Matching the simulated fuel consumption to the measured fuel consumption by varying the initial volume of zone II proved not possible for the four operating points investigated. The initial volume of zone II is varied between 5% and 20% of the total cylinder volume. A smaller initial volume resulted in the combined volume of zone I and zone II much larger than the cylinder volume in the second half of simulation time. Trends where generally unfavorable to use larger initial volumes of zone II.
The air excess ratio in the flame front, initially identified as a tuning parameter, is varied around the advised value of 0.7 between 0.6 and 0.8. Although a shift in fuel consumption is seen, it proved insufficient to match simulated values to the measured values.

In order to investigate wether it is possible at all to match the simulated fuel flow to the measured fuel flow, an adaption to the model is made. The air flow passing the flame front is no longer kept constant. Determining the air flow passing the flame front is possible when detailed information of the injection is available combined with an evaporation-model for the fuel. The measurement set-up only allowed for fuel consumption measurements. Therefore, two different flow profiles for the air passing the flame front, are investigated. One profile started with no air passing the flame front and mass flow linear increasing. The other started with the maximum mass flow passing the flame front and linear decreasing during simulation, reducing to zero at EO. Both profiles kept the original assumption that all mass is contained in zone II at EO.
The linear positive flow makes it possible to match the simulated and measured fuel consumption at the investigated operating point. This supports the hypothesis that a correct choice of the flow profile of the air passing the flame front, makes it possible to match simulated fuel consumption to the measured fuel consumption, by tuning the initial volume of zone II.

The introduction of the initial volume of zone II as an additional tuning parameter and the uncertainty in the flow profile of the air passing the flame front, increase the matching effort required. The initial ease of use of the formulation with only one tuning parameter is reduced. On the other hand, the requirement that the combined volume of zone I and zone II must be equal to the cylinder volume improves the physical representation of the cylinder proces.

6.2.3. Results

A MAN 20L27 diesel engine located at the Royal Netherlands Naval Academy was available for measurements. Engine data and emissions are measured in 18 different operating points within the engine operating envelope. At low loads at all engine speeds, the slipfactor became negative, indicating insufficient scavenging and

back flow. Four operating points at higher load and engine speed are used to investigate the simulation results.
The attempt to match the simulated fuel consumption to the measured fuel consumption by varying the initial volume of zone II, resulted in differences considered too large. For most considered operating points the best found value resulted in a relative difference in fuel consumption over 5%. Since matching the fuel consumption failed for this situation, little can be said regarding the NO-emission simulation results. In general for the four operating points investigated, including the reverse reaction for NO formation, gives some improvement to the results.

For the operating point at 2000 Nm and 1000 RPM the influence of the air excess ratio in the flame front is investigated. A variation of the air excess ratio between 0.6 and 0.8 resulted in the smallest relative difference between simulated and measured fuel consumption of -9% and -6% at the smallest value of initial volume of zone II. The matching could not be performed to sufficient accuracy. The best matching point for the fuel consumption, resulted in the largest deviation between simulated and measured NO-emissions.

For the operating point at 2000 Nm and 1000 RPM, changing the flow profile made it possible to match the simulated fuel consumption to the measured fuel consumption at an initial volume of zone II of 10% of the cylinder volume. The simulated NO emission is 2.7 times larger than the measured NO emission of the diesel engine under consideration in this operating point.

6.3. Recommendations

Adapting the flow profile of the air passing the flame front, made it possible to match the simulated fuel consumption to the measured fuel consumption for the operating point considered. A more complete analysis of the air flow passing the flame front, could give a single satisfying matching procedure.
Measurements of the injection profile where not possible for the engine under consideration. Performing such measurements, would allow analytical evaluation of the air flow passing the flame front, since fuel flow no longer needs to be a controlled variable.
Either of these two options influences the temperature, volume and the composition in zone II, which all influence to the NO formation. This seems an important next step to improve the predictive capability of the model.

The heat loss is modeled using the experimental equation proposed by Woschni, which is commonly used for diesel engine models. Ding [2011] experienced difficulty using this formulation for the MAN engine which is used for the measurements in this thesis. The uncertainty in determination of the parameters should be reduced to increase accuracy of the heat loss model.
Furthermore the ratio of heat loss between zone I and zone II is based on the assumption of Hohlbaum. Since NO-formation is strongly dependent on temperature, the correct estimation of the heat loss in each zone is of importance. Obtaining a more accurate heat loss for each zone, improves the accuracy of the model.

The evaporation of fuel is not modeled, as suggested by Hohlbaum. The simulated fuel flow is lower than the measured fuel flow. The inclusion of a fuel evaporation model might increase the simulated fuel flow. Although it might not completely match the fuel flow or improve the models NO predictive capability, it is interesting to investigate the effect.

The model formulation allows for implementation of the cylinder-model within a complete diesel engine model, such as the DE-B model developed at Delft University. Using such an implementation, more complex interaction between turbo-machinery and the cylinder process can be investigated. Such an approach would require a simulation model for the valves. Simulation time will increase significantly compared with a Seiliger-formulation and time-scales within the model will differ widely in dynamic simulation. Nonetheless insight might be gained in the complex interaction in a diesel engine in dynamic operating conditions.

During measurements a distinct high frequency was present in the pressure signal. This might be a Helmholz frequency. Further analysis of this phenomena, decreasing it by adapting the measurement channel or modeling it in order to convert the measured pressure signal more accurately to the actual in-cylinder pressure is recommended.

A

Model equations

A.1. Two zone model

In both zones of the model conservation of mass, the energy balance and the composition balance are solved. All equations are solved for both zones separately. The resulting output volumina V_1 and V_2 must be equal to the cylinder volume V_{cyl} at each point in time.

Conservation of mass states:

$$\frac{dV}{dt} = \frac{1}{\overline{\rho}}\left(\left[f_{in} - f_{out}\right] - V\xi\frac{d\overline{h}}{dt} - V\psi\frac{dp}{dt} - V\chi_I\frac{dN_i}{dt}\right) \tag{A.1}$$

The energy equation yields:

$$\frac{d\overline{h}}{dt} = \frac{f_{in}\overline{h}_{in} - f_{out}\overline{h}_{out} + \dot{Q}_{\text{loss}} - V\left(1-\overline{h}\psi\right)\frac{dp}{dt} - \overline{\rho}\overline{h}\frac{dV}{dt} - V\overline{h}\chi\frac{dN_i}{dt}}{V\left(\overline{\rho}+\overline{h}\xi\right)} \tag{A.2}$$

The volume and enthalpy are calculated using:

$$V = \int \frac{dV}{dt}dt \tag{A.3}$$

and

$$\overline{h} = \int \frac{d\overline{h}}{dt}dt \tag{A.4}$$

The incoming and leaving mass flows are converted into molair flows:

$$\dot{N}_{i,k} = y_{i,k}\frac{f_k}{M_{k,\text{gas}}} \tag{A.5}$$

for the i-th specie in the k-th flow. The change in composition due to the occurring reaction is calculated in the OHC-equilibrium. The flows in zone 1 are $k = [f_E, f_F, f_A]$ and in zone 2 $k = [f_F, f_A, f_L]$. The change in a specie due to a chemical reaction is:

$$\left.\frac{dN_i}{dt}\right|_{\text{reaction}} = K_{\text{reaction}}\left(N_{i,\text{OHC-equilibrium out}} - N_{i,\text{volume}}\right) \tag{A.6}$$

where $N_{i,\text{volume}}$ is the number of mole of the specie in the volume and $N_{i,\text{OHC-equilibrium out}}$ the number of mole of a specie from the OHC-equilibrium. The parameter K_{reaction} holds the dimension [1/s]. It can be interpreted as 'number of times the content of the cylinder passes through the OHC-equilibrium calculation per second'. The parameter is set to $K_{\text{reaction}} = 10^5$ [1/s].

The total number of mole of each specie is calculated using:

$$N_i = \int\left(\left.\frac{dN_i}{dt}\right|_{\text{reaction}} + \sum_{k=1}^{\mathscr{F}}\dot{N}_{i,k}\right)dt \tag{A.7}$$

for all the $\mathscr{F}$ flows entering and leaving the volume the volume.

The effect of a small change in the amount of one specie δN_i on the density is calculated while keeping the amount of the other species constant:

$$\chi = \left(\frac{\delta\rho}{\delta N_i}\right)_{p,\overline{h},N_{j\neq i}} = \frac{\rho\left(p,\overline{h},\frac{N_1}{N_{\text{tot}}+\delta N_i}\ldots\frac{N_i+\delta N_i}{N_{\text{tot}}+\delta N_i}\ldots\frac{N_{\mathscr{N}}}{dN_{\text{tot}}+\delta N_i}\right)-\rho\left(p,\overline{h},\frac{N_1}{N_{\text{tot}}}\ldots\frac{N_i}{N_{\text{tot}}}\ldots\frac{N_{\mathscr{N}}}{dN_{\text{tot}}}\right)}{\delta N_i} \tag{A.8}$$

where N_{tot} is the total amount of species in the volume. The change in density over time due to the reaction in the flame front and due to the OHC-equilibrium reaction in zone 2 is calculated using:

$$\left.\frac{d\rho}{dt}\right|_{\text{reactions}} = \sum_{i=1}^{\mathscr{N}}\left(\frac{\delta\rho}{\delta N_i}\right)_{p,h,N_{j\neq i}}\left[\left.\frac{dN_i}{dt}\right|_{\text{reaction}}+\left.\frac{dN_i}{dt}\right|_{\text{flame front}}\right] \tag{A.9}$$

The properties of the gas in each zone are calculated using FluidProp.

$$\xi = \left(\frac{\delta\overline{\rho}}{\delta\overline{h}}\right)_{p,N_i} = f(p,\overline{h},[N_1\ldots N_{\mathscr{N}}]) \tag{A.10}$$

$$\psi = \left(\frac{\delta\overline{\rho}}{\delta p}\right)_{\overline{h},N_i} = f(p,\overline{h},[N_1\ldots N_{\mathscr{N}}]) \tag{A.11}$$

$$\overline{\rho} = f(p,\overline{h},[N_1\ldots N_{\mathscr{N}}]) \tag{A.12}$$

$$T = f(p,\overline{h},[N_1\ldots N_{\mathscr{N}}]) \tag{A.13}$$

The leaving enthalpy is assumed to be equal to the average enthalpy in the volume:

$$h_{out} = \overline{h} \tag{A.14}$$

	zone 1	zone 2
flow entering	air from inlet receiver f_E	air from zone 1 f_A and fuel injected f_F
flow leaving	air to zone 2 f_A	air to exhaust receiver f_L
inputs	f_E (zero from IC to EO) h_E (based on IR conditions) f_A(based on assumption) $\dot{Q}_{\text{loss},I}$ (Woschni and Hohlbaum) p (from measurements)	f_L (zero from IC to EO) f_A (based on assumption) f_F (controlled variable using $\frac{dV_I}{dt}+\frac{dV_{II}}{dt}=\frac{dV_{cyl}}{dt}$ $\dot{Q}_{\text{loss},II}$ (Woschni and Hohlbaum) p (from measurements)
outputs	T_I, $N_{i,I}$	T_{II}, $N_{i,II}$
parameters	K_{reaction}	K_{reaction}
initial conditions	V_I $\overline{h}_I$ $N_{i,I}$	V_{II} $\overline{h}_{II}$ $N_{i,II}$

Remarks:

- The flow of air from zone 1 to zone 2 f_A is the combination of two assumptions:
  1. Primary combustion occurs at an air excess ratio of $\lambda = 0.7$. This part of the air flow is directly dependent on the fuel flow into zone 2.
  2. At start of combustion (SOC) volume 1 contains (almost all) gas and volume 2 is (almost) empty. When the exhaust valve opens (EO) zone 1 is empty and volume 2 holds all gas. This part of the air flow is (for now) considered to be constant.
- The amount of fuel injected is a controlled variable. The volume of zone 1 and zone 2 together should equal the cylinder volume. When the combined volume of zone 1 and zone 2 are smaller than the cylinder volume, more fuel is injected. During the first part of combustion (approx. first half between SOC en EO) sufficient accuracy is obtained (within 0.5 %). During the later part of simulation the required amount of fuel injected can become negative. This is physically not possible and therefore limited to zero. This is an indication that the loss predicted using Woschni is too low.

- An initial volume of zone 2 of 2% of the total cylinder volume, results in (very) high temperatures (Hohlbaum suggested that volume 2 holds no mass at SOC). Simulations are now performed at initial volume of zone 2 of 2, 10 and 20 %, to see effects on NO-formation.
- The initial composition of both volume 1 and zone 2 is assumed to be air. Residual gas remaining in the cylinder from previous cycles is neglected.

The cylinder volume is calculated using:

inputs	N_{eng}
outputs	dV/dt, α, $d\alpha/dt$
parameters	L_S, L_{CR}, D_B
initial conditions	$\alpha(t=0)$

The solving system of equations is:

$$\frac{dV}{dt} = \frac{1}{2} V_S \left[\sin\alpha + \lambda_{CR} \left(\frac{\sin\alpha\cos\alpha}{\sqrt{1-\lambda_{CR}^2 \sin^2\alpha}} \right) \right] \frac{d\alpha}{dt}$$

$$V_S = \pi \left(\frac{D_B}{2} \right)^2 L_S$$

$$\frac{d\alpha}{dt} = 2\pi N_{eng}/60$$

$$\lambda_{CR} = \frac{R_{CR}}{L_{CR}} = \frac{L_S/2}{L_{CR}}$$

The empirical formulation for the heat loss according to Woschni is implemented. The total heat loss is given by:

$$\dot{Q}_{loss} = \sum \alpha_{HT} A_i (T_{gas} - T_i) \tag{A.15}$$

where i represents the different parts of the engine (e.g. cylinder liner, piston and cylinder crown). The heat transfer coefficient between gas and wall is given by:

$$\alpha_{HT} = C_1 \frac{1}{D_B^{0.214}} \frac{p^{0.786}}{T^{0.525}} \left(C_3 c_m + C_4 \frac{p - p_0}{p1} \frac{V_S}{V_1} T_1 \right)^{0.786} \tag{A.16}$$

The coefficients in the model are:

$$C_1 = 130 \qquad \text{estimated by Ding} \tag{A.17}$$

$$C_3 = 6.18 + 0.417 \frac{w_t}{c_m} \qquad \text{for the Gas Exchange} \tag{A.18}$$

$$C_3 = 2.28 + 0.308 \frac{w_t}{c_m} \qquad \text{for compression and expansion} \tag{A.19}$$

$$C_4 = 0.00324 \ [\mathrm{m\ s^{-1} K^{-1}}] \qquad \text{for Direct Injection engines} \tag{A.20}$$

where the estimate of $w_t/c_m = 10$ for the MAN-engine at the NLDA is taken from Ding. T

$$p_0 = f(p_{IR}, \alpha) \tag{A.21}$$

The pressure loss over the inlet valve(s) is assumed to be negligible, therefore $p_1 = p_{IR}$. The mean piston speed c_m is calculated using:

$$c_m = 2 L_S N_{eng}/60 \tag{A.22}$$

with the engine speed N_{eng} in [RPM]. The stroke volume is calculated using the bore diameter D_B and the stroke length L_S.
In the 2-zone model a division is made between the loss in zone 1 and the loss in zone 2. The solution proposed by Hohlbaum is adapted:

$$\frac{\dot{Q}_{\mathrm{loss},I}}{\dot{Q}_{\mathrm{loss},II}} = \left(\frac{m_1}{m_2} \right)^2 \frac{T_1}{T_2} \tag{A.23}$$

where the two flows equal the total heat loss $\dot{Q}_{\mathrm{loss},1} + \dot{Q}_{\mathrm{loss},2} = \dot{Q}_{\mathrm{loss,\ tot}}$. Since the division in two flows does not influence the total amount of heat lost.

inputs	p, T, p_{IR}, N_{eng}, α, valve position, A_i, T_i, T_{gas}
outputs	$\dot{Q}_{loss}$, $\dot{Q}_{\text{loss},I}$, $\dot{Q}_{\text{loss},II}$
parameters	D_B, L_S, V_1, T_1, C_1,w_t/c_m,C_4, $p_0 = f(p_{IR})$
initial conditions	-

The rate of formation of NO is given by:

$$\frac{d[NO]}{dt} = 2k_{N,1f}[O]_{eq}[N_2]_{eq} \tag{A.24}$$

The concentration of $[NO]$ (unit $[kmol/m^3]$) can also change as a consequence of a volume change:

$$\frac{d[NO]}{dt} = \frac{d}{dt}\left(\frac{N_{NO}}{V}\right) = \frac{1}{V}\frac{dN_{NO}}{dt} + N_{NO}\frac{d\frac{1}{V}}{dt} \tag{A.25}$$

where the first term on the RHS represents the formation of NO and the second term on RHS represents the effect of volume change on the concentration. Now, only looking at the formation of NO:

$$\frac{1}{V}\frac{dN_{NO}}{dt} = 2k_{N,1f}[O]_{eq}[N_2]_{eq} = 2k_{N,1f}\frac{N_O}{V}\frac{N_{N2}}{V} \tag{A.26}$$

Dividing by the volume results in the expression for the formation of NO:

$$\frac{dN_{NO}}{dt} = 2k_{N,1f}N_O N_{N2}\frac{1}{V} \tag{A.27}$$

where the forward reaction rate coefficient $k_{N,1f} = 1.8 \cdot 10^{11} exp(-38370/T)$ is highly temperature dependent (unit: $[m^3/kmol - s]$ and temperature in [K]). Further more NO-formation depends on the amount of O-radicals, N_2-atoms and the volume available. The total amount of NO formed is calculated based on integration:

$$N_{NO} = \int 2k_{N,1f}N_O N_{N2}\frac{1}{V}dt \tag{A.28}$$

inputs	$N_{O,eq}$, $N_{N_2,eq}$, V
outputs	N_{NO}
parameters	$k_{N,1f}$
initial conditions	N_{NO} (t = 0)

A.2. Single volume model

In the single volume model conservation of mass, the energy balance and the composition balance are solved. The cylinder volume V_{cyl} is calculated based on the crank-angle and engine parameters. The cylinder pressure p is as an output of the model.

Conservation of mass states:

$$\frac{dp}{dt} = \frac{1}{\psi}\left[\frac{1}{V}\left(f_{\text{in}} - f_{\text{out}} - \overline{\rho}(\overline{h}, p)\frac{dV}{dt}\right) - \xi\frac{d\overline{h}}{dt} - \chi\frac{dN_i}{dt}\right] \tag{A.29}$$

The energy equation yields:

$$\frac{d\overline{h}}{dt} = \frac{f_{in}\overline{h}_{in} - f_{out}\overline{h}_{out} + \dot{Q}_{\text{loss}} - V\left(1 - \overline{h}\psi\right)\frac{dp}{dt} - \overline{\rho}\overline{h}\frac{dV}{dt} - V\overline{h}\chi\frac{dN_i}{dt}}{V\left(\overline{\rho} + \overline{h}\xi\right)} \tag{A.30}$$

The pressure and enthalpy are calculated using:

$$p = \int \frac{dp}{dt}dt \tag{A.31}$$

and

$$\overline{h} = \int \frac{d\overline{h}}{dt}dt \tag{A.32}$$

The incoming and leaving mass flows are converted into molair flows:

$$\dot{N}_{i,k} = y_{i,k} \frac{f_k}{M_{k,\text{gas}}} \tag{A.33}$$

for the i-th specie in the k-th flow. The change in composition due to the occurring reaction is calculated in the OHC-equilibrium. The flows in the single volume model are $k = [f_E, f_L]$. The change in a specie due to a chemical reaction is:

$$\left.\frac{dN_i}{dt}\right|_{\text{reaction}} = K_{\text{reaction}} \left(N_{i,\text{OHC-equilibrium out}} - N_{i,\text{volume}}\right) \tag{A.34}$$

where $N_{i,\text{volume}}$ is the number of mole of the specie in the volume and $N_{i,\text{OHC-equilibrium out}}$ the number of mole of a specie from the OHC-equilibrium. The parameter K_{reaction} holds the dimension [1/s]. It can be interpreted as 'number of times the content of the cylinder passes through the OHC-equilibrium calculation per second'. The parameter is set to $K_{\text{reaction}} = 10^5$ [1/s].

The total number of mole of each specie is calculated using:

$$N_i = \int \left(\left.\frac{dN_i}{dt}\right|_{\text{reaction}} + \sum_{k=1}^{\mathscr{F}} \dot{N}_{i,k} \right) dt \tag{A.35}$$

for all the $\mathscr{F}$ flows entering and leaving the volume the volume.

The effect of a small change in the amount of one specie δN_i on the density is calculated while keeping the amount of the other species constant:

$$\chi = \left(\frac{\delta\rho}{\delta N_i}\right)_{p,\overline{h},N_{j\neq i}} = \frac{\rho\left(p,\overline{h},\frac{N_1}{N_{\text{tot}}+\delta N_i}\cdots\frac{N_i+\delta N_i}{N_{\text{tot}}+\delta N_i}\cdots\frac{N_{\mathscr{N}}}{dN_{\text{tot}}+\delta N_i}\right) - \rho\left(p,\overline{h},\frac{N_1}{N_{\text{tot}}}\cdots\frac{N_i}{N_{\text{tot}}}\cdots\frac{N_{\mathscr{N}}}{dN_{\text{tot}}}\right)}{\delta N_i} \tag{A.36}$$

where N_{tot} is the total amount of species in the volume. The change in density over time due to the reaction in the flame front and due to the OHC-equilibrium reaction in zone 2 is calculated using:

$$\left.\frac{d\rho}{dt}\right|_{\text{reactions}} = \sum_{i=1}^{\mathscr{N}} \left(\frac{\delta\rho}{\delta N_i}\right)_{p,h,N_{j\neq i}} \left[\left.\frac{dN_i}{dt}\right|_{\text{reaction}} + \left.\frac{dN_i}{dt}\right|_{\text{flame front}} \right] \tag{A.37}$$

The properties of the gas in each zone are calculated using FluidProp.

$$\xi = \left(\frac{\delta\overline{\rho}}{\delta\overline{h}}\right)_{p,N_i} = f(p,\overline{h},[N_1 ... N_{\mathscr{N}}]) \tag{A.38}$$

$$\psi = \left(\frac{\delta\overline{\rho}}{\delta p}\right)_{\overline{h},N_i} = f(p,\overline{h},[N_1 ... N_{\mathscr{N}}]) \tag{A.39}$$

$$\overline{\rho} = f(p,\overline{h},[N_1 ... N_{\mathscr{N}}]) \tag{A.40}$$

$$T = f(p,\overline{h},[N_1 ... N_{\mathscr{N}}]) \tag{A.41}$$

The leaving enthalpy is assumed to be equal to the average enthalpy in the volume:

$$h_{out} = \overline{h} \tag{A.42}$$

	single volume
flow entering	air from inlet receiver f_E and fuel injected f_F
flow leaving	air to exhaust receiver f_L
inputs	f_E and f_L (zero from IC to EO) h_E (based on IR conditions) f_F $\dot{Q}_{\text{loss, total}}$ (Woschni) V (from crank-angle and engine dimensions)
outputs	T_{SV}, $N_{i,SV}$
parameters	K_{reaction}
initial conditions	p_{SV} $\overline{h}_{SV}$ $N_{i,SV}$

Remarks:

- The amount of fuel injected is an input variable. In this thesis the single volume model is only used from IC to SOC. Therefore, the amount of fuel injected is set to zero (evaporation of the fuel is not taken into account). In order to be able to use the model for complete cycle calculations, fuel input should either be measured, calculated based on a HRR-model or controlled using the measured and calculated cylinder pressure.
- The initial composition of the single volume is assumed to be air. Residual gas remaining in the cylinder from previous cycles is neglected.

The cylinder volume is calculated using:

inputs	N_{eng}
outputs	dV/dt, α, $d\alpha/dt$
parameters	L_S, L_{CR}, D_B
initial conditions	$\alpha(t=0)$

The solving system of equations is:

$$\frac{dV}{dt} = \frac{1}{2} V_S \left[\sin\alpha + \lambda_{CR} \left(\frac{\sin\alpha\cos\alpha}{\sqrt{1-\lambda_{CR}^2 \sin^2\alpha}} \right) \right] \frac{d\alpha}{dt}$$

$$V_S = \pi \left(\frac{D_B}{2} \right)^2 L_S$$

$$\frac{d\alpha}{dt} = 2\pi N_{eng}/60$$

$$\lambda_{CR} = \frac{R_{CR}}{L_{CR}} = \frac{L_S/2}{L_{CR}}$$

The empirical formulation for the heat loss according to Woschni is implemented. The total heat loss is given by:

$$\dot{Q}_{loss} = \sum \alpha_{HT} A_i (T_{gas} - T_i) \tag{A.43}$$

where i represents the different parts of the engine (e.g. cylinder liner, piston and cylinder crown). The heat transfer coefficient between gas and wall is given by:

$$\alpha_{HT} = C_1 \frac{1}{D_B^{0.214}} \frac{p^{0.786}}{T^{0.525}} \left(C_3 c_m + C_4 \frac{p - p_0}{p1} \frac{V_S}{V_1} T_1 \right)^{0.786} \tag{A.44}$$

The coefficients in the model are:

$$C_1 = 130 \qquad \text{estimated by Ding} \tag{A.45}$$

$$C_3 = 6.18 + 0.417 \frac{w_t}{c_m} \qquad \text{for the Gas Exchange} \tag{A.46}$$

$$C_3 = 2.28 + 0.308 \frac{w_t}{c_m} \qquad \text{for compression and expansion} \tag{A.47}$$

$$C_4 = 0.00324 \ [\text{m s}^{-1}\text{K}^{-1}] \qquad \text{for Direct Injection engines} \tag{A.48}$$

where the estimate of $w_t/c_m = 10$ for the MAN-engine at the NLDA is taken from Ding. T

$$p_0 = f(p_{IR}, \alpha) \tag{A.49}$$

The pressure loss over the inlet valve(s) is assumed to be negligible, therefore $p_1 = p_{IR}$. The mean piston speed c_m is calculated using:

$$c_m = 2 L_S N_{eng}/60 \tag{A.50}$$

with the engine speed N_{eng} in [RPM]. The stroke volume is calculated using the bore diameter D_B and the stroke length L_S.

inputs	p, T, p_{IR}, N_{eng}, α, valve position, A_i, T_i, T_{gas}
outputs	$\dot{Q}_{loss}$
parameters	D_B, L_S, V_1, T_1, C_1,w_t/c_m,C_4, $p_0 = f(p_{IR})$
initial conditions	-

B

The difference in fuel consumption between a single zone and a two zone model

B.1. Introduction

A first modeling approach was based on the incorrect hypothesis that the way the in-cylinder process is modeled, does not affect the relation between input and output, since the cylinder proces that is represented by the model does not change. The idea was to combine a single volume model with a two zone model to gain more information (as is done in the model suggested by Heider et al. [15], where the results are based on the process calculation of the zero-dimensional single-zone model Merker et al. [19]).

The single volume model and the two zone model are operated parallel. The amount of fuel injected serves as an input and is calculated based on a HRR-model. The choice is made to use a double Vibe-function, since results obtained by Ding [10] where good for the engine under consideration. The cylinder pressure is calculated using the single volume model. The calculated pressure is assumed to be representative for a specific combination of fuel injected, heat loss and engine speed.
The calculated pressure is used as an input to the two zone model. With the pressure and fuel injection known and the air excess ratio in the flame front set, the only remaining degree of freedom is the air flow passing the flame front. The objective of this modeling approach was to replace the assumption with respect to the air flow passing the flame front with a calculation of the air flow passing the flame front. The air flow passing the flame front goes from zone I to zone II, which are both modeled as volumes. Therefore, the connecting sub-model is viewed as a flow resistance.

B.2. Model description

The single volume model and the two zone model as described in Appendix A are used. The air flow passing the flame front is no longer an input, but based on calculations performed in the resistive element separating zone I and zone II. The fuel injected is no longer a controlled variable based on the volumes of zone I and zone II, but based on a double Vibe heat release function.
As can be seen in Figure B.1, in this combined single volume and two zone model the cylinder pressure is calculated in the single volume model and the two zones are separated by an extra sub-model. In the sub-model separating zone I and zone II the flow going through the flame front is calculated based on the fuel flow and the air excess ratio; and the air passing the flame front is calculated based on knowledge regarding the cylinder volume or cylinder pressure.

B.2.1. Resistive element separating zone I and zone II

Relevant phenomena, hypothesis and assumptions

The volumes of zone I and zone II are separated by a resistive element. The aim of this element is to determine the flow from one zone to the other. Two flows are possible between zone I and zone II: a flow through

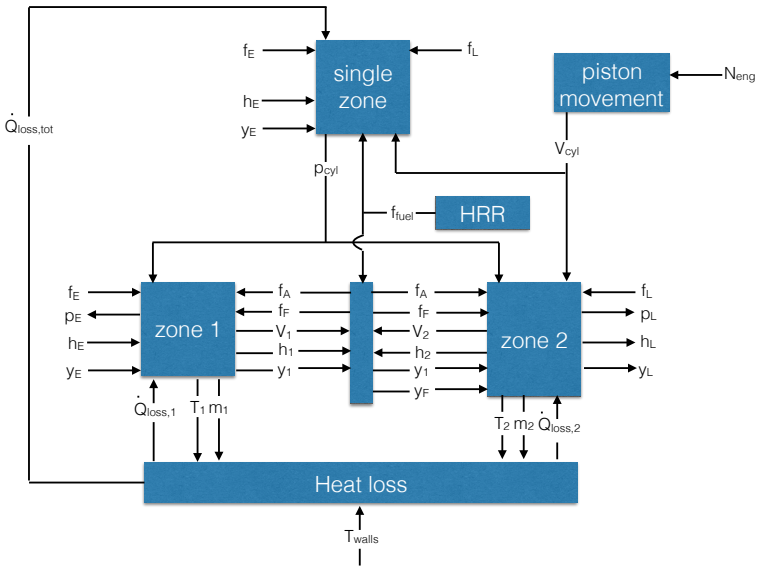

Figure B.1: Overview of sub-models and the main variables in the combined single volume and two zone model

the flame front, in which fuel is added and under-stoichiometric combusted; and a flow (of air) passing the flame front. The flow through the flame front is determined by the amount of fuel that is injected. The fuel injected is based on a Vibe-curve and calculated in the heat release sub-model.
The amount of fuel in combination with the air excess ratio λ_F, determines the amount of air that enters the flame front from zone I. The flame front itself contains no mass and occupies no volume. The OHC-equilibrium is assumed to be reached immediate. This implies that the air and fuel going in to the flame front, directly leave the flame front in an equilibrium condition and enter zone II. The composition is calculated in the OHC-equilibrium sub-model, which is presented in section 3.3.6.
The flow of air passing the flame front f_A is used to satisfy the equation of state.

Model equations

Two different approaches to calculate the air passing the flame front are identified. The first is based on the volume. The combined volume of the two zones is equal to the total cylinder volume:

$$\frac{dV_{II}}{dt} = \frac{dV_{cyl}}{dt} - \frac{dV_I}{dt} \tag{B.1}$$

The change in volume of a zone can be calculated using equation A.1.

$$\frac{dV}{dt} = \frac{1}{\overline{\rho}}\left([f_E - f_L] - V\xi\frac{d\overline{h}}{dt} - V\psi\frac{dp}{dt} - V\chi\frac{dN_i}{dt} \right) \tag{A.1}$$

Combining the above two equations:

$$\begin{aligned} &\frac{1}{\overline{\rho}_{II}}\left([f_F' + f_A - f_L] - V_{II}\xi_{II}\frac{d\overline{h}_{II}}{dt} - V_{II}\psi_{II}\frac{dp}{dt} - V_{II}\chi_{II}\frac{dN_{i,II}}{dt} \right) = \\ &= \frac{dV_{cyl}}{dt} - \frac{1}{\overline{\rho}_I}\left([f_E - f_F - f_A] - V_I\xi_I\frac{d\overline{h}_I}{dt} - V_I\psi_I\frac{dp}{dt} \right) \end{aligned} \tag{B.2}$$

where the parameters f_A is the only unknown since f_F is determined by the heat release, $\frac{dh_I}{dt}$ and $\frac{dh_{II}}{dt}$ from conservation of energy, the pressure change $\frac{dp}{dt}$ from the single volume model and $\frac{dV_{cyl}}{dt}$ from engine speed

and geometry. The leaving and entering flows are either not regarded (the closed cycle model) or are determined by the valve sub-model based on the measurement of the pressure difference over the valves (full-cycle model). The densities and partial derivatives are calculated based on the state parameters pressure p, enthalpy h and composition y.

The equation can be solved for the air flow passing the flame front:

$$f_A = \frac{\frac{1}{\overline{\rho}_I}\left(\left[f_E - f_F\right] - V_I\xi_I\frac{d\overline{h}_I}{dt} - V_I\psi_I\frac{dp}{dt}\right) + \frac{1}{\overline{\rho}_{II}}\left(\left[f'_F - f_L\right] - V_{II}\xi_{II}\frac{d\overline{h}_{II}}{dt} - V_{II}\psi_{II}\frac{dp}{dt} - V_{II}\chi_{II}\frac{dN_{i,II}}{dt}\right) - \frac{dV_{cyl}}{dt}}{\frac{1}{\overline{\rho}_I} - \frac{1}{\overline{\rho}_{II}}} \tag{B.3}$$

No feasible solution will be found, when the densities in zone I and zone II are equal.

A second approach to calculate the air flow passing the flame front is based on the assumption that the pressure in zone I and zone II must be equal, or in differential form:

$$\frac{dp_I}{dt} = \frac{dp_{II}}{dt} = \frac{dp}{dt} \tag{B.4}$$

The pressure change in a volume element is given by equation A.29:

$$\frac{dp}{dt} = \frac{1}{\psi}\left[\frac{1}{V}\left(f_E - f_L - \overline{\rho}\frac{dV}{dt}\right) - \xi\frac{d\overline{h}}{dt} - \chi\frac{dN_i}{dt}\right] \tag{A.29}$$

Therefore:

$$\frac{1}{\psi_I}\left[\frac{1}{V}\left(f_E - f_F - f_A - \overline{\rho}_I\frac{dV_I}{dt}\right) - \xi_I\frac{d\overline{h}_I}{dt}\right] = \frac{1}{\psi_{II}}\left[\frac{1}{V_{II}}\left(f'_F + f_A - f_L - \overline{\rho}_{II}\frac{dV_{II}}{dt}\right) - \xi_{II}\frac{d\overline{h}_{II}}{dt} - \chi_{II}\frac{dN_{i,II}}{dt}\right] \tag{B.5}$$

This equation can also be solved for the flow of air passing the flame front:

$$f_A = \frac{\frac{1}{\psi_I}\left[\frac{1}{V}\left(f_E - f_F - \overline{\rho}_I\frac{dV_I}{dt}\right) - \xi_I\frac{d\overline{h}_I}{dt}\right] - \frac{1}{\psi_{II}}\left[\frac{1}{V_{II}}\left(f'_F - f_L - \overline{\rho}_{II}\frac{dV_{II}}{dt}\right) - \xi_{II}\frac{d\overline{h}_{II}}{dt} - \chi_{II}\frac{dN_{i,II}}{dt}\right]}{\frac{1}{\psi_I} + \frac{1}{\psi_{II}}} \tag{B.6}$$

B.2.2. Heat Release model

Model equations

The heat release is modeled using a double Vibe-function. The dimensionless normalized formulation is adapted from Stapersma (Stapersma [27]). The input of start of combustion (SOC) and end of combustion (EOC) is given in degrees (therefore the symbol φ is introduced to indicate [degree]). The dimensionless combustion time is defined as:

$$\tau = \frac{\varphi(t) - \phi_{SOC}}{\varphi_{SOC} - \varphi_{EOC}} \tag{B.7}$$

and limited between 0 and 1.

$$X = b_1\left(1 - e^{-a\tau^{m_1+1}}\right) + b_2\left(1 - e^{-a\tau^{m_2+1}}\right) \tag{B.8}$$

and

$$Z = \frac{dX}{d\tau} = b_1 a(m_1+1)\tau^{m_1}e^{-a\tau^{m_1+1}} + b_2 a(m_1+1)\tau^{m_2}e^{-a\tau^{m_2+1}} \tag{B.9}$$

To implement the heat release model as input for the volume element, conversion from the dimensionless combustion time to simulation time is necessary.

$$\frac{dX}{dt} = \frac{dX}{d\tau}\frac{360}{2\pi(\varphi_{EOC} - \varphi_{SOC})}\frac{d\alpha}{dt} \tag{B.10}$$

The heat release can be calculated based on the available energy in the fuel (LHV) and the amount of fuel. As model input the total amount of energy entering the cylinder during 1 cycle is used as an input parameter (Q_{in}). The desired output is the flow of fuel f_{fuel}. This can be obtained by dividing by the LHV again or by switching the input to total fuel injected in a single cycle.

$$\dot{Q} = Q_{in}\frac{dX}{dt} \tag{B.11}$$

inputs	α, $d\alpha/dt$
outputs	$\dot{Q}$
parameters	φ_{SOC}, φ_{EOC}, a, b_1, m_1, b_2, m_2, Q_{in}
initial conditions	-

B.3. Results

The objective of this modeling effort was to gain more insight in the air flow passing the flame front. In the formulation proposed by Hohlbaum [18] the air flow passing the flame front was based on an assumption. The calculation used in this combined single volume and two zone model gives a division of the two zones in which all gas in the cylinder quickly flow to zone II, leaving zone I empty. Simulation results can also ly outside the boundary conditions, when zone II becomes larger than the cylinder volume and zone I negative . The two formulations to calculate the air passing the flame front (one based on volume and the other based on pressure) give the same result for the flow.

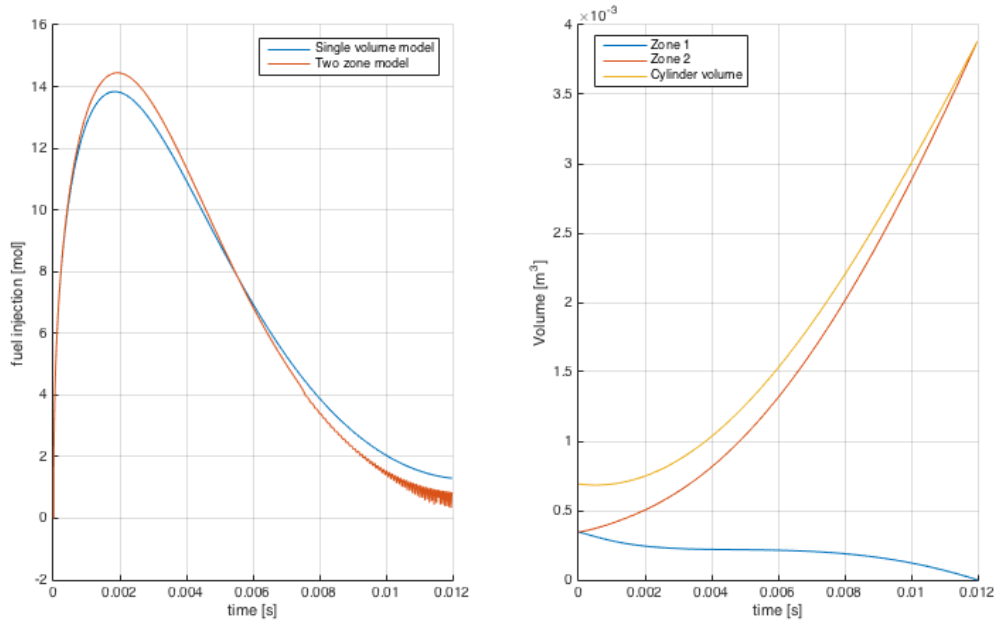

Figure B.2: The fuel injected in the single volume sub-model and the two zone sub-model (left) and the volume of the two zones and the single volume model (right)

In order to investigate how an air flow passing the flame front would be more in line with the assumptions proposed by Hohlbaum, a comparison is made between the fuel flow in the single volume model and the two zone model. The fuel flow in the single volume model and the two zone model with a constant air flow passing the flame front are presented in Figure B.2. A different fuel flow and therefore heat release is required to obtain the same pressure and volume in two zones as in a single volume.
The proposed method in this section would require a detailed measurement of the fuel injection over time and an accurate evaporation sub-model. Also, the measured cylinder pressure would have to be an input for the two zone model, since the simulated pressure from the single volume model would differ from the pressure in the two zone model with the same amount of fuel injected. Furthermore, the quality of the heat loss model must be high in order to obtain a stable and feasible solution.

Detailed information regarding the fuel injection over time is neither available for the engine under consideration, nor is it widely available or easily measured on engines onboard ships. Therefore, this modeling approach does not fulfill the requirements stated in the research proposal.

C

Measurement data

In order to validate the proposed model, measurements are performed on the MAN engine located at the Royal Netherlands Naval College. Not all results are presented within the main text, since they are not required to 'tell the story'. However, for reasons of completeness and to give the interested reader an opportunity to look into more details, some additional measurement results are presented in this appendix.

The speed of the turbo-charger and the gas temperatures, which where not presented in the main text, are depicted in Figure C.1. The temperature of the air after the compressor (but before the intercooler) increases with power. The temperature in the exhaust receiver is presented for the cylinders 2 and 3. Due to the pulse-type turbo-charger, the gas flow to the turbine is split. The temperatures in the exhaust receiver for the cylinders 1 and 4 is similar to the temperatures presented.

The amount of oxygen and carbon-dioxide in the flue gas is measured. The results are presented in figure C.2. The amount of carbon-dioxide increases with fuel flow. The amount of oxygen left in the flue gas decreases with engine load.
Over a period of three weeks time, the same measurement grid is performed multiple times. The results of all NO and NO_x measurements are presented in Figure C.3 and C.4, respectively. As expected the composition of NO_x is mainly NO. The fraction NO varies with operating conditions, but lies between 90 and 99.9%.

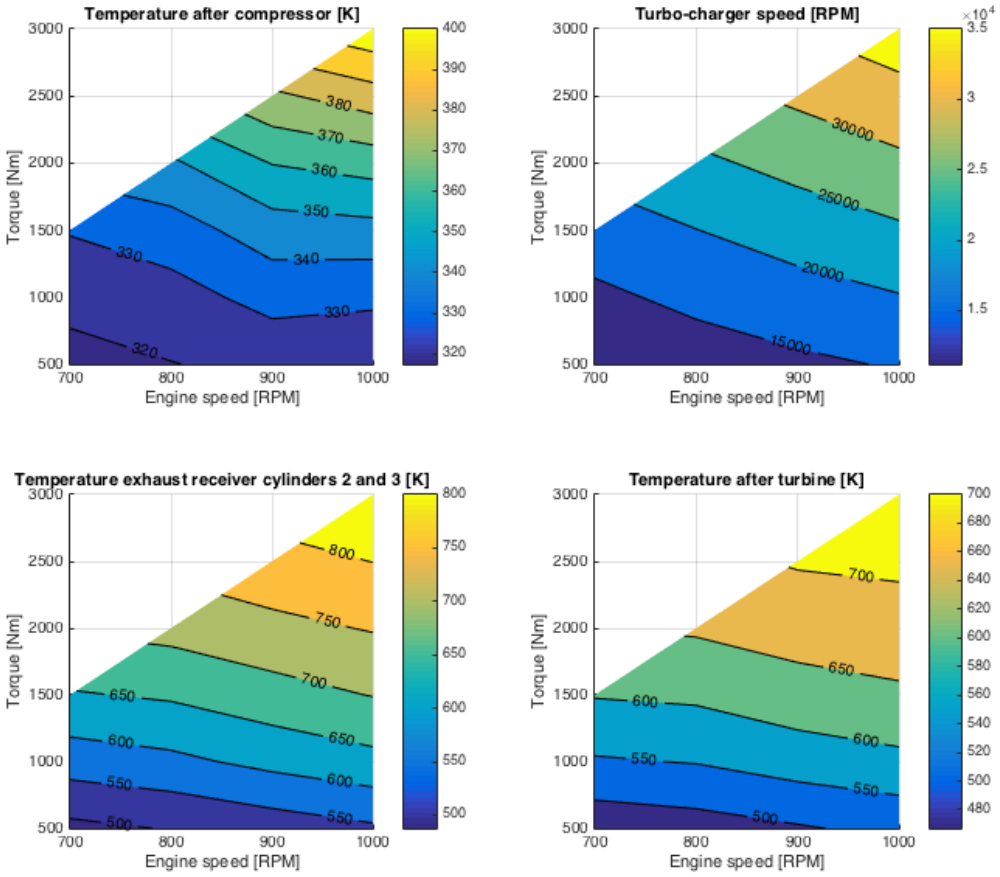

Figure C.1: Turbo-charger speed and gas temperatures

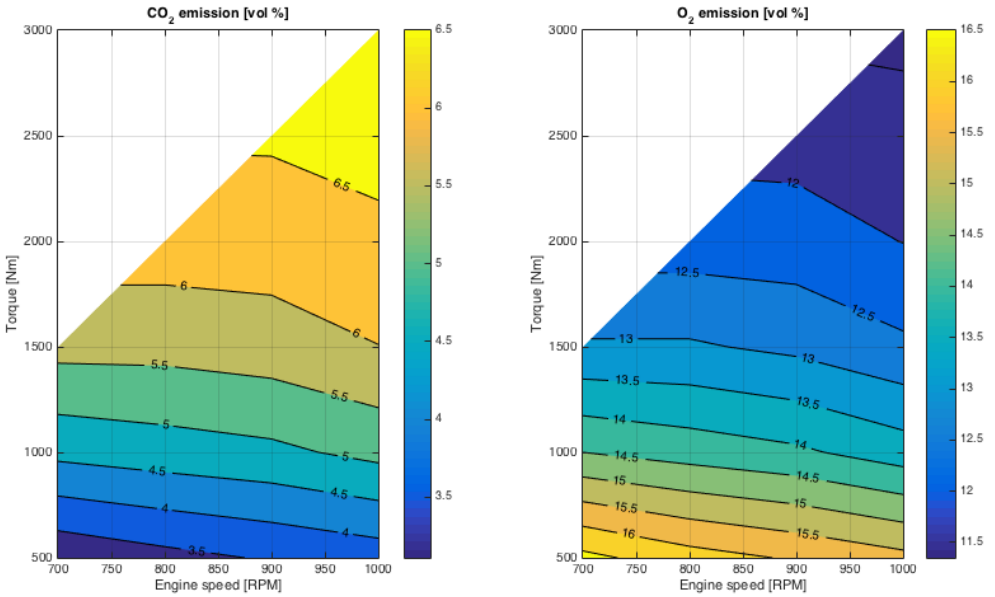

Figure C.2: Volume fractions of carbon-dioxide (left) and oxygen (right) in the flue gas

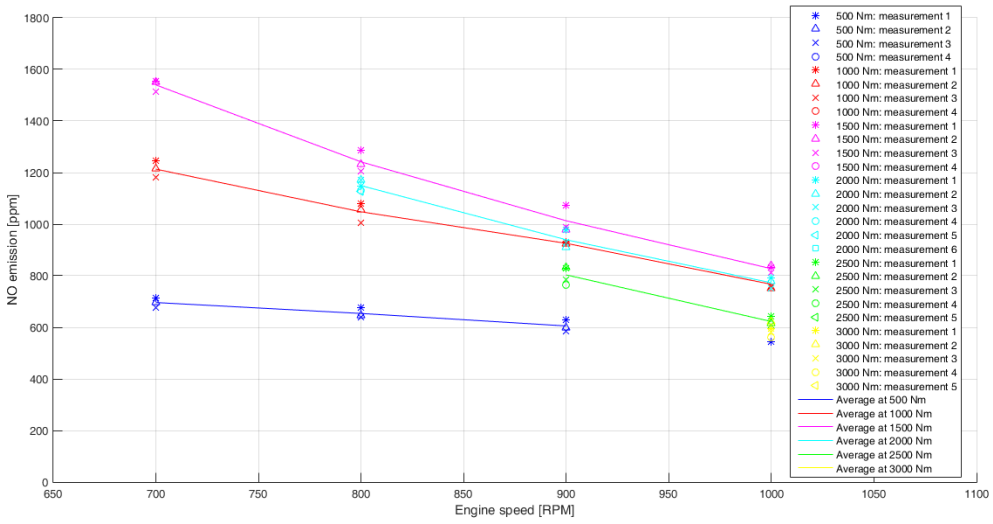

Figure C.3: *NO* measured in the flue gas

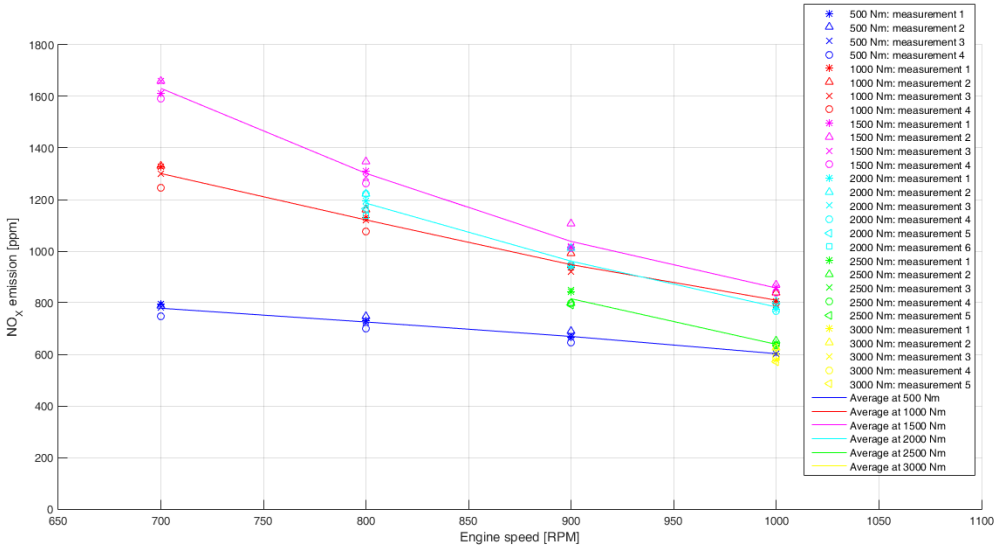

Figure C.4: NO_x measured in the flue gas

D

Input variables for the *NO*-formation sub-model

The input of the *NO*-formation sub-model is a result of the two zone model. The input, which is obtained by simulation is presented in this appendix. The results for a load of 2000 Nm at 900 RPM are presented in Figure D.1 and at 1000 RPM in Figure D.3. Figures D.2 and D.4 show the results for a load of 2500 Nm at 900 and 1000 RPM, respectively.

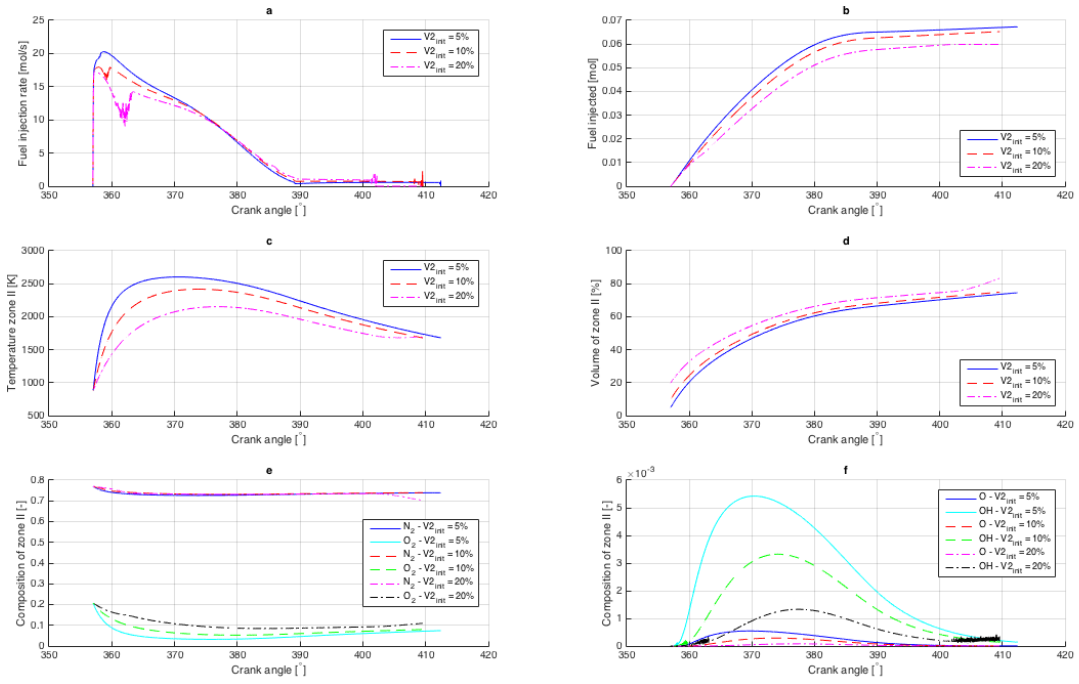

Figure D.1: The fuel injection rate (a), total amount of fuel injected (b) and the temperature (c), volume (d) and composition (e and f) of zone *II* for a load of 2000Nm at 900 RPM

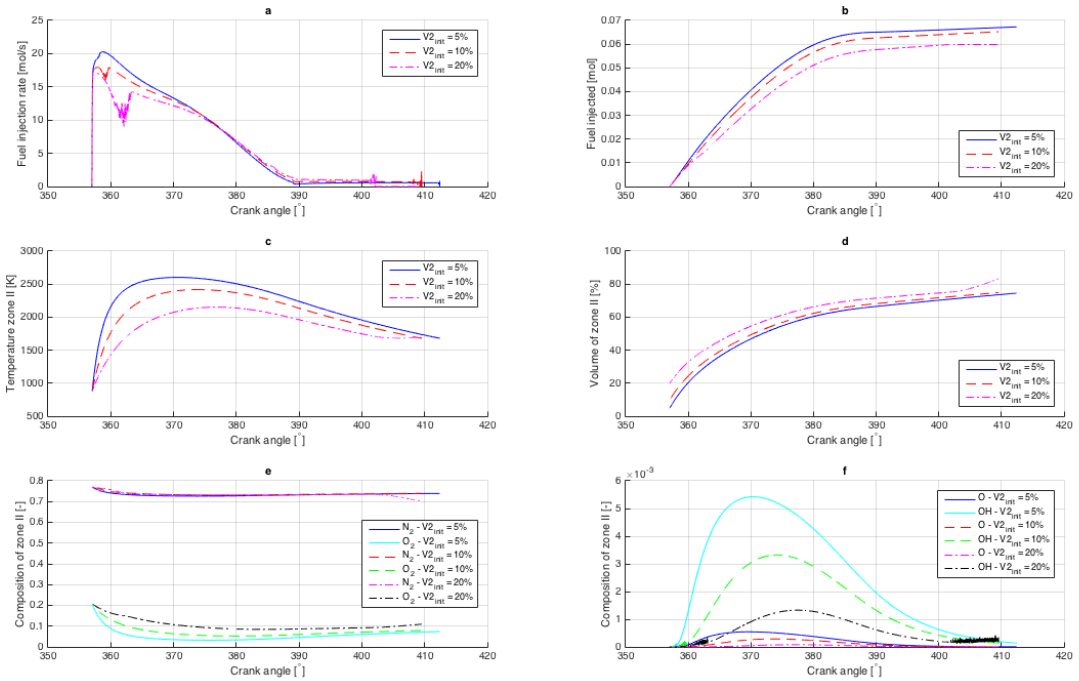

Figure D.2: The fuel injection rate (a), total amount of fuel injected (b) and the temperature (c), volume (d) and composition (e and f) of zone *II* for a load of 2500Nm at 900 RPM

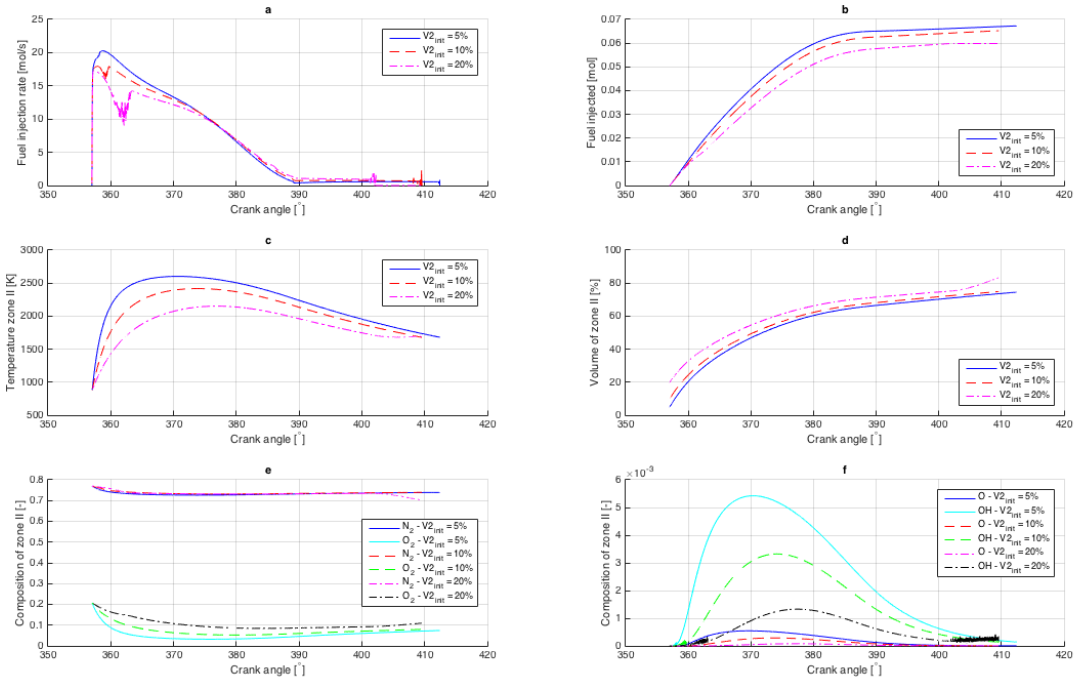

Figure D.3: The fuel injection rate (a), total amount of fuel injected (b) and the temperature (c), volume (d) and composition (e and f) of zone *II* for a load of 2000Nm at 1000 RPM

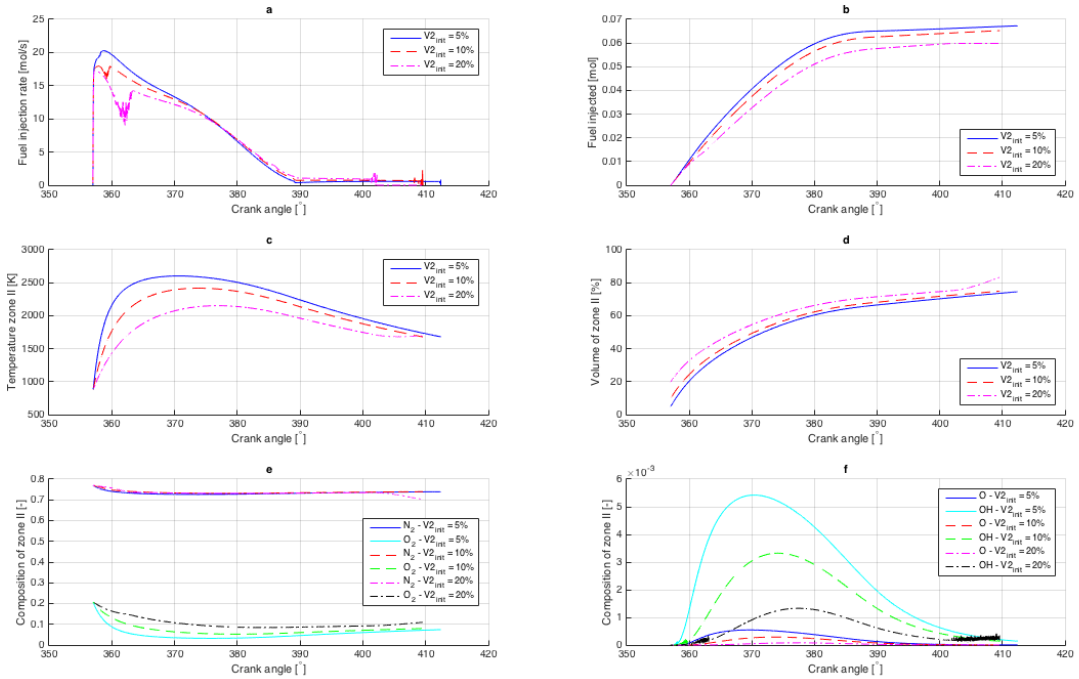

Figure D.4: The fuel injection rate (a), total amount of fuel injected (b) and the temperature (c), volume (d) and composition (e and f) of zone *II* for a load of 2500Nm at 1000 RPM

Bibliography

[1] J. Arrègle, J.J. López, J.M. Garcıa, and C. Fenollosa. Development of a zero-dimensional diesel combustion model. part 1: Analysis of the quasi-steady diffusion combustion phase. *Applied Thermal Engineering*, 23(11):1301 – 1317, 2003.

[2] J. Arrègle, J.J. López, J.M. Garcıa, and C. Fenollosa. Development of a zero-dimensional diesel combustion model: Part 2: Analysis of the transient initial and final diffusion combustion phases. *Applied Thermal Engineering*, 23(11):1319 – 1331, 2003.

[3] Jonas Asprion, Oscar Chinellato, and Lino Guzzella. Optimisation-oriented modelling of the {NOx} emissions of a diesel engine. *Energy Conversion and Management*, 75:61 – 73, 2013. ISSN 0196-8904. doi: http://dx.doi.org/10.1016/j.enconman.2013.05.039. URL `http://www.sciencedirect.com/science/article/pii/S0196890413003038`.

[4] Jonas Asprion, Oscar Chinellato, and Lino Guzzella. A fast and accurate physics-based model for the {NOx} emissions of diesel engines. *Applied Energy*, 103:221 – 233, 2013. ISSN 0306-2619. doi: http://dx.doi.org/10.1016/j.apenergy.2012.09.038. URL `http://www.sciencedirect.com/science/article/pii/S0306261912006794`.

[5] Francesco Baldi, Gerasimos Theotokatos, and Karin Andersson. Development of a combined mean value-zero dimensional model and application for a large marine four-stroke diesel engine simulation. *Applied Energy*, 154:402–415, 2015.

[6] J.S. Barsingerhorn, J.S. Limburg, E.C. de Man, and V.A. Wieleman. Turbodrive. Bachelor thesis, Delft University of Technology, Delft, The Netherlands, 2016.

[7] Xiaobei Cheng, Liang Chen, Fangqin Yan, and Shijun Dong. Study on soot formation characteristics in the diesel combustion process based on an improved detailed soot model. *Energy Conversion and Management*, 75:1 – 10, 2013. ISSN 0196-8904. doi: http://dx.doi.org/10.1016/j.enconman.2013.05.033. URL `http://www.sciencedirect.com/science/article/pii/S0196890413002938`.

[8] Franz G. Chmela, Gerhard H. Pirker, and Andreas Wimmer. Zero-dimensional {ROHR} simulation for {DI} diesel engines – a generic approach. *Energy Conversion and Management*, 48(11):2942 – 2950, 2007. ISSN 0196-8904. doi: http://dx.doi.org/10.1016/j.enconman.2007.07.004. URL `http://www.sciencedirect.com/science/article/pii/S0196890407002051`. 19th International Conference on Efficiency, Cost, Optimization, Simulation and Environmental Impact of Energy Systems.

[9] J. Deng, M. Bastian, and R.K. Stobart. Particulate matter prediction in both steady state and transient operation of diesel engines. *Proc. IMechE*, 226:260–274, 2011.

[10] Yu Ding. *Characterising Combustion in Diesel Engines using parameterised finite stage cylinder process models*. PhD thesis, Delft University of Technology, Delft, The Netherlands, 2011.

[11] EEA. The impact of international shipping on european air quality and climate forcing. ISBN 978-92-9213-357-3 4/2013, European Environment Agency, Luxembourg: Publications Office of the European Union, 2013.

[12] EEA. Eea-32 nitrogen oxides (nox) emissions. European Environment Agency Kongens Nytorv 6 1050 Copenhagen K Denmark, 2014. URL `http://www.eea.europa.eu/data-and-maps/indicators/eea-32-nitrogen-oxides-nox-emissions/eea-32-nitrogen-oxides-nox`.

[13] S. Galindo Lopez. Three-zone in-cylinder process model for di diesel engines. Master's thesis, Delft University of Technology, Delft, The Netherlands, April 2014.

[14] M. Ghazikhani and I. Mirzaii. Soot emission prediction of a waste-gated turbo-charged di diesel engine using artificial neural network. *Neural Comput & Applic*, 20:303–308, 2011.

[15] G. Heider, G. Woschni, and K. Zeilinger. Two-zone calculation model for the prediction of no emissions from diesel engines. In *21st International conference on combustion engines*, Interlaken, 1995.

[16] J.J. Hernandez, M. Lpuerta, and J. Perez-Collado. A combustion kinetic model for estimating diesel engine nox emissions. *Combustion Theory and Modelling*, 10(4):639 – 657, 2006.

[17] Eds. P.J. Linstrom and W.G. Mallard. Thermophysical properties of fluid systems. In National Institute of Standards and Technology, editor, *NIST Standard Reference Database Number 69*. NIST Chemistry Webbook, Gaithersburg MD, 20899, http://webbook.nist.gov, (retrieved November 30, 2016), 11 2016. URL `http://webbook.nist.gov/cgi/cbook.cgi?ID=C7732185&Mask=4&Type=ANTOINE&Plot=on`.

[18] G.P. Merker, B. Hohlbaum, and M. Rauscher. Two-zone model for calculation of nitrogen-oxide formation in direct-injection diesel engines. SAE Technical Paper 932454, SAE International, Warrendale, PA, Sept 1993.

[19] Prof. Dr.-Ing. Günter P. Merker, Prof. Dr.-Ing. Christian Schwarz, Dr.-Ing. habil Gunnar Stiesch, and Dr. rer. nat. Frank Otto. *Simulating Combustion - Simulation of combustion and pollutant formation for engine-development*. Springer Berlin Heidelberg, 2006.

[20] H. van Putten P. Colonna. Dynamic modeling of steam power cycles. part i—modeling paradigm and validation. *Applied Thermal Engineering*, 27:467 – 480, 2007.

[21] T.W.J. Peeters. *Numerical modeling of turbulent natural-gas diffusion flames*. PhD thesis, Technische Universiteit Delft, Sept 1995.

[22] C.D. Rakopoulos, D.C. Rakopoulos, and D.C. kyritsis. Development and validation of a comprehensive two-zone model for combustion and emissions formation in a di diesel engine. *International Journal of Energy Research*, 27:1221–1249, 2003.

[23] Stanley I. Sandler. *Chemical, Biochemical, and Engineering Thermodynamics*. John Wiley & Sons, Inc, fourth edition, 2006.

[24] P.J.M. Schulten. *The interaction between diesel engines, ship and propellers during manoeuvring*. PhD thesis, Delft University of Technology, Delft, The Netherlands, 2005.

[25] D. Stapersma. Performance analysis. In *Diesel Engines*, volume 1. Faculty of Mechanical, Maritime and Materials Engineering - Delft University of Technology, 2010.

[26] D. Stapersma. Turbocharging. In *Diesel Engines*, volume 2. Faculty of Mechanical, Maritime and Materials Engineering - Delft University of Technology, 2010.

[27] D. Stapersma. Combustion. In *Diesel Engines*, volume 3. Faculty of Mechanical, Maritime and Materials Engineering - Delft University of Technology, 2010.

[28] D. Stapersma. Emissions and heat transfer. In *Diesel Engines*, volume 4. Faculty of Mechanical, Maritime and Materials Engineering - Delft University of Technology, 2010.

[29] D. Stapersma. Thermodynamical principles i. In *Diesel Engines*, volume 5. Faculty of Mechanical, Maritime and Materials Engineering - Delft University of Technology, 2010.

[30] Xavier Tauzia, Alain Maiboom, Pascal Chesse, and Nicolas Thouvenel. A new phenomenological heat release model for thermodynamical simulation of modern turbocharged heavy duty diesel engines. *Applied Thermal Engineering*, 26(16):1851 – 1857, 2006. ISSN 1359-4311. doi: http://dx.doi.org/10.1016/j.applthermaleng.2006.02.009. URL `http://www.sciencedirect.com/science/article/pii/S1359431106000342`.

[31] Stephen R. Turns. *An Introduction to Combustion - Concepts and Applications*. Mechenical Engineering Series. McGraw-Hill International editions, second edition, 2006.

[32] UNCTAD. Review of maritme transport. ISBN 978-92-1-112892-5, UNITED NATIONS CONFERENCE ON TRADE AND DEVELOPMENT - New York and Geneva, 2015.

[33] Prof. Dr. Dr. Jürgen Warnatz, Prof. Dr. Ulrich Maas, and Prof. Dr. Robert W. Dibble. *Combustion - Physical and Chemical Fundamentals, Modeling and Simulation, Experiments, Pollutant Formation*. Springer Berlin Heidelberg, 2006.

[34] J. Xi and B. J. Zhong. Soot in diesel combustion systems. *Chemical Engineering & Technology*, 29(6): 665–673, 2006. doi: 10.1002/ceat.200600016. URL http://dx.doi.org/10.1002/ceat.200600016.

[35] Xingyu Xue and Jerald A Caton. Detailed multi-zone thermodynamic simulation for direct-injection diesel engine combustion. *International Journal of Engine Research*, 13(4):340 – 356, August 2012.